http://www.icact.org/journal.asp

ICACT-TACT JOURNAL

Transactions on Advanced Communications Technology

Volume 1 Issue 3, Nov 2012, ISSN: 2288-0003

Editor-in-Chief
Prof. Thomas Byeongnam YOON, PhD.

Global IT
Research Institute

Journal Editorial Board

■ Editor-in-Chief

■ Editors

Dr. Youssef SAID, Tunisie Telecom, Tunisia
Dr. Noor Zaman, King Faisal University, Al Ahsa Hofuf, Saudi Arabia
Dr. Srinivas Mantha, SASTRA University, Thanjavur, India
Dr. Shahriar Mohammadi, KNTU University, Iran
Prof. Beonsku An, Hongik University, korea
Dr. Guanbo Zheng, University of Houston, USA
Prof. Sangho Choe, The Catholic University of Korea, korea
Dr. Gyanendra Prasad Joshi, Yeungnam University, korea
Dr. Tae-Gyu Lee, Korea Institue of Industrial Technology(KITECH), korea
Prof. Ilkyeun Ra, University of Colorado Denver, USA
Dr. Yong Sun, Beijing University of Posts and Telecommunications, China
Dr. Yulei Wu, Chinese Academy of Sciences, China
Mr. Anup Thapa, Chosun University, korea
Dr. Vo Nguyen Quoc Bao, Posts and Telecommunications Institute of Technology, Vietnam
Dr. Harish Kumar, Bhagwant institute of technology, India
Dr. Jin REN, North china university of technology, China
Dr. Joseph Kandath, Electronics & Commn Engg, India
Dr. Mohamed M. A. Moustafa, Arab Information Union (AIU), Egypt
Dr. Mostafa Zaman Chowdhury, Kookmin University, Korea
Prof. Francis C.M. Lau, Hong Kong Polytechnic University, Hong Kong
Prof. Ju Bin Song, Kyung Hee University, korea
Prof. KyungHi Chang, Inha University, Korea
Prof. Sherif Welsen Shaker, Kuang-Chi Institute of Advanced Technology, China
Prof. Seung-Hoon Hwang, Dongguk University, Korea
Prof. Dal-Hwan Yoon, Semyung University, korea
Prof. Chongyang ZHANG, Shanghai Jiao Tong University, China
Dr. H K Lau, The Open University of Hong Kong, Honh Kong
Prof. Ying-Ren Chien, Department of Electrical Engineering, National Ilan University, Taiwan
Prof. Mai Yi-Ting, Hsiuping University of Science and Technology, Taiwan
Dr. Sang-Hwan Ryu, Korea Railroad Research Institute, Korea
Dr. Yung-Chien Shih, MediaTek Inc., Taiwan
Dr. Kuan Hoong Poo, Multimedia University, Malaysia
Dr. Michael Leung, CEng MIET SMIEEE, Hong Kong
Dr. Abu sahman Bin mohd Supa'at, Universiti Teknologi Malaysia, Malaysia
Prof. Amit Kumar Garg, Deenbandhu Chhotu Ram University of Science & Technology, India
Dr. Jens Myrup Pedersen, Aalborg University, Denmark
Dr. Augustine Ikechi Ukaegbu, KAIST, Korea
Dr. Jamshid Sangirov, KAIST, Korea
Prof. Ahmed Dooguy KORA, Ecole Sup. Multinationale des Telecommunications, Senegal
Dr. Se-Jin Oh, Korea Astronomy & Space Science Institute, Korea
Dr. Rajendra Prasad Mahajan, RGPV Bhopal, India
Dr. Woo-Jin Byun, ETRI, Korea
Dr. Mohammed M. Kadhum, School of Computing, Goodwin Hall, Queen's University , Canada
Prof. Seong Gon Choi, Chungbuk National University, Korea
Prof. Yao-Chung Chang, National Taitung University, Taiwan
Dr. Abdallah Handoura, Engineering school of Gabes - Tunisia, Tunisia
Dr. Gopal Chandra Manna, BSNL, India

Dr. Il Kwon Cho, National Information Society Agency, Korea
Prof. Jiann-Liang Chen, National Taiwan University of Science and Technology, Taiwan
Prof. Ruay-Shiung Chang, National Dong Hwa University, Taiwan
Dr. Vasaka Visoottiviseth, Mahidol University, Thailand
Prof. Dae-Ki Kang, Dongseo University, Korea
Dr. Yong-Sik Choi, Research Institute, IDLE co., ltd, Korea
Dr. Xuena Peng, Northeastern University, China
Dr. Ming-Shen Jian, National Formosa University, Taiwan
Dr. Soobin Lee, KAIST Institute for IT Convergence, Korea
Prof. Yongpan Liu, Tsinghua University, China
Prof. Chih-Lin HU, National Central University, Taiwan
Prof. Chen-Shie Ho, Oriental Institute of Technology, Taiwan
Dr. Hyoung-Jun Kim, ETRI, Korea
Prof. Bernard Cousin, IRISA/Universite de Rennes 1, France
Prof. Eun-young Lee, Dongduk Woman s University, Korea
Dr. Porkumaran K, NGP institute of technology India, India
Dr. Feng CHENG, Hasso Plattner Institute at University of Potsdam, Germany
Prof. El-Sayed M. El-Alfy, King Fahd University of Petroleum and Minerals, Saudi Arabia
Prof. Lin You, Hangzhou Dianzi Univ, China
Mr. Nicolai Kuntze, Fraunhofer Institute for Secure Information Technology, Germany
Dr. Min-Hong Yun, ETRI, Korea
Dr. Seong Joon Lee, Korea Electrotechnology Research Institute, korea
Dr. Kwihoon Kim, ETRI, Korea
Dr. Jin Woo HONG, Electronics and Telecommunications Research Inst., Korea
Dr. Heeseok Choi, KISTI(Korea Institute of Science and Technology Information), korea
Dr. Somkiat Kitjongthawonkul, Australian Catholic University, St Patrick's Campus, Australia
Dr. Dae Won Kim, ETRI, Korea
Dr. Ho-Jin CHOI, KAIST(Univ), Korea
Dr. Su-Cheng HAW, Multimedia University, Faculty of Information Technology, Malaysia
Dr. Myoung-Jin Kim, Soongsil University, Korea
Dr. Gyu Myoung Lee, Institut Mines-Telecom, Telecom SudParis, France
Dr. Dongkyun Kim, KISTI(Korea Institute of Science and Technology Information), Korea
Prof. Yoonhee Kim, Sookmyung Women s University, Korea
Prof. Li-Der Chou, National Central University, Taiwan
Prof. Young Woong Ko, Hallym University, Korea
Prof. Dimiter G. Velev, UNWE(University of National and World Economy), Bulgaria
Dr. Tadasuke Minagawa, Meiji University, Japan
Prof. Jun-Kyun Choi, KAIST (Univ.), Korea
Dr. Brownson ObaridoaObele, Hyundai Mobis Multimedia R&D Lab , Korea
Prof. Anisha Lal, VIT university, India
Dr. kyeong kang, University of technology sydney, faculty of engineering and IT , Australia
Prof. Chwen-Yea Lin, Tatung Institute of Commerce and Technology, Taiwan
Dr. Ting Peng, Chang'an University, China
Prof. ChaeSoo Kim, Donga University in Korea, Korea
Prof. kirankumar M. joshi, m.s.uni.of baroda, India
Dr. Chin-Feng Lin, National Taiwan Ocean University, Taiwan
Dr. Chang-shin Chung, TTA(Telecommunications Technology Association), Korea

Editor Guide

■ Introduction for Editor or Reviewer

All the editor group members are to be assigned as a evaluator(editor or reviewer) to submitted journal papers at the discretion of the Editor-in-Chief. It will be informed by eMail with a Member Login ID and Password.

Once logined the Website via the Member Login menu in left as a evaluator, you can find out the paper assigned to you. You can evaluate it there. All the results of the evaluation are supposed to be shown in the Author Homepage in the real time manner. You can also enter the Author Homepage assigned to you by the Paper ID and the author's eMail address shown in your Evaluation Webpage. In the Author Homepage, you can communicate each other efficiently under the peer review policy. Please don't miss it!

All the editor group members are supposed to be candidates of a part of the editorial board, depending on their contribution which comes from history of ICACT TACT as an active evaluator. Because the main contribution comes from sincere paper reviewing role.

■ Role of the Editor

The editor's primary responsibilities are to conduct the peer review process, and check the final camera-ready manuscripts for any technical, grammatical or typographical errors.

As a member of the editorial board of the publication, the editor is responsible for ensuring that the publication maintains the highest quality while adhering to the publication policies and procedures of the ICACT TACT(Transactions on the Advanced Communications Technology).

For each paper that the editor-in-chief gets assigned, the Secretariat of ICACT Journal will send the editor an eMail requesting the review process of the paper.

The editor is responsible to make a decision on an "accept", "reject", or "revision" to the Editor-in-Chief via the Evaluation Webpage that can be shown in the Author Homepage also.

■ Deadlines for Regular Review

Editor-in-Chief will assign a evalaution group(a Editor and 2 reviewers) in a week upon receiving a completed Journal paper submission. Evaluators are given 2 weeks to review the paper. Editors are given a week to submit a recommendation to the Editor-in-Chief via the evaluation Webpage, once all or enough of the reviews have come in. In revision case, authors have a maximum of a month to submit their revised manuscripts. The deadlines for the regular review process are as follows:

Evalution Procedure	Deadline
Selection of Evaluation Group	1 week
Review processing	2 weeks
Editor's recommendation	1 week
Final Decision Noticing	1 week

■ Making Decisions on Manuscript

Editor will make a decision on the disposition of the manuscript, based on remarks of the reviewers. The editor's recommendation must be well justified and explained in detail. In cases where the revision is requested, these should be clearly indicated and explained. The editor must then promptly convey this decision to the author. The author may contact the editor if instructions regarding amendments to the manuscript are unclear. All these actions could be done via the evaluation system in this Website. The guidelines of decisions for publication are as follows:

Decision	Description
Accept	An accept decision means that an editor is accepting the paper with no further modifications. The paper will not be seen again by the editor or by the reviewers.
Reject	The manuscript is not suitable for the ICACT TACT publication.
Revision	The paper is conditionally accepted with some requirements. A revision means that the paper should go back to the original reviewers for a second round of reviews. We strongly discourage editors from making a decision based on their own review of the manuscript if a revision had been previously required.

■ Role of the Reviewer

Reviewer Webpage:

Once logined the Member Login menu in left, you can find out papers assigned to you. You can also login the Author Homepage assigned to you with the paper ID and author's eMail address. In there you can communicate each other via a Communication Channel Box.

Quick Review Required:

You are given 2 weeks for the first round of review and 1 week for the second round of review. You must agree that time is so important for the rapidly changing IT technologies and applications trend. Please respect the deadline. Authors undoubtedly appreciate your quick review.

Anonymity:

Do not identify yourself or your organization within the review text.

Review:

Reviewer will perform the paper review based on the main criteria provided below. Please provide detailed public comments for each criterion, also available to the author.

- How this manuscript advances this field of research and/or contributes something new to the literature?
- Relevance of this manuscript to the readers of TACT?
- Is the manuscript technically sound?
- Is the paper clearly written and well organized?
- Are all figures and tables appropriately provided and are their resolution good quality?
- Does the introduction state the objectives of the manuscript encouraging the reader to read on?
- Are the references relevant and complete?

Supply missing references:

Please supply any information that you think will be useful to the author in revision for enhancing quality of the paperor for convincing him/her of the mistakes.

Review Comments:

If you find any already known results related to the manuscript, please give references to earlier papers which contain these or similar results. If the reasoning is incorrect or ambiguous, please indicate specifically where and why. If you would like to suggest that the paper be rewritten, give specific suggestions regarding which parts of the paper should be deleted, added or modified, and please indicate how.

Journal Procedure

Dear Author,

- **You can see all your paper information & progress.**

- **Step 1. Journal Full Paper Submission**

Using the Submit button, submit your journal paper through ICACT Website, then you will get new paper ID of your journal, and send your journal Paper ID to the Secretariat@icact.org for the review and editorial processing. Once you got your Journal paper ID, never submit again! Journal Paper/CRF Template

- **Step 2. Full Paper Review**

Using the evaluation system in the ICACT Website, the editor, reviewer and author can communicate each other for the good quality publication. It may take about 1 month.

- **Step 3. Acceptance Notification**

It officially informs acceptance, revision, or reject of submitted full paper after the full paper review process.

Status	Action
Acceptance	Go to next Step.
Revision	Re-submit Full Paper within 1 month after Revision Notification.
Reject	Drop everything.

- **Step 4. Payment Registration**

So far it's free of charge in case of the journal promotion paper from the registered ICACT conference paper! But you have to regist it, because you need your Journal Paper Registration ID for submission of the final CRF manuscripts in the next step's process. Once you get your Registration ID, send it to Secretariat@icact.org for further process.

- **Step 5. Camera Ready Form (CRF) Manuscripts Submission**

After you have received the confirmation notice from secretariat of ICACT, and then you are allowed to submit the final CRF manuscripts in PDF file form, the full paper and the Copyright Transfer Agreement. Journal Paper Template, Copyright Form Template, BioAbstract Template,

Journal Submission Guide

All the Out-Standing ICACT conference papers have been invited to this "ICACT Transactions on the Advanced Communications Technology" Journal, and also welcome all the authors whose conference paper has been accepted by the ICACT Technical Program Committee, if you could extend new contents at least 30% more than pure content of your conference paper. Journal paper must be followed to ensure full compliance with the IEEE Journal Template Form attached on this page.

➢ How to submit your Journal paper and check the progress?

Step 1. Submit	Using the Submit button, submit your journal paper through ICACT Website, then you will get new paper ID of your journal, and send your journal Paper ID to the Secretariat@icact.org for the review and editorial processing. Once you got your Journal paper ID, never submit again! Using the Update button, you can change any information of journal paper related or upload new full journal paper.
Step 2. Confirm	Secretariat is supposed to confirm all the necessary conditions of your journal paper to make it ready to review. In case of promotion from the conference paper to Journal paper, send us all the .DOC(or Latex) files of your ICACT conference paper and journal paper to evaluate the difference of the pure contents in between at least 30% more to avoid the self replication violation under scrutiny. The pure content does not include any reference list, acknowledgement, Appendix and author biography information.
Step 3. Review	Upon completing the confirmation, it gets started the review process thru the Editor & Reviewer Guideline. Whenever you visit the Author Homepage, you can check the progress status of your paper there from start to end like this, " Confirm OK! -> Gets started the review process -> ...", in the Review Status column. Please don't miss it!

Volume 1, Issue 3

WPBR: Weekly Prediction based Bandwidth Reservation Scheme for Macrocellular Wireless Networks in Urban Areas

Adel Amani *, Hossein Pedram *

** Department of Computer Engineering and Information Technology, Amirkabir University of Technology, Tehran, Iran*
a.amani64@gmail.com, pedram@aut.ac.ir

***Abstract*—One of the major challenges in the cellular networks is to guarantee the quality of service of the ongoing calls by prioritizing them over the new calls. An operative approach to prioritize the hand off calls over the new calls is by reserving bandwidth for the ongoing calls of mobile stations in the potential next cell that they may visit. Improving the prediction of potential next cell that a mobile station may visit will cause better bandwidth utilization. In this paper, we propose weekly prediction based bandwidth reservation scheme. The proposed scheme, WPBR, improves prediction by means of storing weekly movement probabilities of mobile station based on Markov modeling techniques. In order to decreasing the storage space that is needed for storing the mobile station's movement probabilities, we adopted a dynamic hashing approach. Simulation results show that the weekly prediction in the proposed scheme, significantly improves bandwidth utilization, and the adopted dynamic hashing approach caused the overhead of storage space to be acceptable.**

Index Terms*—Macrocellular Wireless Networks, Bandwidth Reservation, Mobility Prediction, Markov Modeling Techniques, Dynamic Hashing.

I. INTRODUCTION

IN recent years there has been a rapid development in mobile and wireless cellular networks. One of the most major challenges in the mobile and wireless cellular networks is to efficiently utilize the bandwidth while the quality of service (QoS) of the ongoing calls should be guaranteed. However, due to user mobility, establishment and management of connections are very difficult.

A mobile and wireless cellular network consists of a lot of cells that serve a large number of mobile users with various mobility patterns and a number of applications. A cell involves a base station (BS) and a number of mobile stations (MSs). When an MS moves from the coverage of a cell into the coverage of another cell and there is an ongoing call, the call should be handed over from the prior cell to the new cell. This process is called hand off. If there is no available bandwidth to serve the hand off call in the new cell, then this call will not complete and will be dropped by the new BS. There are three elementary QoS parameters in the cellular networks: the hand off call dropping probability (CDP), the new call blocking probability (CBP) and the bandwidth utilization (BWU).

From the user point of view, dropping of an ongoing call is more undesirable than blocking of a new call. In the other word, ongoing calls must prioritized over new calls. In literature, several approaches have been proposed to give priorities to hand off calls [1]. One most common approach to prioritize hand off calls over new calls is by reserving channels for hand off calls. Schemes that utilize mentioned approach are classified as *channel reservation schemes* [1].

Reserving some bandwidth at each BS could only be utilized by hand off calls. Since any such reservation inevitably increases the CBP, and decreases the system's BWU, it is very important to make reservations as sparingly as possible. One astute way for the purpose of sparing reservation is to reserve bandwidth for each MS based on its predicted path through the cellular network. At first, the potential next cell that an MS may visit during its lifetime is predicted based on some information about the MS's mobility, and then, bandwidth reservation will be made only in the potential next cell that the mobile station may visit. In [1], schemes that utilize mobility prediction approach to reserve bandwidth are classified as *predictive mobile-oriented channel reservation schemes* (PMOCR).

The information that employed in the mobility prediction could be categorized into two types: current mobility parameters of MSs and observation histories of MSs. The schemes that using current mobility parameters like velocity, direction, angle or distance in their prediction, typically compute the probability of events occurring, depending on the values of these parameters. In [1], it mentioned that the key limitation of prediction by means of current mobility parameters is the requirement of positioning hardware.

Manuscript received July 9, 2012.
Hossein Pedram is with Department of Computer Engineering and Information Technology, Amirkabir University of Technology, Tehran, Iran (Tel: +98-2164542701; email: pedram@aut.ac.ir).
Adel Amani was with Department of Computer Engineering and Information Technology, Amirkabir University of Technology, Tehran, Iran (Tel: +98-9183733912; email: a_amani@aut.ac.ir).

Another problem in these approaches is the overhead to obtain mobility parameters. However, the serious problem with these schemes is hidden behind the parameters and the mobility models that used in their predictions. The majority of these approaches utilize mobility models like random waypoint or its variants that fail to represent all or some of mobility characteristics (temporal and spatial dependency of velocity and geographic restrictions) that mentioned in [2]. But the predictions are unrealistic without representing mobility characteristics.

History-based schemes use historical mobility patterns of MSs to calculate their potential next cell. These schemes are based on a reasonable assumption that mobility of an MS shows some regularity in urban areas. In [1], it mentioned that the key limitation with all history-based schemes is the overhead to store and update observation histories for the MS's mobility.

There are two common approaches to work with observation histories: data mining techniques and markov modeling techniques. In data mining approach, user mobility patterns are mined from the history of mobile user trajectories. The MS's next movement is predicted by using mobility rules, which are extracted from the user mobility patterns. These trajectories are saved over time and the needed storage space will grow over time too. In markov modeling approach, potential next cell for an MS predicted based on historical mobility of the MS using Markov modeling. The Markovian mobility model defines distinct probabilities for movement from a given cell to each of its neighbors. Thus the needed space for storing movement probabilities in markov modeling approaches does not exceed a particular limit.

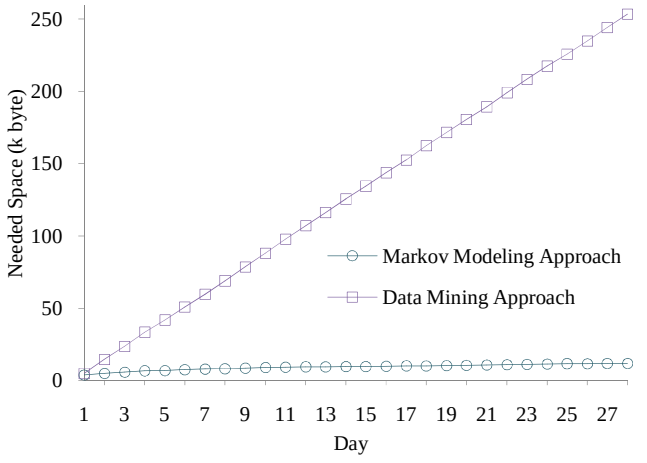

Figure 1.Comparison of needed storage space by data mining approach and markov modeling approach

In Figure 1 needed storage space of the markov modeling approach that suggested in [3], is compared to the data mining approach that explained in [4]. The comparison is done in a macrocellular wireless network with 25 cells and 95 mobile stations that move based on real time traces that have obtained through the reality mining project [7]. Our simulation results show that the needed space of data mining approach is extremely more than needed space of markov modeling approach. Thus the data mining approaches are not right choices for mobility prediction in the macrocellular wireless networks with a large number of mobile stations in urban area.

In this paper, we propose a predictive mobile-oriented bandwidth reservation scheme that improves prediction by means of storing weekly movement probabilities of MSs based on Markov modeling techniques. Also, we adopted a dynamic hashing approach in order to decreasing the storage space that is needed for storing the movement probabilities. Simulation results show that the weekly prediction in this novel strategy significantly improves bandwidth utilization, and the adopted dynamic hashing approach fairly overcomes the overhead of storage space.

The remainder of this paper is organized as follows: Section II gives an overview of related works. In section III the novel weekly-prediction-based bandwidth reservation (WPBR) strategy will be introduced. Section IV describes simulation environment and provides simulation results and discussions. Section V gives a plan for future works and concludes the paper.

II. Related Works

Many history-based mobility prediction schemes have been proposed to estimate the potential next cell that an MS may visit. In [3], a *dynamic location management* scheme have been introduced, in which potential next cell for an MS predicted based on historical mobility of the MS using Markov modeling. The Markovian mobility model defines distinct probabilities for movement from a given cell to each of its neighbors. These probabilities are stored in a matrix that called transition matrix. Each cell records movement probabilities based on the frequency of hand offs to its adjacent cells for each MS that is on a call inside the cell. Movement probabilities are updated at specified refresh intervals. Refreshing process may take place hourly, daily or more infrequently. The proposed algorithm for obtaining the movement probabilities is given as follows:

1) For every hand off to a neighbor cell, the hand off tally for that particular neighbor is incremented, or the cell is recorded as a neighbor if not previously seen.
2) On a cell refresh, each individual hand off tally is divided by the total number of hand offs to obtain the probability of moving to each cell.
3) Stored movement probabilities are smoothed using a simple exponentially weighted moving average as in (1).
4) Each hand off tally is reset to zero and the process is continued.

$$prob(c,i) = w \times prob(c,i-1) + (1-w) \times newProb(c). \quad (1)$$

For each MS the probability of moving to cell c in the interval i obtained from (1), in which w is the smoothing factor. Each cell requires two hash maps, one to store the hand

off frequencies that resulted in *newProb(c)*, and one to store the smoothed movement probabilities that used to predict potential next cell. MS's mobility patterns attain a steady state and are predictable after a series of repeated cell refreshes.

However, a single transition matrix for the whole day will cause unrealistic predictions [5]. In urban areas, a considerable number of MSs are moving from home to work every morning, and coming back from work to home in the afternoon. So, if an MS came back to home in the same path that has gone to work and refresh interval was greater than or equal to a day, a single transition matrix will give equal probability of occurrence for both of the movement paths (to work and to home) at any time of the day. In order to overcome this problem, the day is divided into eight fixed time slots (00:00-6:00, 6:00-8:00, 8:00-10:00, 10:00-12:00, 12:00-14:00, 14:00-16:00, 16:00-18:00, 18:00-24:00). Individual transition matrixes are created and maintained for each of the eight time slots [5]. This approach will cause more realistic mobility prediction, but on the other hand it increases the storage space that is needed for storing the movement probabilities.

III. Weekly Prediction based Bandwidth Reservation Scheme

In this section, proposed radio resource management scheme would be introduced. When MS *i* moves into the coverage of cell *c* in time slot *t* of day *d* and there is an ongoing call, a hand over request will be sent to call admission control module of cell *c*. Then call admission control module gets the available radio resources from radio resource management module. If there was not enough resource, the call request will be rejected. If there was enough resource, call admission control module will allocate the resources to MS *i*. Subsequently call admission control module will get the potential next cell from prediction module and will send a bandwidth reservation request to the resource reservation module of potential next cell, and then resource reservation module reserves requested bandwidth if possible. The structure of proposed radio resource management scheme has been depicted in Figure 2.

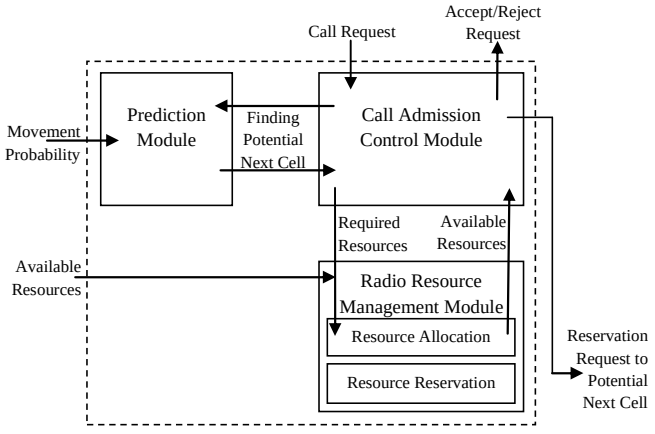

Figure 2. The structure of proposed radio resource management scheme

In Table I, the main steps of the call admission control module are described using pseudo code. In the rest of this section, the structure and the action of prediction module would be introduced.

TABLE I. Pseudo Code Describing The Call Admission Control Module

```
//method gets MS id,i , and required radio resource, rrr, as input
arr = available radio resource from radio resource management module
if(rrr<arr)
    accept the request
    nCell = get the potential next cell from prediction module
    send reservation request to nCell
else
    reject the request
```

A. Weekly Behavior Similarity

In [6], authors have tried to expand the comprehending of pragmatic user behavior in macrocellular wireless networks, utilizing real time traces. The traces have obtained through the reality mining project [7]. We use their traces in this paper too. In [6], the parameter pr_1 defined as in (2):

$$pr_1 = \frac{Number\ of\ newly\ visited\ cells}{Total\ visits}. \quad (2)$$

The ratio pr_1 indicates that to what extent the user mobility behavior is predictable. The swing in value pr_1 from the day i to the day i+7 of each week is seen to follow a periodic pattern. Comparable weekly patterns suggest repetitive patterns in user movements. It seems that mobility pattern of MSs is repetitive with a period equal to a week.

Now, we introduce another parameter to indicate to what extent the user mobility behavior is similar to its mobility behavior in the previous days. Behavior similarity of MS *i* in the day *n* to its behavior in the day *n-j* that indicated by $S_i(n, n-j)$ defined as in (4):

$$N_i(c_k, n) = \text{Number of times that MS } i \text{ visits cell } k \text{ in day } n. \quad (3)$$

$$S_i(n, n-j) = \frac{\sum_{for\ all\ k} min(N_i(c_k,n), N_i(c_k,n-j))}{\sum_{for\ all\ k} N_i(c_k,n)}. \quad (4)$$

Also, behavior similarity of all MSs in the day *n* to their behaviors in the day *n-j* that indicated by $\bar{S}(n, n-j)$ defined as mean of similarity ratios of all the MSs in the network as in (5):

$$\bar{S}(n, n-j) = \frac{\sum_{for\ all\ i} S_i(n,n-j)}{number\ of\ MSs}. \quad (5)$$

A plot of $\bar{S}(28,28-j)$ for $0 \leq j < 28$ is given in Figure 3. It is obvious that $S_i(n,n)$=1 and so $\bar{S}(n,n)$=1.

$\bar{S}(n, n-j)$ could be used as a parameter to indicate that to what extent the mobility behavior in the network is similar to the previous days. Figure 3 illustrates that in the macrocellular wireless networks, the mobility behavior in the day *i* is similar to the mobility behavior in the day *i-7*. Therefore, it seems that

mobility prediction based on weekly observations is more pragmatic than mobility prediction based on daily observations.

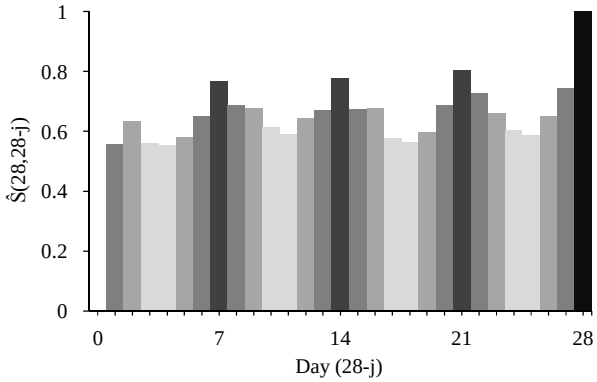

Figure 3. Behavior similarity of MSs in day 28 to their behavior in the previous days

Similarity ratio could be defined for time slots either. Assume $N_i(c_k, n, t)$ indicates the number of times that MS i visits cell k in time slot t of day n. Behavior similarity of MS *i* in the time slot *t* of day *n*, to its behavior in the time slot *t'* of day *n-j* that indicated by $TS_i(n, t; n-j, t')$ defined as in (6):

$$TS_i(n,t;n-j,t') = \frac{\sum_{for\ all\ k} min(N_i(c_k,n,t), N_i(c_k,n-j,t'))}{\sum_{for\ all\ k} N_i(c_k,n,t)}. \quad (6)$$

Behavior similarity of all MSs in the time slot *t* of day *n* to their behaviors in the time slot *t'* of day *n-j* that indicated by $\overline{TS}(n,t;n-j,t')$ defined as mean of similarity ratios of all the MSs in the network as in (7):

$$\overline{TS}(n,t;\ n-j,t') = \frac{\sum_{for\ all\ i} TS_i(n,t;n-j,t')}{number\ of\ MSs}. \quad (7)$$

A plot of $\overline{TS}(28,10;28-j,t')$ for *14≤ j<28* and *0≤t'≤10* is given in Figure 4. It is obvious that $TS_i(n,t;n,t)=1$ and so $\overline{TS}(n,t;n,t)=1$.

The time slot similarity ratio, $\overline{TS}(n,t;n-j,t')$, could be used as a parameter to indicate that to what extent the mobility behavior in the network is similar to the previous time slots. Figure 4 illustrates that in the macrocellular wireless networks, the mobility behavior in the time slot *t* of day *d* is similar to the mobility behavior in the time slot *t* of day *d-(x*7)* that *x* ϵ {1, 2, 3, …}.

B. Weekly Prediction

And now, we introduce our weekly predictive bandwidth reservation strategy. In order to predict movement of each MS, the week is divided into 56 fixed time slots (each day is divided into eight time slots as explained in [5]). Individual transition matrixes are created and maintained for each of the 56 time slots during the week. For MS *i* the probability of moving to cell *c* in time slot *t* of the day *d* indicated by $p_i(c,t,d)$ which obtained through the frequency of hand offs to cell *c* during time slot *t* of day *d*. Movement probabilities will be updated using (8) at the end of each time slot. The transition matrix for MS *i* in time slot *t* of day *d* indicated by $M(i,t,d)$.

$$P_i(c,t,d) = w \times P_i(c,t,d) + (1-w) \times newProb(c). \quad (8)$$

When MS *i* moves into the coverage of new cell in time slot *t* of day *d* and there is an ongoing call, *prediction module* of the cell detects the corresponding transition matrix and then, searches the matrix for maximum transition probability

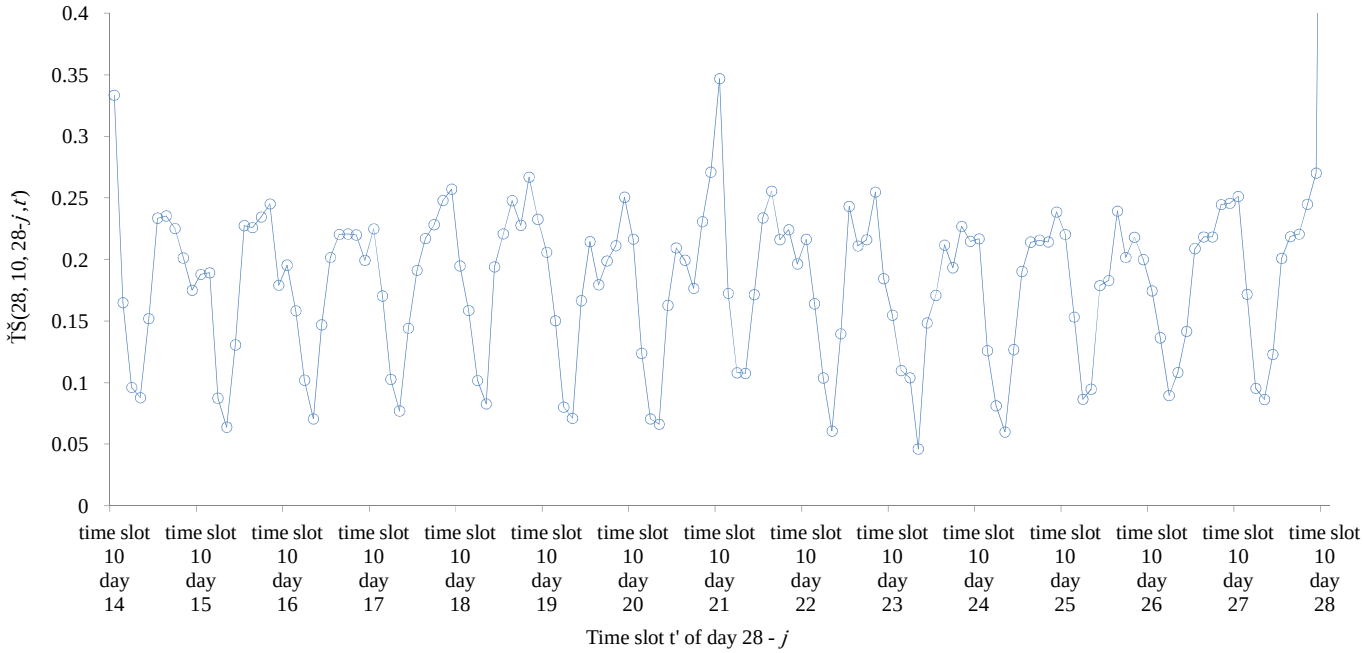

Figure 4. Behavior similarity of MSs in time slot 10 of day 28 to their behavior in the previous time slots

(p_i^{max}).

$$p_i^{max} = max_{for\ each\ adjacent\ cell\ c}\{p_i(c,t,d)\}. \quad (9)$$

As it mentioned, time slots are fixed and the MS behavior fluctuates from day to day. Hence a movement might be captured in the adjacent time slots which may result in incorrect predictions. It is difficult to use variable time slots and this problem will not be solved even if variable time slots be used.

In order to overcome this problem, the prediction could be made with the aid of transition matrix of the adjacent time slots. The mobility behavior of MSs in time slot *t* of day d is moderately similar to their mobility behavior in time slot *t-1*and *t+1*of day d of the previous weeks as it could be seen in Figure 4. Thus, in order to resolve the problem of MS's behavior fluctuation, prediction module could make predictions based on the transition matrixes $M(i,t-1,d)$, $M(i,t,d)$ and$M(i,t+1,d)$.

If p_i^{max} was greater than or equal to a minimum threshold p_{min}, the bandwidth reservation request will be sent to the cell that maximizes (9). Otherwise, if $p_i^{max}$was less than p_{min}, the prediction will be made based on $\bar{p}_i^{max}$ that obtained from (10). In the other word, if p_i^{max} was less than p_{min}, the bandwidth reservation request will be sent to the cell that maximizes (10).

$$\bar{p}_i^{max} = \max_{for\ each\ adjacent\ cell\ c}\{q \times p_i(c,t,d) +$$

$$\frac{1-q}{2} \times p_i(c,t-1,d) + \frac{1-q}{2} \times p_i(c,t+1,d)\}. \quad (10)$$

The algorithm effectiveness affected by choosing appropriate value for p_{min}. Choosing a high value for p_{min} results in smoothed prediction, but also, increases the number of accesses to the transition matrixes from 1 to 3. For each adjacent cell *c*, the probability $p_i(c,t,d)$ will be equal to 0, and so, p_i^{max} will be equal to 0 until the first movement is captured in the time slot *t* in the day *d*. After capturing the first movement in the time slot *t* of day *d*, $\sum_{\forall c} p_i(c,t,d)$ will be equal to 1. Hence, if the number of adjacent cells is *n*, the minimum value for p_i^{max} will be $1/\eta$. Thus, p_{min} should be greater than or equal to $1/\eta$.Assuming the number of adjacent cells to be 6, p_{min} should be greater than or equal to $0.1\overline{6}$. The value of p_{min} was chosen to be 0.2 to make more accurate predictions.

The weighting factor q in (10) indicates that to what extent $\bar{p}_i^{max}$is affected by adjacent time slots. If any movement still not captured, q should be equal to 0 in that time slot. Otherwise, it should be greater than 0. So, q obtained from (11):

$$q = q' \times \sum_{foreachadjacentcellc} p_i(c,t,d). \quad (11)$$

It seems that q' should be greater than or equal to $0.\overline{3}$. If q' was less than $0.\overline{3}$, the current time slot movement probabilities is less effective than adjacent time slot movement probabilities in calculating $\bar{p}_i^{max}$, and it does not makes sense. The value of q' must be proportionate to behavior similarity of MSs to their behavior in time slots *t*, *t-1* and *t+1*. Thus, there is a direct correlation between q' and time slot similarity ratio ($\overline{TS}$). The parameter q' could be obtained from (13) for each time slot *t*.

$$q'_{(j)} = \frac{\overline{TS}(n,t;n-(j\times 7),t)}{\overline{TS}(n,t;n-(j\times 7),t-1)+\overline{TS}(n,t;n-(j\times 7),t)+\overline{TS}(n,t;n-(j\times 7),t+1)}. \quad (12)$$

$$q' = \frac{\sum_{j=1}^{[n/7]}(q'_{(j)})}{[n/7]}. \quad (13)$$

In (12) the parameter $\overline{TS}$ is the time slot similarity ratio and $q'_{(j)}$ indicates the correlation of mobility behavior in time slot *t* to mobility behavior in time slot *t* of *j* weeks ago.q' obtained from averaging out the values of $q'_{(j)}$ for j={1, 2, …, $[n/7]$}. The parameter q' could be obtained at the beginning of each time slot or could be obtained for all time slots after an initial period (about a month). Based on reality mining traces that used in this article, the value of q' was chosen to be between 0.4 and 0.5 to make more accurate predictions.

TABLE II. PSEUDO CODE DESCRIBING THE PREDICTION MODULE

```
//method gets i, t and d as input
p_min = 0.2
σ = 0
p_i^max = 0
c_i^max = null
while(there is another adjacent cell)
    c = next adjacent cell
    σ += p_i(c,t,d)
    if(p_i(c,t,d)>p_i^max)
        p_i^max = p_i(c,t,d)
        c_i^max = c
if(p_i^max>p_min)
    return c_i^max
else
    p̄_i^max = 0, q = 0.5*σ
    while(there is another adjacent cell)
        c = next adjacent cell
        p = q × p_i(c,t,d) + ((1-q)/2)(p_i(c,t-1,d) + p_i(c,t+1,d))
        if(p>p̄_i^max)
            p̄_i^max = p
            c_i^max = c
if(p̄_i^max= =0)
    σ← = 0
    p←_i^max = 0
    while(there is another adjacent cell)
        c = next adjacent cell
        σ← += p_i(c,t,d-1)
        if(p_i(c,t,d)>p←_i^max)
            p←_i^max = p_i(c,t,d-1)
            c_i^max = c
return c_i^max
```

When a BS attaches to the cellular network, it has no background information about the mobility patterns. Hence any prediction and reservation will not be made in the initial period. The mobility pattern of MSs in day d, is moderately similar to the mobility pattern in day $d-1$ and day $d+1$ of the previous weeks as it could be seen in Figure 3. So, in order to improve prediction in the initial period, prediction module could make prediction based on the transition matrix for the MS in time slot t of day $d-1$, $M(i,t,d-1)$.

The prediction module of each cell gets i, t and d as inputs that indicate the MS id, the time slot and the day of week respectively. At the end, prediction module returns the potential next cell that MS i may visit, and subsequently bandwidth will be reserved in the predicted cell. In Table II, the main steps of the prediction module are described using pseudo code.

C. Storing Movement Probabilities

Weekly prediction needs to store and update transition matrixes weekly that require more storage space. In weekly prediction, for each MS, there are 56 time slots whereas in daily prediction 8 time slots should be traced for each MS. It seems that required storage space for weekly prediction is 7 times the required storage space for daily prediction. However, in practice, some time slots will never capture any movements. Simulation results show that in actual traces, required storage space for weekly prediction is 3 to 4 times the required storage space for daily prediction. This ratio could be decreased to 2.5 using dynamic hashing approach. Decreasing the required storage space in macrocellular wireless networks is crucial due to existence of a large number of MSs.

In order to storing movement probabilities, hashing has been suggested in [3]. The hash function maps MS id into the stored probabilities. When an MS, for the first time, moves into the coverage of new cell, all the space that is needed for movement probabilities will be allocated to it. However, as it mentioned, some of the time slots will never capture any probabilities. In this work, a dynamic hashing approach has been introduced to allocate just the required storage space to an MS.

Dynamic hashing promises the flexibility of needed storage space while preserving the fast access times expected from hashing [8]. Dynamic hashing is a type of hashing which treats a hash as a bit string. The hash function $h(k)$ returns a unique binary number that its first b bits will be used to figure out where they will go in the hash table. Additionally, b is the smallest number such that the first b bits could be the same for utmost b_{max} keys, that b_{max} is the bucket size.

In this article, in order to simplify hashing, the binary format of keys is used as the bit string. The transition matrix of MS i in time slot t of day d indicated by $M(i,t,d)$. So the key may consist of 3 fields, MS id, time slot and the day. Now the question is, how first b bits should be structured and what fields must first b bits consist of?

The plot of time slot similarity that had been depicted in Figure 4 has been shown again for the last week in Figure 5. In this sample, similarity of last week time slots to the reference point, time slot 10 of day 28, has been depicted. Square shape data points indicate the most similar time slots of the most dissimilar days to the reference point time slot in the last week. As it mentioned, the most similar time slot in previous days to a reference point time slot is the same time slot in previous days. Triangle shape data point indicates the most dissimilar time slot of the most similar day to the reference point time slot in the last week. As it mentioned, the most similar day in

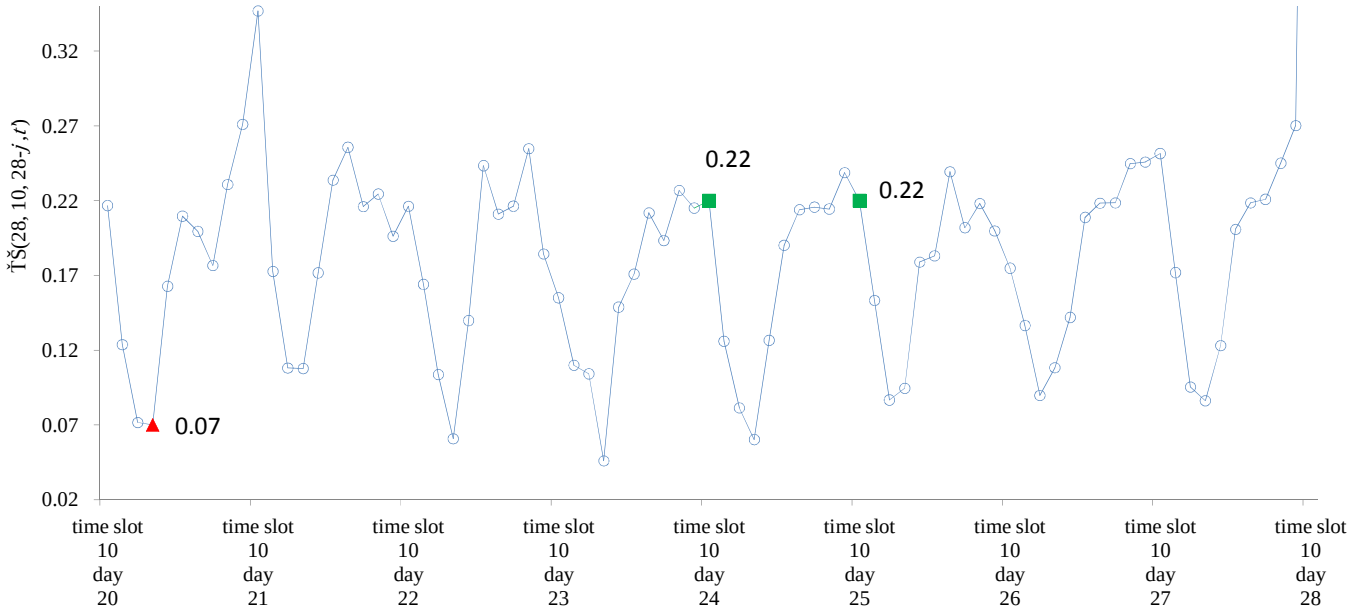

Figure 5. Behavior similarity of MSs in time slot 10 of day 28 to their behavior in the last week time slots

previous weeks to a reference point day is the same day in previous weeks. As it could be seen in Figure 5, square shape data points are more similar to the reference point time slot than triangle shape data point. In the other word, mobility behavior of MSs in different time slots of a day varies more than mobility behavior of MSs in the same time slots of different days. Thus, the number of new entries that captured in different time slots is more than new entries that captured in different days. Hence hash could be structured as following:

1) First *b* bits could consist of MS id, *i*.
2) First *b* bits could consist of some of the most significant bits of time slot, *t*.
3) If first *b* bits were same for more than b_{max} keys, first *b* bits shall extend. The extension shall done to the remaining bits of time slot and then encompass the day bits, *d*.

At first, the set of *i* and 2 most significant bits of *t* could be used in construction of the hash table. For example, the entry $M(6,5,3)$ will go into the index 11010 of hash table. In some cells, this set could be adequate to construct the hash table. If there was an entry that causes the bucket size exceeds b_{max}, the hash table size will be doubled.

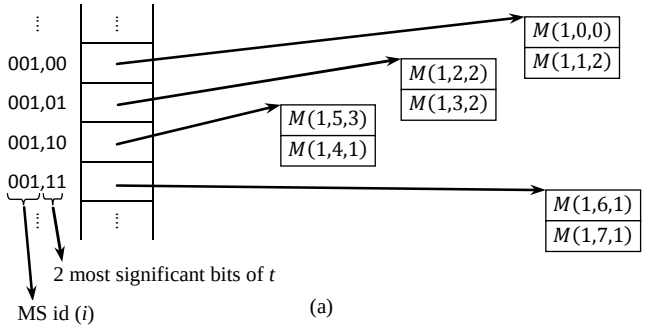

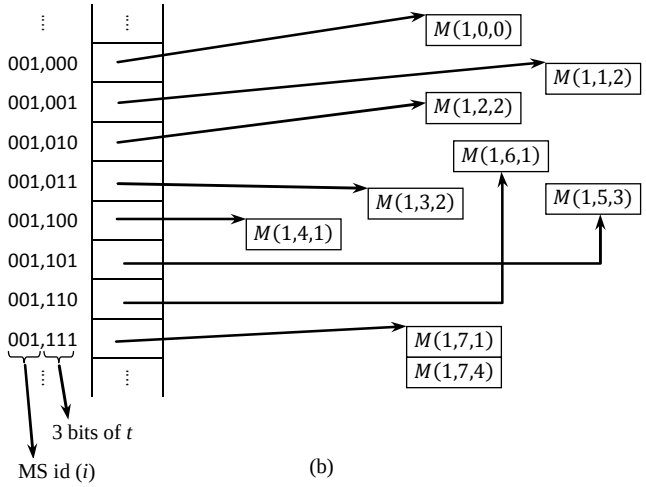

Figure 6. An example of adopted dynamic hashing approach, (a) before entering $\mathbf{M(1,7,4)}$, (b) after entering $\mathbf{M(1,7,4)}$

An example of dynamic hashing approach has been depicted in Figure 6. It has been assumed that for this particular example, the bucket size is 2. Before entering $M(1,7,4)$, the set of *i* and 2 most significant bits of *t* is adequate to construct the hash table as it has been shown in Figure 6(a). In order to enter $M(1,7,4)$, the hash table should be doubled as in Figure 6(b). Likewise, other bits of the key could be included in the set and the hash table size could increase.

Simulation results show that for the majority of cells, the undesirable increase in the hash table size will persist to a certain extent, and the dynamic hashing approach moderately overcomes the overhead of storage space. Moreover, dynamic hashing causes storage space to increase imperceptibly. Also it is possible to decrease the storage space by deleting transition matrixes that will not be used any more. However, opportunity to decrease storage space is not investigated here.

IV. Simulation And Results

In order to evaluate the performance of proposed weekly-prediction-based bandwidth reservation (WPBR) strategy, the daily prediction based bandwidth reservation (DPBR) scheme has been implemented and simulated for comparison. The algorithms of daily prediction that described in section II and weekly prediction that described in section III have been implemented using Java.

A. Simulation Model

The data set that have been used in this study, developed by researchers at MIT Media Laboratory, and came from Nokia 6600 phones programmed to automatically run the ContextLog application as a background process at all times [7]. These real time mobility traces have been mapped into a macrocellular network with 25 hexagonal cells that each cell has 6 adjacent cells. Table III summarizes the various simulation parameters whose values were empirically chosen to represent the most realistic scenario for the simulation. Each simulation was carried out for 28 days of real time traces in the macrocellular network. It is assumed that the arrival rate of new calls is a Poisson distribution with a mean arrival value of 0.5.

TABLE III. Simulation Parameters

Parameter	Value	Description of parameter
N_C	25	Number of cells simulated
N_{ms} [a]	95	Number of mobile stations in system
B_c	30Mbps	Maximum bandwidth capacity of a cell
B_{req}	3Mbps	Average bandwidth requirement for a call
$\bar{C}_r$	0.5req/s	Average connection arrival rate
$\bar{C}_d$	235 s	Average call duration
w	0.5	The weighting factor that used in (1)
q	0.5	The weighting factor that used in (8)
p_{min}	0.2	The threshold that indicates which time slots should participate in prediction

a. This number came from number of MSs that have been traced in reality mining project [7]

B. Experimental Results

Figure 7 compares the bandwidth utilization of the WPBR strategy with the DPBR scheme for 28 days of simulation and average connection arrival rate 0.5. There is no background information about the mobility patterns in the first day, hence no prediction will made and bandwidth utilization values are high for both schemes. As time passed, mobility information is gradually gathered. Prediction and the respective bandwidth reservation will cause bandwidth utilization value to decrease. For the DPBR scheme, bandwidth utilization values decrease to an extent and after that leveled off at about 0.4. The subsequent negligible fluctuation in the bandwidth utilization values of the DPBR scheme has arisen from alteration in the behavior of MSs. For the WPBR scheme, bandwidth utilization values decrease for an initial period (about a week) and then increase with improvement in the prediction. The accurate and sparing prediction caused the WPBR scheme to gain higher bandwidth utilization.

Figure 8 compares the new call blocking probability of the WPBR strategy with the DPBR scheme for average connection arrival rate 0.5. March of progress in CBP is similar to what expressed about bandwidth utilization before. For the WPBR scheme, CBP increases for an initial period (about a week) and then decreases with improvement in the prediction and cause the WPBR scheme to gain lower CBP.

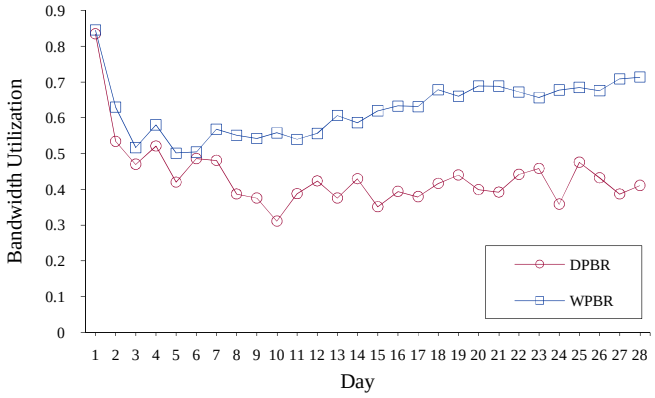

Figure 7. Comparison of bandwidth utilization by the two schemes for average connection arrival rate 0.5

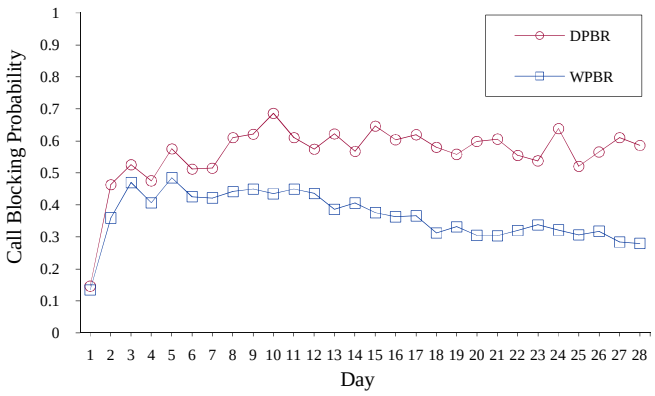

Figure 8. Comparison of new call blocking probability by the two schemes for average connection arrival rate 0.5

Figure 9 compares the hand off call dropping probability of the WPBR strategy with the DPBR scheme for average connection arrival rate 0.5. For the DPBR scheme, CDP decrease to an extent and after that leveled off at about 0.15×10^{-2}. For the WPBR scheme, decrease in CDP for an initial period is less than decrease in CDP for the DPBR. The trend line of the WPBR scheme shows that CDP is dwindling by the time. . As the WPBR scheme distinguishes between days of the week, its CDP fluctuates in the course of a week. The weekly fluctuation in the CDP of the WPBR scheme shows that the behavior of MSs is more predictable in some days of the week. For example the MS behavior on workdays could be more predictable than weekends.

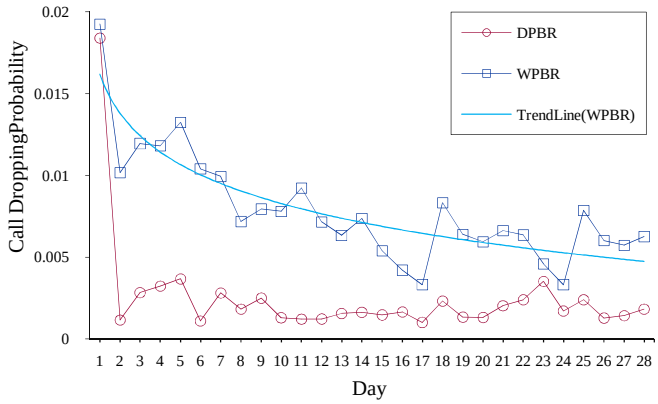

Figure 9.Comparison of hand off call dropping probability by the two schemes for average connection arrival rate 0.5

From the MS's point of view, the objective is to minimize CBP and specially CDP in order to improve the performance of the network. Another objective, from the service provider's perspective is to decrease the cost by increasing BWU of the network. In order to make a fair balance between both user satisfaction and service provider satisfaction, one should consider the cost/performance ratio (Z) which is defined in [9] as (14) where *r* is the penalty factor used to reflect the effect of the hand off dropping over the new call blocking. A penalty of 5–20 times is commonly recommended [9].The design goals of a call admission control scheme are increasing the performance and decreasing the cost, which means minimizing Z.

$$Z = \frac{cost}{performance} = \frac{r \times CDP + CBP}{BWU}. \quad (14)$$

Figure 10 depicts Z versus *r* on the day 28 of simulation. It shows that the proposed WPBR scheme, for penalty of 5–20 times, has a lower Z value than DPBR scheme.

Figure 11 compares the required storage space of the WPBR strategy with the DPBR scheme for 28 days of simulation. It seemed that required storage space for the WPBR was 7 times the required storage space for the DPBR. But simulation results show that in actual traces, required storage space for the WPBR is approximately 2.5 times the required storage space

for the DPBR. So, the adopted dynamic hashing approach moderately obviates the overhead of storage space.

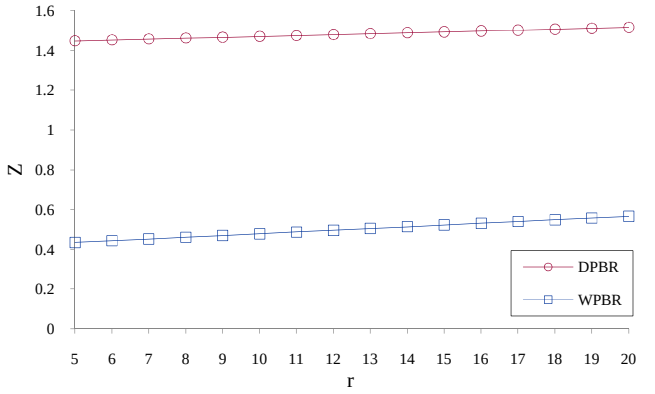

Figure 10. Z versus r on the day 28 of simulation

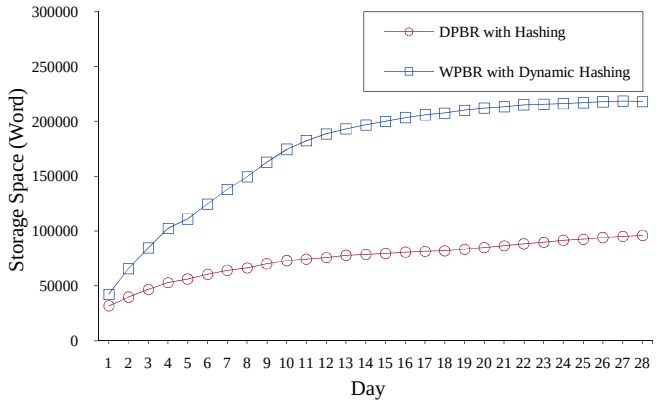

Figure 11. Comparison of used storage space by the two schemes

V. Conclusions

A weekly predictive mobile-oriented bandwidth reservation strategy has been proposed that improves prediction by weekly storing movement probabilities based on Markov modeling techniques. And also, a dynamic hashing approach has been adopted to decrease the required storage space. Simulation results show that the weekly prediction in this novel strategy significantly improves bandwidth utilization, and the adopted dynamic hashing approach moderately overcomes the overhead of storage space.

Unfortunately, the cell residence time of mobile stations is not included in the bandwidth reservation strategy. When a mobile station moves into the coverage of new cell and there is an ongoing call, bandwidth will be reserved in the potential next cell and the cell residence time of the mobile station has not been taken into account. This topic is an interesting area for further researches.

Acknowledgment

This work was supported by Iran Telecommunication Research Center (ITRC). The authors would like to thank the anonymous reviewers and the associate editor for their valuable comments and time spent in handling this paper. And also we would like to express our gratitude to Xalid Barmasida for his care in helping with English editing of the manuscript.

References

[1] V. Abdulova and I. Aybay, “Predictive mobile-oriented channel reservation schemes in wireless cellular networks,”*Wireless Networks*, vol. 17, pp.149-166, 2011.

[2] P. Prabhakaran and R. Sankar, “Impact of Realistic Mobility Models on Wireless Networks Performance,”*in Proceedings ofIEEE International Conference on Wireless and Mobile Computing, Networking and Communications (WiMob)*, pp. 329-334, 2006.

[3] J. Cowling, “Dynamic Location Management in Heterogeneous Cellular Networks,”*Bachelor Thesis*, University of Sydney, Australia, 2004.

[4] S. Rashad, M. Kantardzic, and A. Kumar, "User mobility oriented predictive call admission control and resource reservation for next-generation mobile networks," Journal of Parallel and Distributed Computing, Elsevier, vol. 66, pp. 971-988, 2006.

[5] R.V. Mathivaruni and V.Vaidehi, “An activity based mobility prediction strategy using markov modeling for wireless networks,”*in Proceedings of the World Congress on Engineering and Computer Science (WCECS)*, San Francisco, USA, 2008.

[6] M. S. Sricharan and V. Vaidehi, “A pragmatic analysis of user mobility patterns in macrocellular wireless networks,”*Pervasive and Mobile Computing*, vol. 4, pp. 616-632, 2008.

[7] N. Eagle, A. Pentland, and D. Lazer,“Inferring Social Network Structure using Mobile Phone Data,”*in Proceedings of the National Academy of Sciences (PNAS)*, Vol 106 (36), pp.15274-15278, 2009.

[8] R. J. Enbody and H. C. Du, “Dynamic Hashing Schemes,”*ACM Computing Surveys (CSUR)*, vol. 20, pp. 850-113, 1988.

[9] I. Candan, M. Salamah, "Analytical modeling of a time-threshold based bandwidth allocation scheme for cellular networks,"*Computer Communications*, vol. 30, pp.1036-1043, 2007.

Adel Amani received his BS degree from Kordestan University and Allame Rafiee University in 2008 in Computer Engineering. He received his MS degree from Amirkabir University of Technology in 2012 in Information Technology. His research interests include computer networks, distributed systems, wireless cellular networks, mobility prediction in mobile networks, multimedia networks, and wireless sensor networks.

Hossein Pedram received his BS degree from Sharif University in 1977 and an MS degree from Ohio State University in 1980, both in Electrical Engineering. He received his PhD degree from Washington State University in 1992 in Computer Engineering. He has served as a faculty member in the Computer Engineering Department of Amirkabir University of Technology since 1992. He teaches courses in Computer architecture and distributed systems. His research interests include innovative methods in computer architecture such as asynchronous circuits, management of computer networks, distributed systems, and robotics.

Online Adaptive Fuzzy Logic Controller Using Genetic Algorithm and Neural Network for Networked Control Systems

Pooya Hajebi*, Seyed Mohammad Taghi AlModarresi*

*Department of Electrical and Computer Engineering, Yazd University, Yazd, Iran

Hajebi@stu.yazd.ac.ir, smta@yazd.ac.ir

***Abstract*—Networked Control Systems are used for controlling remote plants via shared data communication networks such as Ethernet. These systems have found many applications in industrial, medical and space sciences fields. However there are some drawbacks in these systems, which make them challenging to design. One of the most common problems in these systems is the stochastic time delay. Packet switching in internet brings about the randomly varying time delay and consequently makes these systems instable. Convenient controllers such as PID and PI type controllers which are just matched with a constant time delay could not be a solution for these systems. Fuzzy logic controllers due to their nonlinear characteristic which is compatible with these systems are potentially a wise option for their control purpose. Fuzzy logic controller could become adaptive by means of neural networks and beneficial to deal with the varying time delay problem. Further, they do have more capabilities to tackle packet dropouts and dynamically system variables. This paper introduces a novel control method which addresses the varying time delay problem effectively. This novel method suggests an online adaptive fuzzy logic controller which has been controlled and adapted through the neural network. This method takes the advantage of the genetic algorithm to optimize the membership functions for its fuzzy logic controller. This designed controller is applied to an AC 400 W servo motor as a remote plant in order to control its position via Ethernet. The measurement of round-trip time (RTT) is used to estimate the online time delay as a parameter in online adaptive fuzzy logic controller. The rule-based table of designed fuzzy logic controller rotates in relation to this estimated time delay. The value of rotating is obtained from a trained neural network. Comparison of simulation results for different controllers indicates that this novel designed controller provides a better performance over the varying time delay. The proposed method follows the input easily, despite classical methods which result in an unstable system especially over the large time delays as large as 600 ms. Results get even more improved when genetic algorithm is applied to fuzzy logic controller.**

***Index Terms*—Data Communication Networks, Genetic Algorithm, Networked Control Systems, Neural Networks, Online Adaptive Optimized Fuzzy Logic Controller, Rules-Table Rotation.**

Manuscript received June 29, 2012. This work was supported in part by the ICT Research Institute (ITRC), Iran, under Grant T-500-12192.

P. Hajebi is with the Department of Electrical and Computer Engineering, Yazd University, Yazd, Iran (phone: +98-351-8122377; fax: +98-351-8200144; e-mail: Hajebi@stu.yazd.ac.ir).

S.M.T. AlModarresi is with the Department of Electrical and Computer Engineering, Yazd University, Yazd, Iran (e-mail: smta@yazd.ac.ir).

I. Introduction

NETWORKED control systems (NCSs) are spatially distributed systems in which the communication between sensors, actuators and controllers occurs through a shared band-limited digital communication network [1], [2]. This multipurpose shared network connecting, spatially distributed elements, creates a flexible architecture which generally reduces installation and maintenance costs. NCSs have been finding application in a broad range of areas such as mobile sensor networks [3], remote surgery [4], haptics collaboration over the Internet [5]–[7], and automated highway systems and unmanned aerial vehicles [8], [9]. Murry et al. in [10] have identified control over networks as one of the key future directions for control. However, application of a shared network versus several dedicated independent connections, introduces new challenges. Drops and variable delays in NCSs are two major problematic issues that were addressed in [11], [12]. Packet dropouts and finite level quantization make NCSs unstable [12]. When the delay time is less than the sampling time of NCSs, results show that the time delay has insignificant effect on control system. However, delay time greater than the sampling time degrade the performance of the NCSs [13]. Many controllers such as conventional PID and fuzzy logic controllers are utilized to stabilize the NCS closed loop feedback and to reduce the error. Classical Smith predictor is one of the controllers which are efficient for time delay processes [13], [14]. Lai and Hsu proposed an adaptive Smith predictor as a controller for NCS in [14]. Despite showing relatively a good performance, there are some drawbacks in these controllers. For instance, the accuracy of the model depends on plant transfer function estimation. Moreover, each new plant requires changing the controller design. Practically estimation of plant transfer function is not exact. Recently Pan et al. in [15] and Zhao et al. in [16] have shown that fuzzy logic controllers offer a better performance in tackling packet dropouts and varying time delay, at the same time are more compatible with nonlinear processes. W. Du and F. Du proposed a Smith predictor integrated with fuzzy adaptive PID

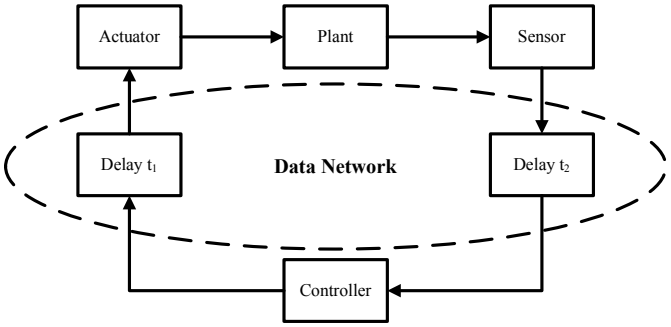

Fig. 1. A SISO networked control system structure.

controller for the NCSs in [17]. However they did not measure the network delay online. They applied fuzzy logic controller for tuning the coefficients of PID controller. This paper first, suggests a fuzzy logic controller (without PID controller) to control the position of an AC 400 W servo motor via Ethernet. At the next step, it proposes a novel control method which is an online adaptive fuzzy logic controller for the similar application. This research provides the advantages of no PID controllers application while offers an adaptive controller which its fuzzy logic rules are rotating during the plant control. The round-trip time (RTT) is measured online and this value is utilized as, t_m, time delay parameter. Then, this time delay value is mapped to an angle by means of trained neural network. This neural network has been already trained by different time delays in adaptive fuzzy logic controller. Results verify the better performance of this novel design which its fuzzy logic controller rules-table rotates through a trained neural network. The fact is that in communication networks time delay could exceed 200 ms (vs. 400 ms, 600 ms). However, results from [17], [18] show that the response would be degraded in these systems for time delays over 200 ms despite the application of designed offline controllers. This paper's proposed method has shown an improved response especially in the case of time delays over 200 ms. Even with time delay of 600 ms, there is no degradation in step response. Genetic algorithm could be implied in order to optimize a suitable objective function for tuning the fuzzy logic controller membership functions. The results indicate that this optimized controller shows better performance in comparison with a non-optimized fuzzy logic controller.

This paper includes the following sections; In Section II, NCSs, stochastic time delay and packet dropouts are introduced. Section III, first describes, designing a fuzzy logic controller in order to control the position of an AC 400 W servo motor and next introduces a novel adaptive fuzzy logic controller with a rotating rules-table by means of trained neural network. Section IV introduces the genetic algorithm and describes its application in optimization of membership functions of the designed fuzzy controller. Section V contains the related simulations and equations. This paper ends with conclusion in section VI.

II. Networked Control Systems

Due to quantum leaps in communication systems, in recent years, it has become more common to apply a shared

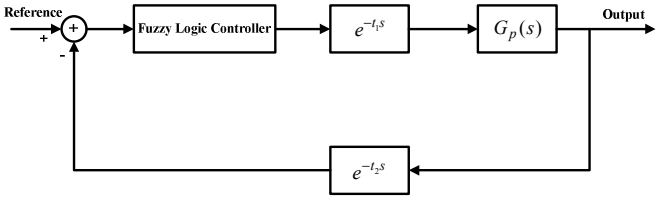

Fig. 2. Fuzzy logic controller.

communication channel such as Ethernet or Controller Area Network (CAN) bus etc. for transmission of the control signal and the measured output. This method helps reducing the wiring costs as well as eliminates the necessity for maintaining dedicated communication channels for each control parameter [15]. However, this type of networked control system is not a perfect solution and own its various unsolved issues such as transmission delays and packet dropouts [12], [15] which can degrade control performance. The SISO (single input-single output) NCS structure in the closed loop model is shown in Fig. 1. As illustrated in this figure, t_1 and t_2 indicate, time-delays induced in the network structure for the controller-to-actuator direction and the sensor-to-controller direction, respectively. Basically, the induced network delay varies according to the network load, scheduling policies, number of nodes, and different protocols. Time-varying characteristic of these NCSs makes the design and modeling of them more complicated. The total time-delay can be categorized into three classes, based on the parts where they occur, namely, the server node, the network channel, and the client node [19]. In addition, the round-trip time (RTT) measurement is crucial as it provides of accurate delay measurements periodically [19]–[21]. RTT is defined as the total time delay in SISO NCSs. Obviously the longer distances increase, the time delay of a network since more nodes are involved and consequently results in a larger RTT. In a classical Smith predictor design, the value of t_m is constant and usually equals to average approximation of time delay between two nodes in the network. The value of RTT could be applied to fuzzy logic controller for compensating of variable delay. Normally in a fuzzy logic controller, rule-based table is constant during the control process action. In this paper's suggested method, RTT applied by neural network mapping, generates a rotating rules-table.

III. Fuzzy Logic Controller Using Rules-Table Rotation

As it has been already mentioned, an online adaptive fuzzy logic controller could be a solution for tackling the stochastic time delay problem in NCSs. However it controls with simple PID or PI controllers which shows limited potentials, especially in nonlinearity processes. Recently it is proved that fuzzy logic controller is the best option for controlling nonlinear processes while make the system more robust against the varying time delay [15], [16]. In the following parts, first a fuzzy logic controller is designed then a classical Smith predictor would be integrated with this designed fuzzy logic controller based on our plant. Finally a novel rotating rules-table online adaptive fuzzy logic controller is described.

A. Designing Fuzzy Logic Controller

To implement a NCS controller, first the output of plant is measured and then it would be compared with a reference signal. This comparison generates the error signal. The error signal and its derivative are both inputs for the fuzzy logic controller shown in Fig. 2. Here in this paper, the plant is an AC 400 W servo motor which its position as an output is measured with an encoder with gain 10^4 P/R. The coefficients of the equivalent PI controller for this plant are K_p=0.0001 and K_i= 0.00000001, [14]. The open loop position control is obtained from (1). Equations (2) and (3) represent the continuous-state space form of transfer function described in (1). In Fig. 3, seven triangular membership functions have been devoted to either, input (error and derivative of error) and output. In Fig. 3, the fuzzy linguistic variables ("NB", "NM", "NS", "ZE", "PS", "PM", "PB") represent (Negative Big, Negative Medium, Negative Small, Zero, Positive Small, Positive Medium and Positive Big) respectively. In position control, the output follows the input. Therefore, at first they are assumed to have similar membership functions. However in the following section, output memberships would be optimized using an objective function. Here are provided some design specifications, applied in this fuzzy logic controller: 1) The inference, used in this design is Mamdani-type [22], 2) Fuzzy logic "and operator" was implemented by "min" method while the fuzzy logic implication is based on the "min" method as well and rules are aggregated using fuzzy "max" operator, 3) The fuzzy logic output has been determined through the center of gravity method by means of defuzzification, 4) Fuzzy rules are opted based on Table I which contains 49 rules, 5) Due to

$$G_P(s) = \frac{10^4 (0.058\,s + 3.221)}{s\,(0.0001\,s^2 + 0.019\,s + 1)} \tag{1}$$

$$\dot{x} = \begin{bmatrix} -190 & -78.125 & 0 \\ 128 & 0 & 0 \\ 0 & 1 & 0 \end{bmatrix} x + \begin{bmatrix} 2048 \\ 0 \\ 0 \end{bmatrix} U \tag{2}$$

$$y = \begin{bmatrix} 0 & 22.13 & 1228.7 \end{bmatrix} x \tag{3}$$

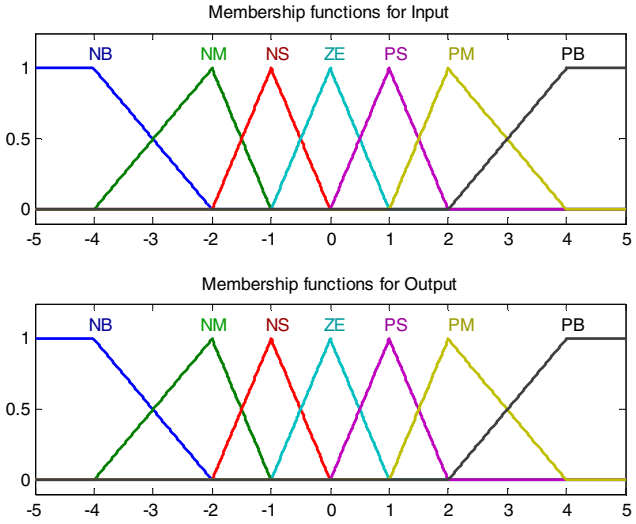

Fig. 3. Membership functions for input and output.

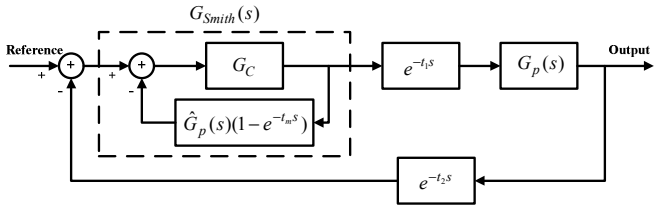

Fig. 4. A control structure of Smith predictor.

high gain of encoder the scaling factor value selected for fuzzy logic controller output is ,10^{-4}.

B. Classical Smith Predictor with Fuzzy Logic Controller

Classical Smith predictor is one of the controllers which are efficient for time delay process [13], [14]. Here a classical Smith predictor is designed for comparing the results. In this classical Smith predictor which is shown in Fig. 4, G_C is the designed fuzzy logic controller described in section III. A., G_P is the transfer function of the plant while $\hat{G}_P$ is the estimation of plant transfer function. Usually t_m is the approximation of total time delay from controller to plant and plant to controller. If t_m is the appropriate estimation of overall time delay the performance of system will be reasonable. t_m is assumed 200 ms in the simulation. $\hat{G}_P$, is the estimation of G_P, and practically difference between these two transfer functions results in instabilities and increases of the error of response. This is the main problem for classical Smith predictor and online adaptive Smith predictor. In this paper classical Smith predictor with fuzzy logic controller was assumed ideal, thus the G_P and $\hat{G}_P$ are equal in the simulations. The fuzzy rules are selected based on Table I.

C. Designing Rules-Table Rotation of Online Adaptive Fuzzy Logic Controller Using Neural Network

RTT is estimated in network [19], [20] and then this measurement would be applied to online fuzzy logic controller. In this stage the designed fuzzy logic controller in part A would be integrated with an online neural network. The measurement of round-trip time (RTT) is applied for estimating of online time delay which in turn provides the value for rotation angle of fuzzy rules-table. As already mentioned, the controller in this paper has not included any PID or PI method.

TABLE I
RULE BASE FOR ERROR, ERROR DERIVATIVE AND FLC OUTPUT (WITHOUT ROTATION).

de \ e	NB	NM	NS	ZE	PS	PM	PB
NB	NB	NB	NB	NB	NM	NS	ZE
NM	NB	NB	NB	NM	NS	ZE	PS
NS	NB	NB	NM	NS	ZE	PS	PM
ZE	NB	NM	NS	ZE	PS	PM	PB
PS	NM	NS	ZE	PS	PM	PB	PB
PM	NS	ZE	PS	PM	PB	PB	PB
PB	ZE	PS	PM	PB	PB	PB	PB

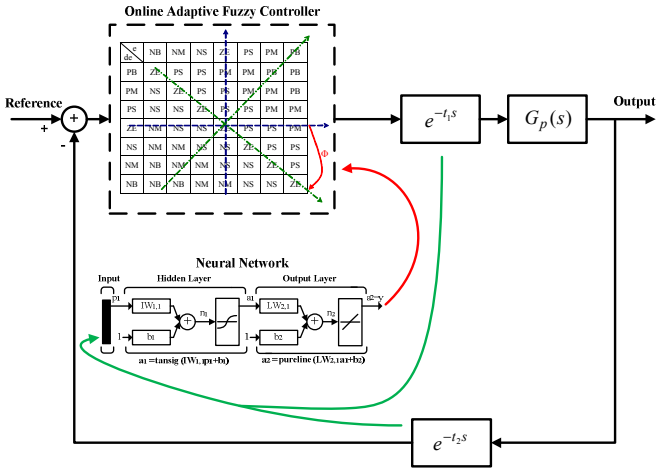

Fig. 5. Structure of online adaptive fuzzy logic controller using neural network.

The nonlinear fuzzy logic controller does have the potential to control the complicated and nonlinear processes while is more robust against the dynamically system variables specially occurs at the beginning of the process. In a control process with no delay, the error and the derivative of the error change periodically. However, these changes suggests nonlinear function pattern. During the control process and based on the taken time, the error and derivative of the error move on the fuzzy rules-table in a circular path. While delays caused the error and derivative of error do not have desired time values, application of this suggested rotation method could overcome problem of delays. Thus, this paper has suggested a control method which integrated fuzzy logic controller with a neural network. Fig. 5, shows the structure of this proposed controller. Here in this figure, the value of RTT is mapped to an angle by neural network. The structure of neural network has two-layer feedforward. First this neural network is trained by several set point time delays. It means the value of rotation for several time delays is obtained manually then these values will be applied for training the neural network.

The value of angle for rotating rules-table in online adaptive fuzzy logic controller, changes periodically based on the RTT value. Fuzzy rules are opted based on Table II, but other parameters (membership functions, fuzzy logic operators and fuzzy logic method) are similar to data in section III. A. Equation (4) shows the mapping relation of the error and variation of the error in new coordinate. Matrix A, in (5) is the rotation transform matrix which rotates coordinates by the angle

TABLE II
RULE BASE FOR ERROR, ERROR DERIVATIVE AND FLC OUTPUT (ROTATION TABLE).

de \ e	NB	NM	NS	ZE	PS	PM	PB
PB	ZE	PS	PS	PM	PM	PB	PB
PM	NS	ZE	PS	PS	PM	PM	PB
PS	NS	NS	ZE	PS	PS	PM	PM
ZE	NM	NS	NS	ZE	PS	PS	PM
NS	NM	NM	NS	NS	ZE	PS	PS
NM	NB	NM	NM	NS	NS	ZE	PS
NB	NB	NB	NM	NM	NS	NS	ZE

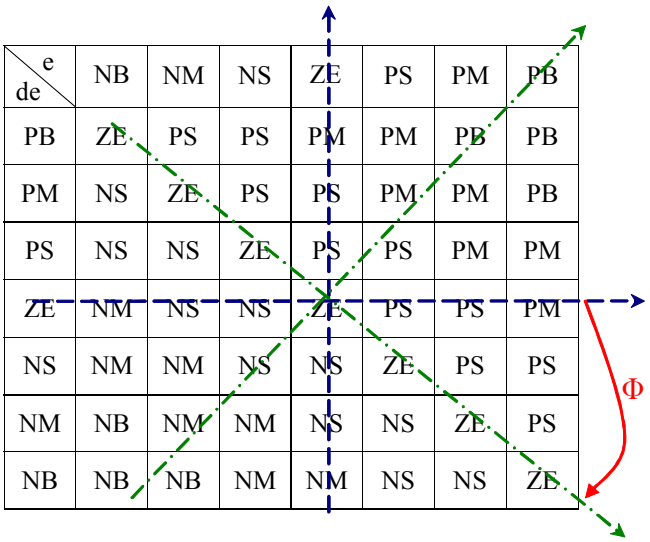

Fig. 6. Rotating of fuzzy rules-table.

of φ radian. The rules-table rotation structure of fuzzy logic controller and trend of rotation are shown in Fig. 6.

$$\begin{bmatrix} e_{new} \\ \dot{e}_{new} \end{bmatrix} = A \begin{bmatrix} e \\ \dot{e} \end{bmatrix} \tag{4}$$

$$A = \begin{bmatrix} \cos\phi & -\sin\phi \\ \sin\phi & \cos\phi \end{bmatrix} \tag{5}$$

IV. OPTIMIZATION OF FUZZY LOGIC CONTROLLER USING GENETIC ALGORITHM

To improve the proposed fuzzy logic controller, genetic algorithm is used to find the optimal membership functions [15]. Here, firstly the genetic algorithm is explained, and then the optimization of fuzzy logic controller by means of genetic algorithm is discussed.

A. Genetic Algorithm

Genetic algorithm was firstly introduced by John Holland and developed by him, his student and colleagues [23]. These algorithms are heuristic optimization process inspired by natural evolution and could be used to minimize a suitable objective function or fitness function for tuning the fuzzy logic controller parameters. It is more effective at avoiding local minima than differentiation based methods.

The genetic algorithm will generally include three fundamental genetic operations of selection, crossover and mutation. These operations are used to modify the chosen solutions and select the most appropriate offspring to succeeding generations [23].

In a genetic algorithm, a population of strings (called chromosomes), which encode candidate solutions (called individuals) to an optimization problem, evolves toward better solutions. Traditionally, solutions represented in binary as strings of “0”s and “1”s. The evolution usually starts from a population of randomly generated individuals and happens in generations. In each generation, the fitness of every individual in the population is evaluated, multiple individuals are stochastically selected from current population (based on their

fitness), and modified (recombined and possibly randomly mutated) to form a new population. The new population is then used in the next iteration of the algorithm. Commonly the algorithm terminates when either a maximum number of generations has been produced, or satisfactory fitness level has been reached for the population.

The basic iterations of genetic algorithm can be summarized as follows [23]–[25]:

1) Genetic representation: encoding the variables. Genetic algorithm often encodes solutions as fixed length "bitstrings" (e.g. 101110, 111111, and 000101).

2) A method for generating the initial population: population may be generated randomly or problem specific knowledge can be used to construct the chromosomes with the populations.

3) An evaluation function, which assign a real number to measure the fitness of each chromosome.

4) A reproduction selection scheme, which is used to select chromosome to be exposed to genetic operations. One of the most famous approaches is "roulette wheel", which selects chromosomes proportional to their fitness values.

5) Genetic operators: crossover and mutation are two main operators in genetic algorithm. These operators are applied to modify the chosen chromosomes (parents) and select the most appropriate offspring to pass on to succeed generations. The basic mechanism of genetic algorithm, crossover of the parental and mutation illustrated in Fig. 7. Crossover is done by selecting two parents during reproduction and combining genes to produce offspring. Two selected parents are combined with some probability (crossover rate); therefore two new offspring will be born. One gene or several genes of each offspring may then change randomly (mutation) with some probability (mutation rate). Usually the crossover has high probability (typically values are between 0.8 and 0.95) and mutation has small probability (typically values are between 0.1 and 0.001).

6) Termination: The cycle of genetic algorithm will be continued until the genetic algorithm reaches to stopping criteria. There are several approaches to terminate the genetic algorithm. A common approach is to terminate genetic algorithm when the number of generations reaches to specific value. The genetic algorithm process may also run just for limited time duration. It is also possible to terminate a genetic algorithm when the objective function of the best chromosome has not improved in the several generations.

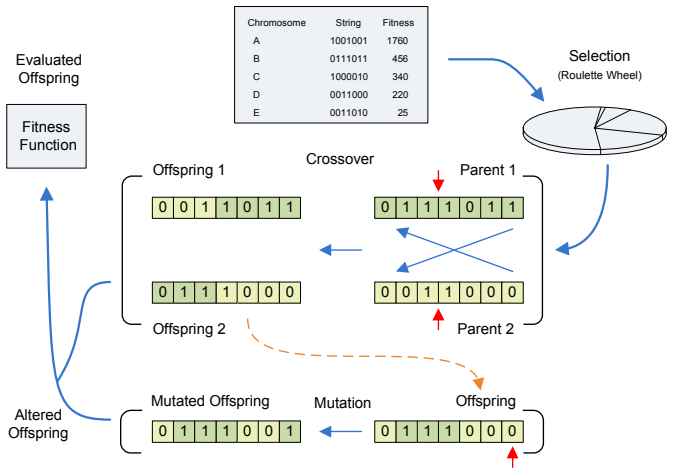

Fig. 7. Mechanism of genetic algorithm.

B. Using Genetic Algorithm for Optimizing of Fuzzy Logic Controller Membership functions

In section III. A., input and output memberships of fuzzy logic controller are assumed similar. Now, with taking to consider the values from the last input membership functions, the output membership functions could be optimized. The shapes of membership functions in fuzzy logic controller are triangular. Therefore in the case of triangular fuzzy sets, three characteristic points (center and two widths) are used as the parameters should be optimized. Here, the number of triangular membership functions is seven ("NB", "NM", "NS", "ZE", "PS", "PM", "PB"). To design symmetric controller for positive and negative input pulses, the membership functions are assumed symmetric to Y axis. Also the center of ZE is assumed zero. Therefore there are nine points or variables for optimizing the output membership functions; two points for "NB", three points for "NM", three points for "NS" and one point for "ZE". The range of changes in these variables is between 0.1 and 4. Moreover, there are constraints in optimization which guarantee that the membership functions are ordered according to their values (e.g. NB<NM<NS<ZE<PS<PM<PB); for instance, the center of "NB" must be less than the center of "NM". These constraints are considered to optimize the membership functions. The number of initial population is assumed 100. Minimizing integral of time-weighted absolute error (ITAE) is commonly referred to as good performance index in designing PID controllers. Thus the ITAE assumed as objective function. Equation (6) shows the mathematical formula of ITAE. Where t is the time and e is the different between output and reference in control process.

$$ITAE = \int_0^\infty t\,|e(t)|\,dt \tag{6}$$

Selection of parents is based on "roulette wheel". The rate of crossover which applied to parents is 0.8. Crossover trends to make the chromosomes within the population more similar, whereas mutation trends them more divers and usually has low rate. Here, because of existing constraints for membership functions, the mutation is not applied. Also here the genetic algorithm is terminated when 32 generations have been produced.

V. Simulation Results

A closed loop NCS unit in this paper includes these sections: online adaptive fuzzy logic controller, neural network, plant, data communication network. In order to analyse the whole unit each section should be analysed separately. This paper has applied the state equations to plot the step response of this NCS. At this first stage, transfer functions of plant and controller are converted to state equations. Since the data transmitted over the network is digital these equation states need to be discretized state space equation to be able to simulate the processes. Equation (7) shows the discrete state-space form of process. While A, B, C and D are the continuous state space matrices

then their equal discrete state space matrices (A_d, B_d, C_d, D_d) would be obtained from (8), (9), (10), (11). By substituting the (2), (3) in to (7)-(11), discrete state space form of plant is obtained and represented in (12), (13).

$$\begin{cases} x[k+1] = A_d x[k] + B_d u[k] \\ y[k] = C_d x[k] + D_d u[k] \end{cases} \tag{7}$$

$$A_d = e^{AT} \tag{8}$$

$$B_d = \left(\int_0^T e^{A\tau} d\tau \right) B \tag{9}$$

$$C_d = C \tag{10}$$

$$D_d = D \tag{11}$$

$$x[k+1] = \begin{bmatrix} 0.0066 & -0.2973 & 0 \\ 0.4870 & 0.7295 & 0 \\ 0.0035 & 0.0089 & 1 \end{bmatrix} x[k] + \begin{bmatrix} 7.7924 \\ 7.0909 \\ 0.0277 \end{bmatrix} U[k] \tag{12}$$

$$y[k] = \begin{bmatrix} 0 & 22.13 & 1228.7 \end{bmatrix} x[k] \tag{13}$$

In these simulations a random time delay is provided to analyse the performance of NCS. The total of command delay, t_1, and feedback delay, t_2, generates the total time delay (RTT) which is shown in Fig. 8. After training of neural network, the biases and weights values are obtained shown in Table III. Neural network transfer functions for layer 1 (hidden layer) and layer 2 (output layer) are "tansig" and "purelin" respectively. Equations (14) and (15) show these two transfer functions in mathematical forms, while figures of these transfer functions are plotted in Fig. 9.

$$tansig\,(n) = \frac{2}{1+e^{-2n}} - 1 \tag{14}$$

$$purelin\,(n) = n \tag{15}$$

The sampling time is assumed 0.01 second and the model of NCS is based on the model described in [26]. Here in this paper the simulations and comparisons of the step response are provided among three controller types: 1) Online adaptive fuzzy logic controller, 2) Classical Smith predictor with fuzzy logic controller and 3) Pure fuzzy logic controller. The results are illustrated in Fig. 12. Results show that the online adaptive fuzzy logic controller offer a better performance compared to other two controllers.

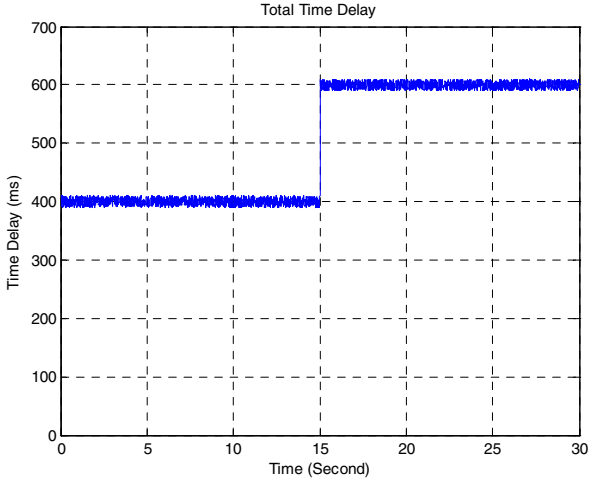

Fig. 8. A sample of simulated varying time delay in NCS.

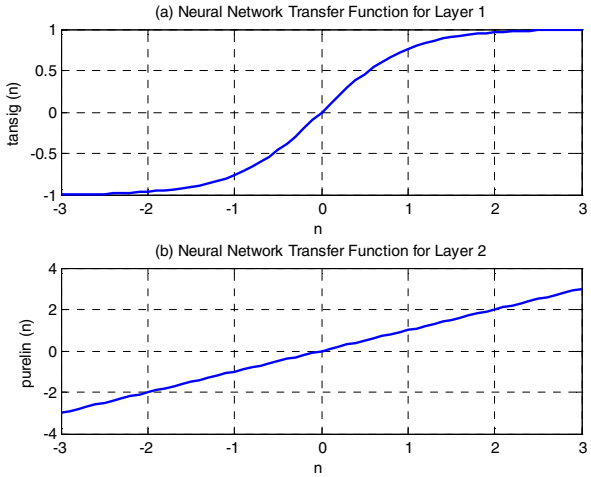

Fig. 9. Neural networks transfer functions; a) tansig; b) purelin.

As can be seen the output signal of online adaptive fuzzy logic method does have small overshoot and fast response. Therefore this controller is recommended for networked control systems purposes. W. Du and F. Du have suggested a Smith predictor integrated with adaptive fuzzy-PID controller for the NCSs in [17]. However they did not measure the network delay online. They applied a fuzzy logic controller just for tuning the coefficients of PID controller, which means that their suggested controller works offline. They also have designed in [18] a RBF neural network control with Smith predictor for NCSs which works offline as well. In communication networks time delay could exceeds 200 ms (vs. 400 ms, 600 ms). The results from [17], [18] show that response would degrade with time delays over 200 ms. In [17], [18], it was assumed that the maximum of burst time delay is about 200 ms while this time delay was applied discretely. Our proposed method has more improved response especially when the time delay is over 200 ms even with the time delay of 600 ms there is no degradation in step response. In the spite of applying this large value of time delay continuously, results in Fig. 13 show that this does not have any more effects on the step response as well.

As described in section IV, This paper takes the advantage of genetic algorithm method to optimize the fuzzy controller membership functions and consequently improve the overall results. For this propose, it starts with assumption of a no delay system while optimizes the fuzzy logic controller. The applied objective function type in this paper is ITAE. In this case, which is a position control example, the goal is that the output follows the input more closely. The closer output follows the input the more accurate is the performance. Tuning of an online adaptive fuzzy logic controller reduces the error value even with the presence of time delay in the system. Hence genetic algorithm is applied for some input pulses, and as a result, the output membership functions become tuned. The values of objective functions in each generation are shown in Fig. 10. As could be perceived, the objective function values in each generation become smaller compared to their previous generation which is inherently a genetic algorithm characteristic. Another point is that objective functions do not

show significant changes in last four generations, which indicates that, this genetic algorithm roughly obtains its best answer. The best value of ITAE in 32th generation is 0.05292. After applying the genetic algorithm to fuzzy logic controller, tuned output membership function shapes could be illustrated in Fig. 11. These membership functions are used for last three types of controller. For online adaptive fuzzy logic controller, the neural network is trained based on new optimized membership functions. Obtained biases and weights values are shown in Table IV. Rotation values are obtained according to different delays in experiments. Then the neural network is trained by these values. Experiments in Fig. 12 and Fig. 13 are repeated and are shown in Fig. 14 and Fig. 15. Results of online adaptive fuzzy logic controller are better compared to the other two controllers. Since the pure fuzzy logic controller is tuned in conditions with no delay, changes in membership make it unstable with the presence of time delay. Moreover, classical Smith predictor as shown in Fig .15 becomes unstable for delay times over 200 ms similar to pure fuzzy logic controller. It is even worse when the time it is not tuned. Table V shows the comparison of results. Two main evaluation indexes for comparison of results are the rise time (T_r) and the Percent Overshoot ($P.O.$). Rise time is that time taken for the output of plant to rise from 10% to 90% of its final value when simulated by step input. The Percent Overshoot is defined as (16). For a unit step input, where M_{Pt}, is the first peak value of the time response, and f_v is the final value of the response. Normally, f_v is the magnitude of the input.

$$P.O. = \frac{M_{Pt} - f_v}{f_v} \times 100\,\% \tag{16}$$

Peak time (T_p) is the time that takes for output of plant to reaches the peak value. The smaller the $P.O.$ and M_{Pt} values, the better is the controller performance. The results from Table V show that our proposed method has no overshoot. Furthermore, when the membership functions are optimized with genetic algorithm, the T_r is more smaller compared to the non-optimized case. Since the Smith predictor controller is tuned for 200 ms delay, when optimization is applied, this controller shows better results with the time delay of 200 ms. However, for other induced delays, its performance will decrease. Pure fuzzy logic controller tuned with no time delay and shows poor performance result compared to other two controllers.

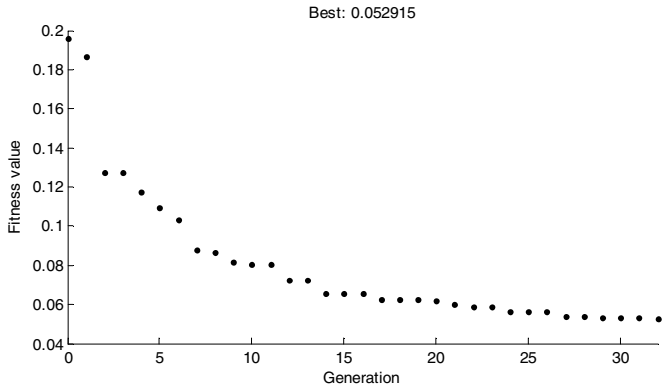

Fig. 10. Objective functions values for different generations of genetic algorithm.

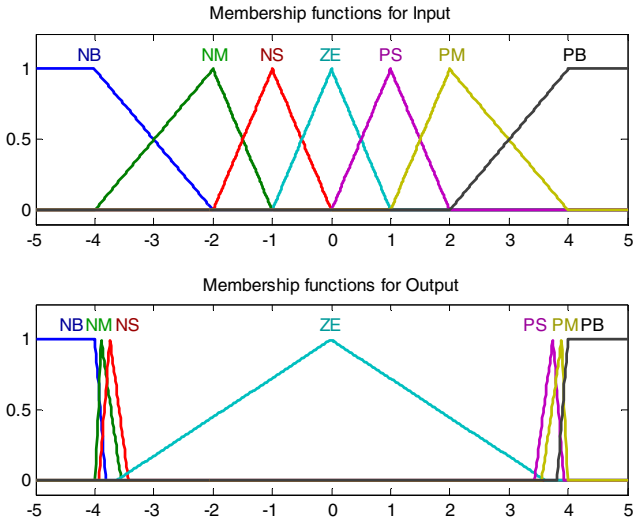

Fig. 11. Optimal fuzzy logic membership functions.

VI. Conclusion

NCSs have found widely application in various fields recently. However there are some drawbacks in their structures such as varying time delay and packet dropouts, which makes the control design of these systems challenging. Conventional PID and fuzzy logic controllers are mostly designed to address the instability problems in NCSs. Fuzzy logic controllers with the great potential in tackling the nonlinear processes and making NCSs more robust against the dynamically variable parameters could be a more reasonable option for NCSs. Moreover, a rotating rules-table fuzzy logic controller is a great solution for stochastic time delay. Thus according to above mentioned characteristic of both fuzzy logic controller and rules-table rotation, this paper has proposed a novel controller for NCSs. This novel design has integrated a rotating rules-table fuzzy logic controller with a neural network to control the position of an AC 400 W servo motor as a remote plant via Ethernet. Simulation results and their comparison for three different methods of controlling over this plant verified that this novel controller design is more beneficial especially over the big value of delay times as large as 600 ms. The proposed method shows better performance when the fuzzy logic membership functions are optimized by means of genetic algorithm.

TABLE III
Weights and Biases Values for Neural Network.

$IW_{1,1} = \begin{bmatrix} -0.0057 \\ -0.2547 \end{bmatrix}$	$LW_{2,1} = \begin{bmatrix} 0.3566 & 0.8011 \end{bmatrix}$
$b_1 = \begin{bmatrix} 1.1243 \\ 24.6125 \end{bmatrix}$	$b_2 = 0.5684$

TABLE IV
WEIGHTS AND BIASES VALUES FOR NEURAL NETWORK.
(FOR OPTIMIZED FUZZY LOGIC CONTROLLER)

$IW_{1,1} = \begin{bmatrix} 0.0036 \\ 0.0154 \end{bmatrix}$	$LW_{2,1} = \begin{bmatrix} -2.9954 & -15.2386 \end{bmatrix}$
$b_1 = \begin{bmatrix} 1.286 \\ 1.4904 \end{bmatrix}$	$b_2 = 17.5069$

REFERENCES

[1] J. P. Hespanha, P. Naghshtabrizi, and Y. Xu, "A survey of recent results in networked control systems," *Proc. IEEE*, vol. 95, no. 1, pp. 138–161, Jan. 2007.

[2] F. L. Lian, J. R. Moyne, and D. M. Tilbury, "Performance evaluation of control networks: Ethernet control net and device net," *IEEE Control Syst. Mag.*, pp. 66–83, Feb. 2001.

[3] P. Ogren, E. Fiorelli, and N. E. Leonard, "Cooperative control of mobile sensor networks: Adaptive gradient climbing in a distributed environment," *IEEE Trans. Automat. Contr.*, vol. 49, no. 8, pp. 1292–1302, Aug. 2004.

[4] C. Meng, T. Wang, W. Chou, S. Luan, Y. Zhang, and Z. Tian, "Remote surgery case: Robot-assisted teleneurosurgery," in *IEEE Int. Conf. Robot. and Auto. (ICRA'04)*, Apr. 2004, vol. 1, pp. 819–823.

[5] J. P. Hespanha, M. L. McLaughlin, and G. Sukhatme, "Haptic collaboration over the Internet," in *Proc. 5th Phantom Users Group Workshop*, Oct. 2000.

[6] K. Hikichi, H. Morino, I. Arimoto, K. Sezaki, and Y. Yasuda, "The evaluation of delay jitter for haptics collaboration over the Internet," in *Proc. IEEE Global Telecomm. Conf. (GLOBECOM)*, Nov. 2002, vol. 2, pp. 1492–1496.

[7] S. Shirmohammadi and N. H. Woo, "Evaluating decorators for haptic collaboration over the Internet," in *Proc. 3rd IEEE Int. Workshop Haptic, Audio and Visual Env. Applic.*, Oct. 2004, pp. 105–109.

[8] P. Seiler and R. Sengupta, "Analysis of communication losses in vehicle control problems," in *Proc. 2001 Amer. Contr. Conf.*, Jun. 2001, vol. 2, pp. 1491–1496.

[9] P. Seiler and R. Sengupta, "An H_∞ approach to networked control," *IEEE Trans. Automat. Contr.*, vol. 50, no. 3, pp. 356–364, Mar. 2005.

[10] R. M. Murray, K. J. Astrom, S. P. Boyd, R. W. Brockett, and G. Stein, "Control in an information rich world, " *IEEE Contr. Syst. Mag.*, vol. 23, no. 2, pp. 20–33, Apr. 2003.

[11] M. G. Rivera and A. Barreiro, "Analysis of networked control systems with drops and variable delays," *Automatica*, vol. 43, no. 12, pp. 2054–2059, Dec. 2007.

[12] Y. Ishido, K. Takaba, and D. E. Quevedo, "Stability analysis of networked control systems subject to packet-dropouts and finite-level quantization," *Syst. & Control Lett.*, vol. 60, no. 5, pp. 325–332, May 2011.

[13] C. W. Cheng, C. L. Lai, B. C. Wang, and P. L. Hsu, "The time-delay effect of multiple-networks systems in NCS," in *Proc. SICE Annu. Conf.*, Sep. 2007, pp. 929–934.

[14] C. L. Lai and P. L. Hsu, "Design the remote control system with the time-delay estimator and the adaptive smith predictor," *IEEE Trans. Ind. Inform.* , vol. 6, no. 1, pp. 73–80, Feb. 2010.

[15] I. Pan, S. Das, and A. Gupta, "Tuning of an optimal fuzzy PID controller with stochastic algorithms for networked control systems with random time delay," *ISA Trans.*, vol. 50, no. 1 , pp. 28–36, Jan. 2011.

[16] D. Zhao, C. Li, and J. Ren, "Fuzzy speed control and stability analysis of a networked induction motor system with time delays and packet dropouts," *Nonlinear Anal.: Real World Applicat.*, vol. 12, no. 1, pp. 273–287, Feb. 2011.

[17] W. Du and F. Du, "Novel smith predictor and fuzzy control for networked control systems," in *Proc. Asia-Pacific Conf. Inform. Process. (APCIP)*, July 2009, pp. 75–78.

[18] F. Du and W. Du, "RBF neural network control and novel smith predictor for networked control systems," in *Proc. Asia-Pacific Conf. Inform. Process. (APCIP)*, July 2009, pp. 67–70.

[19] C. L. Lai, P. L. Hsu, and B. C. Wang, "Design of the adaptive smith predictor for time-varying network control system," in *Proc. SICE Annu. Conf.*, Aug. 2008, pp. 2933–2938.

[20] C. L. Lai and P. L. Hsu, "Realization of networked control systems on Ethernet with varied time delay," in *Proc. IEEE Int. Conf. Syst., Man, Cybern. (SMC)*, Oct. 2010, pp. 66–73.

[21] N. Vatanski, J. P. Georges, C. Aubrun, E. Rondeau, and S. L. J. Jounela, "Networked control with delay measurement and estimation," *Control Eng. Practice*, vol. 17, no. 2, pp. 231–244, Feb. 2009.

[22] T. J. Ross, *Fuzzy Logic with Engineering Applications.* 2nd ed. John Wiley & Sons, Ltd., 2004, pp. 151–161.

[23] A. Mellit and S.A. Kalogirou, "Artificial intelligence techniques for photovoltaic applications: A review," *Progress in Energy and Combustion Sci.*, vol. 34, no. 5, pp. 574–632, Oct. 2008.

[24] C. Hicks, "A genetic algorithm tool for optimising cellular or functional layouts in the capital goods industry," *Int. J. Prod. Econ.*, vol. 104, no. 2, pp. 598–614, Dec. 2006.

[25] A. Messai, A. Mellit, A. Guessoum, and S.A. Kalogirou, "Maximum power point tracking using a GA optimized fuzzy logic controller and its FPGA implementation," *Solar Energy*, vol. 85, no. 2, pp. 265–277, Feb. 2011.

[26] M. Y. Chow and Y. Tipsuwan, "Network-based control systems: A tutorial," in *Proc. 27th Annu. Conf. IEEE Ind. Electro. Soc.*, 2001, pp. 1593–1602.

Pooya Hajebi (S'10) was born in Isfahan, Iran, in 1981. He received the B.S. degree in electrical engineering (Electronics) and the M.S. degree in electrical engineering (Communication Systems), both from Yazd University, Yazd, Iran, in 2005 and 2009, respectively. Currently, He is working toward the Ph.D. degree in the Department of Electrical and Computer Engineering, Yazd University, Yazd, Iran. His research interests include Networked Control Systems, Fuzzy Systems, Neural Networks, Data Communication Networks, Digital Signal Processing, Biological Signal Processing, Digital Image Processing, Cellular Networks, Optimizations, Time Delay Systems and Real Time Systems.

Seyed Mohammad Taghi AlModarresi obtained his B.S. degree in Electronics Engineering and M.S. degree in Communication Systems, both from the Isfahan University of Technology, Isfahan, Iran. He also holds Ph.D. in Electronics (Intelligent Signal Processing) from University of Southampton, UK (Department of Electrical and Computer Science: ECS). He works at the Department of Electrical and Computer Engineering in Yazd University where he pursues his research interests in: (i) Networked Control Systems (NCS) (ii) Neuro-Fuzzy Networks (iii) Wireless Networks.

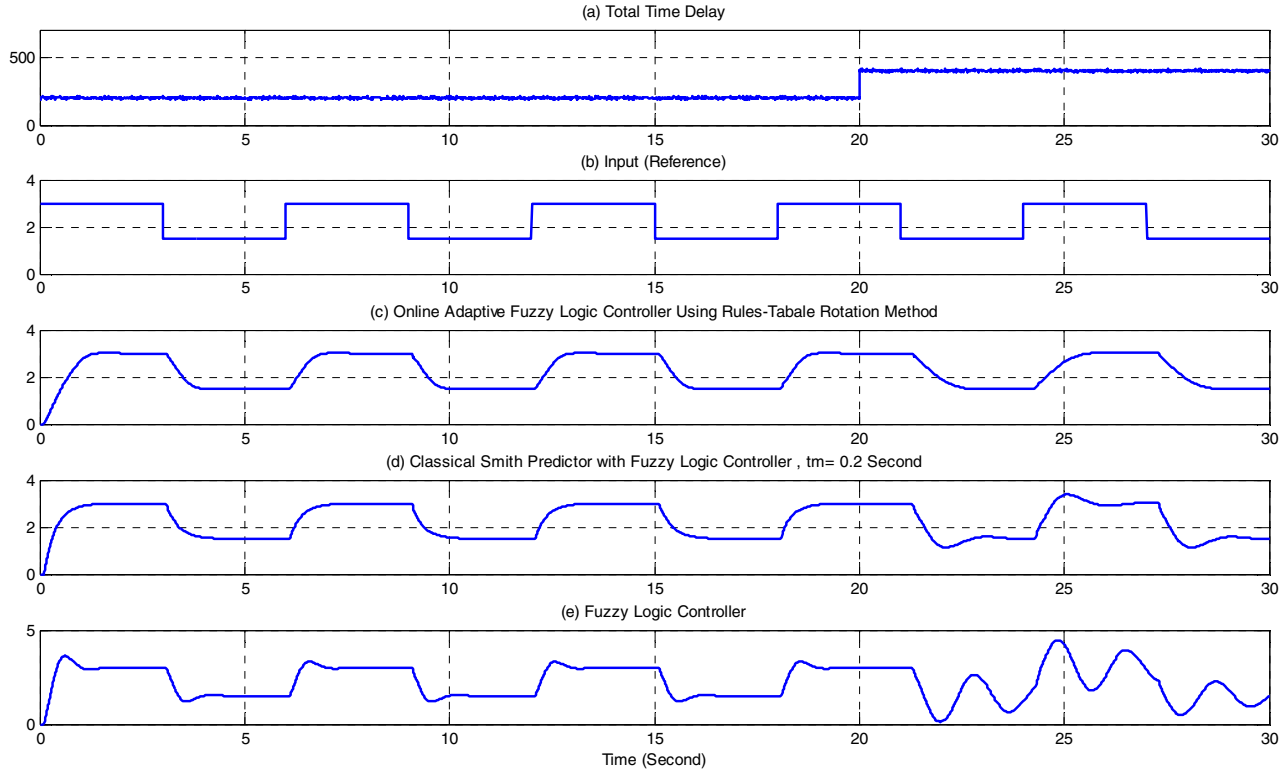

Fig. 12. Simulation results (The maximum time delay is about 400 ms); a) Time delay; b) Reference signal; c) Position (revolution of the motor shaft) for online adaptive fuzzy logic controller using rules-table rotation; d) Position (revolution of the motor shaft) for classical Smith predictor with fuzzy logic controller; e) Position (revolution of the motor shaft) for fuzzy logic controller.

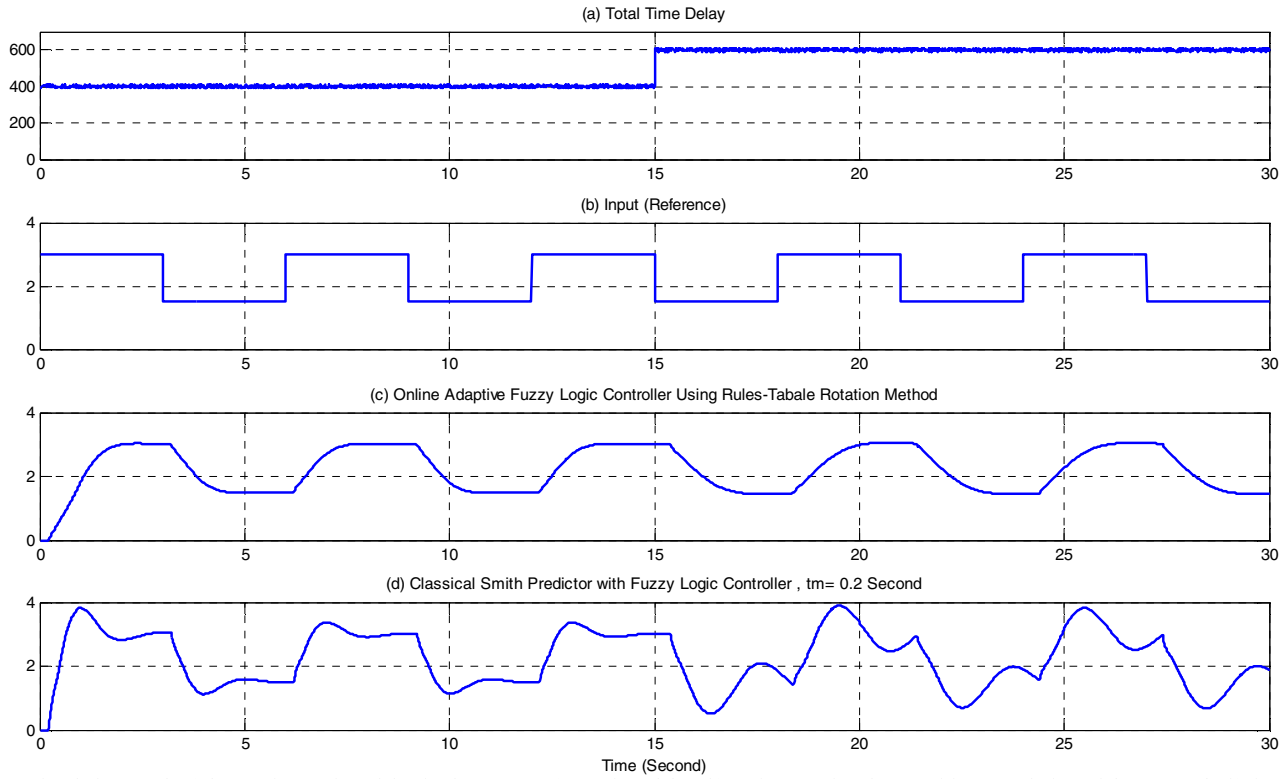

Fig. 13. Simulation results (The maximum time delay is about 600 ms); a) Time delay; b) Reference signal; c) Position (revolution of the motor shaft) for online adaptive fuzzy logic controller using rules-table rotation; d) Position (revolution of the motor shaft) for classical Smith predictor with fuzzy logic controller.

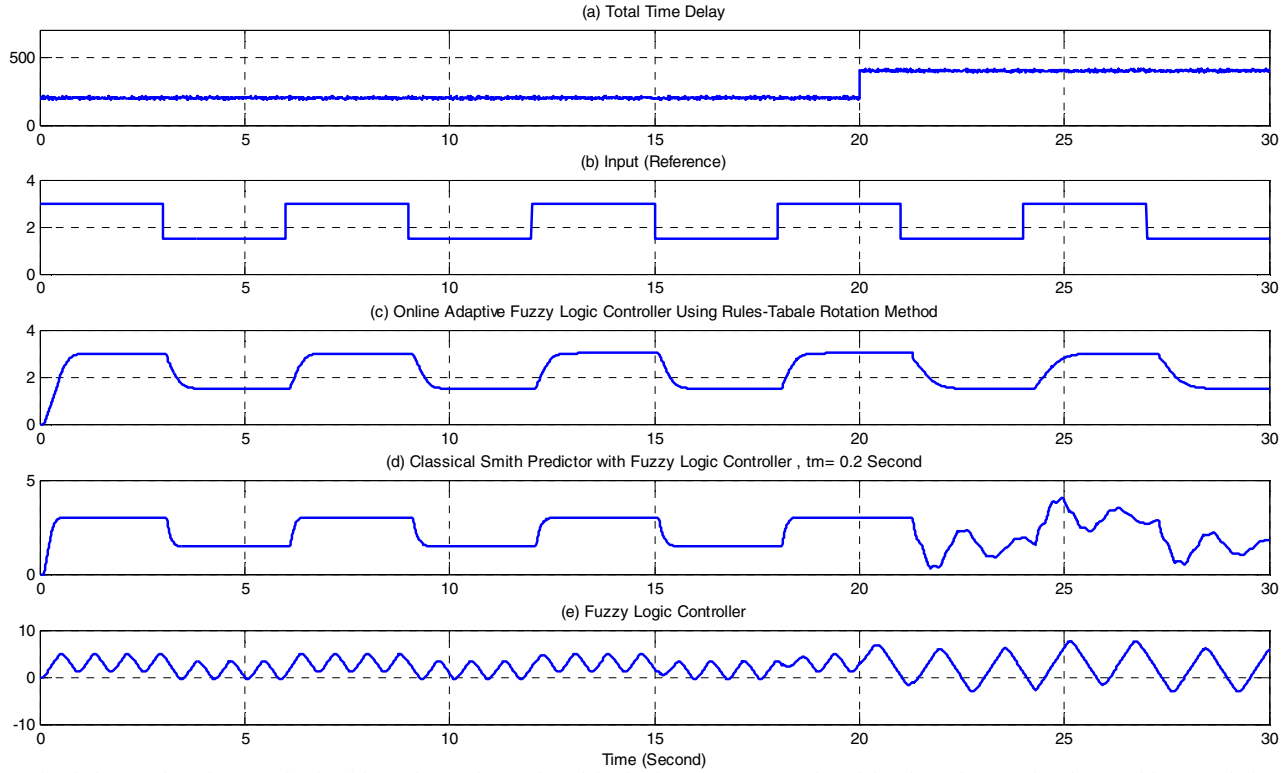

Fig. 14. Simulation results using genetic algorithm (The maximum time delay is about 400 ms); a) Time delay; b) Reference signal; c) Position (revolution of the motor shaft) for online adaptive optimized fuzzy logic controller using rules-table rotation; d) Position (revolution of the motor shaft) for Classical Smith predictor with optimized fuzzy logic controller; e) Position (revolution of the motor shaft) for optimized fuzzy logic controller.

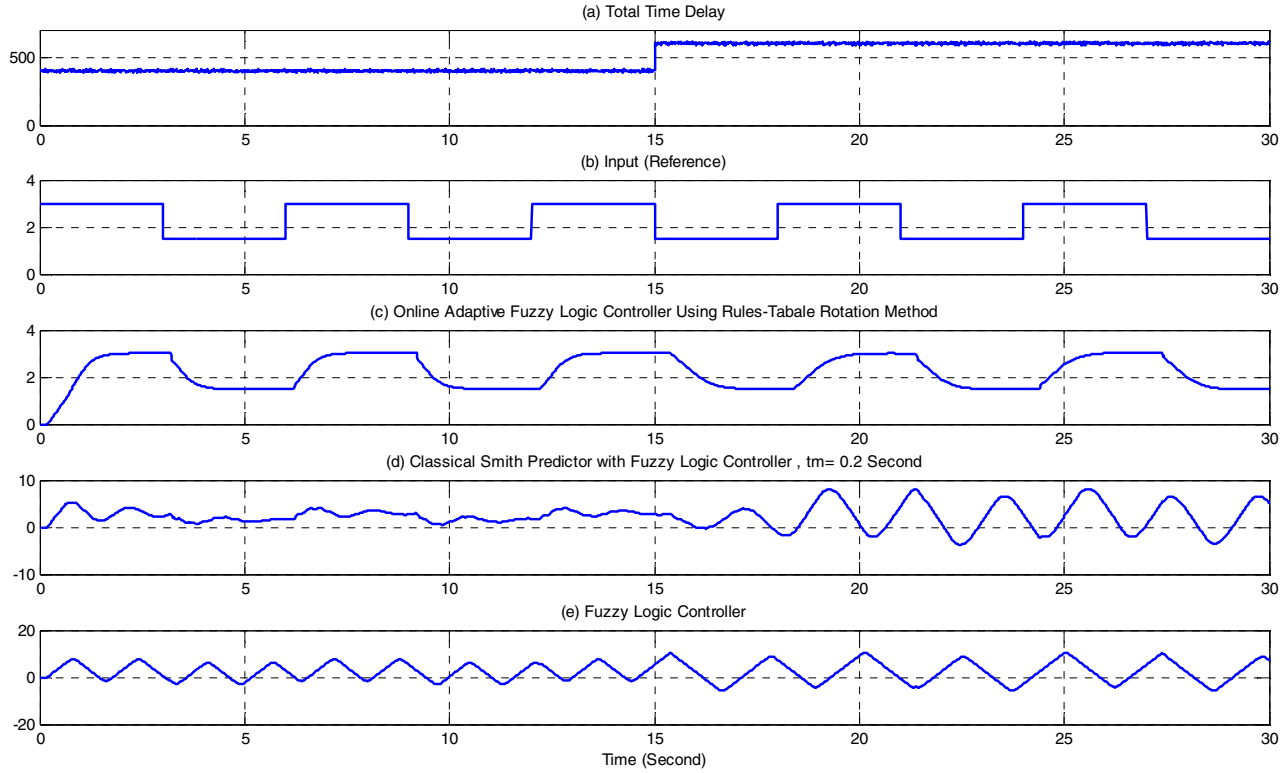

Fig. 15. Simulation results using genetic algorithm (The maximum time delay is about 600 ms); a) Time delay; b) Reference signal; c) Position (revolution of the motor shaft) for online adaptive optimized fuzzy logic controller using rules-table rotation; d) Position (revolution of the motor shaft) for classical Smith predictor with optimized fuzzy logic controller. e) Position (revolution of the motor shaft) for optimized fuzzy logic controller.

TABLE V
COMPARISON OF RESULTS

Approximate value of delay	Method	Optimization	T_r (s)	*P.O.* (%)	ITAE	T_p (s)
20 ms	Online Adaptive FLC	Optimized	**0.1990**	**0**	**0.0429**	-
		Non-Optimized	0.8289	0	0.4959	-
	Classical Smith Predictor	Optimized	0.6863	0	0.2858	-
		Non-Optimized	1.0869	0	0.7152	-
	FLC	Optimized	0.2075	0	0.0436	-
		Non-Optimized	0.5899	0	0.2355	-
200 ms	Online Adaptive FLC	Optimized	**0.5062**	**0**	**0.3034**	-
		Non-Optimized	0.7876	0	0.5937	-
	Classical Smith Predictor	Optimized	0.2195	2.04	0.0972	0.5600
		Non-Optimized	0.6026	0	0.3355	-
	FLC	Optimized	0.2439	24.45	4.7879	0.5400
		Non-Optimized	0.2432	21.77	0.3322	0.6300
400 ms	Online Adaptive FLC	Optimized	**1.0146**	**0**	**1.2863**	-
		Non-Optimized	1.2394	0	1.6309	-
	Classical Smith Predictor	Optimized	0.1388	144.38	3.8189	0.8600
		Non-Optimized	0.3538	26.91	1.0856	1
	FLC	Optimized	0.1506	202.66	10.6089	0.8400
		Non-Optimized	0.2941	52.25	6.4426	0.9100
600 ms	Online Adaptive FLC	Optimized	**1.2878**	**0**	**2.2986**	-
		Non-Optimized	1.5202	0	2.6264	-
	Classical Smith Predictor	Optimized	0.3932	36.03	11.2648	1.1600
		Non-Optimized	0.2371	144.27	5.0326	1.3000
	FLC	Optimized	0.1379	343.67	16.8155	1.1400
		Non-Optimized	-	-	-	-

Improving Coverage and Capacity in Underwater Acoustic Cellular Networks

Amirmansour Nabavinejad *, Samar Shahabi Ghahfarokhi **

* *Department of Electrical Engineering, Najafabad Branch, Islamic Azad University, Isfahan, Iran*

** *Faculty of Electrical Engineering and Information Technology, Ilmenau University of Technology, Ilmenau, Germany*

dc.nabavinejad@gmail.com , samar.shahabi-ghahfarokhi@tu-ilmenau.de

***Abstract*— Underwater acoustic communications systems are challenged by the characteristics of acoustic propagation through the underwater environment. There are a wide range of physical processes that impact underwater acoustic communications and the relative importance of these processes are different in different environments. Acoustic propagation is characterized by three major factors: time-varying multipath propagation, low speed of sound and attenuation that increases with signal frequency. Limited bandwidth in these systems is of paramount obstacles. To overcome this problem the idea of frequency reuse pattern seems to be useful. The key characteristic of a cellular network is the ability to re-use frequencies to increase both coverage and capacity. One element that determines frequency reuse is the reuse distance depending on the cell radius and the number of cells per cluster. Analysis of frequency reuse between adjacent clusters and optimal cell-radius selection criteria has been carried out recently. In other recent woks, the parameters of the cellular networks designing have been calculated based on a rough approximation of the attenuation and propagation model. In our work, after driving the ratio of signal to interference for underwater acoustic channels with more accuracy, the constraints for the cell radius are determined. One of the most important results of this contribution is that, for special parameters like bandwidth, it may be impossible to provide the required signal to interference ratio and bandwidth for the network users. Furthermore, in this paper, the number of supportable users, per-user bandwidth, and the user capacity for a cellular underwater network are determined.**

***Index Terms*— Cell Radius, Frequency Reuse, Signal to Interference Ratio, Underwater Cellular Networks, User Capacity**

I. INTRODUCTION

THE surface of the earth covered 70% by ocean and most of which are unexplored. There is a lot of potential applications in underwater environment such as oceanographic monitoring, scientific exploration, disaster monitoring and also especially for oil/gas field exploration. The underwater channel remains one of the most challenging communication environments. Designing a reliable communication system remains an active area of research. The underwater is a time and spatially varying propagation environment whose characteristics pose significant challenges to the development of effective underwater wireless communications systems. For several decades, electromagnetic waves, especially radio waves, have seen extensive use in long range communications. When the propagating medium is water, however, electromagnetic waves find limited use. The high rate of absorption of electromagnetic signals in underwater has limited the development of electromagnetic communications systems. Similarly, optical signals are also rapidly absorbed in underwater and have the added disadvantage of scattering by suspended particles and high levels of ambient light in the upper part of the water column. As a result, the development of underwater optical communications systems has also been limited to few applications. Thus, acoustic signalling is primary form of wireless underwater communication. Despite its favourable characteristics relative to electromagnetic and optical propagation in the underwater environment, the physics of acoustic propagation pose significant challenge to underwater acoustic communications systems [1]. Acoustic propagation is best supported at low frequencies, and the bandwidth available for communication is extremely limited. An underwater acoustic channel is different from a ground-based radio channel from many aspects, including [2]-[7].

1) Bandwidth is extremely limited. Lack of available bandwidth is the biggest issue for underwater acoustic communication /network. The attenuation of acoustic signal increases with frequency and range. Consequently, the available bandwidth of underwater acoustic channels is limited and dramatically depends on both transmission range and frequency.

2) Propagation delay is long. Sound propagates through water much more slowly than electromagnetic waves through air. Sound speed underwater depends on several factors, such as pressure, salinity, and temperature, but has a nominal value around 1500m/s [4]. The slower acoustic propagation speed, five orders of magnitude below the speed of light, greatly impacts communication protocols. Low sound speed combined

Manuscript received Jun 29, 2012.

A. Nabavinejad is with the Najafabad Branch, Islamic Azad University, Isfahan, Iran (phone: +98-311-6250695; e-mail: dc.nabavinejad@gmail.com).

S. Shahabi Ghahfarokhi is with the Faculty of Electrical Engineering and Information Technology, Ilmenau University of Technology, Ilmenau, Germany (e-mail: samar.shahabi-ghahfarokhi@tu-ilmenau.de).

with the large distances common in underwater networks makes propagation delays on the order of several seconds common. Long propagation delays in validate or decrease the usefulness of many techniques used in RF networks, such as carrier sensing and handshaking protocols.

3) The channel impulse response is not only spatially varied but also temporarily varied. In fact, the ocean is a dynamic and complex environment. Water movements are never-ceasing, and conditions are always changing with the time of day and weather. It is generally very difficult to predict. The fluctuation nature of the channel causes the received signals easily distorted. Acoustic signals travelling through it are distorted by a variety of factors. The major contributors are absorption, refraction and reflection (reverberation). Through these three factors, the signals picked up by receivers are duplicated forms of the original, of varying levels of strength and distorted by a certain degree of spreading or compression.

4) Probability of bit error is much higher and temporary loss of connectivity (shadow zone) sometimes occurs, due to the extreme characteristics of the channel. Underwater acoustic communication channels are affected by many factors such as path loss, noise, multi-path, and doppler spread. All these factors cause high bit-error and delay variance.

5) In RF networks, the capacity of a channel depends primarily on the bandwidth utilized and the SNR at the receiver. The familiar equation from Shannon describes this relationship as $C = B\log_2(1+SNR)$ where C equals the channel capacity and B equals the channel bandwidth. Acoustic channels, however, involve a more complicated relationship between capacity and device distance, as we will discuss in more detail later. Since the available bandwidth in underwater is severely limited, frequency reuse and cellular networks concepts are very important. The key characteristic of a cellular network is the ability to re-use frequencies to increase both coverage and capacity. Adjacent cells must utilize different frequencies; however there is no problem with two cells sufficiently far apart operating on the same frequency. Since bandwidth is at premium in an acoustic channel, the concept of frequency reuse is an appealing one and, given the immense Success and practicality of terrestrial cellular systems, the question naturally arises as to how the cellular concept applies to an underwater acoustic environment. The first task in the design of a cellular network is the selection of network topology, i.e. determination of the cell size (radius) and the reuse pattern. In other words, the practical questions that one wants to answer are the following: For a given distribution of users and the desired information throughput, what should the coverage area of one base station be? How far should another base station operating in the same frequency band be? According to what pattern should the frequency bands be reused? In a terrestrial radio environment, this problem has a very simple solution, but in an underwater acoustic environment, the solution is complicated by the fact that the path loss does not consist only of the spreading loss (which grows with distances r^k, where k is usually a number between 1 and 2), But the absorption loss as well (which grows with distance as a^r, and depends on the frequency through the factor a) [8]. In other recent woks, the parameters of the cellular networks designing have been calculated based on a rough approximation of the attenuation and propagation model. In section II, after driving the ratio of signal to interference for underwater acoustic channels with more accuracy, the constraints for the cell radius are determined. In section III, we determine the cell size and the frequency reuse pattern needed to support a desired number of users operating over a given area within a given system bandwidth. In section IV we define the capacity of an underwater acoustic cellular networks and the maximal user density that can be supported within a given bandwidth. Conclusions are summarized in Section V.

II. UNDERWATER CELLULAR NETWORKS PARAMETERS

The concept of frequency reuse is employed often in wireless communication technologies, cellular systems are widely used today and cellular technology needs to offer very efficient use of the available frequency spectrum. The basic principle of frequency reuse establishes its foundations over the idea of utilizing a limited number of available (or assigned) frequency channels in different and distant geographical locations. Actually, a cellular network is usually divided into small geographical segments or "cells" contained within a larger set called "cluster," and each cell has its own set of uplink and downlink carrier frequencies. In this manner, all the neighboring cells have different sets of career frequencies, and this difference is kept in order to avoid interference between their transmission and reception. This is in accord with a basic law of wireless communication, which states that similar frequencies cannot be used repetitively in a limited geographical area, as doing so results in their cancellation or creation of interference, which results in interrupting the process of communication. Analysis of frequency reuse between adjacent clusters and optimal cell-radius selection criteria has been carried out recently [8]. In this section, we try to obtain underwater cellular network parameters with attention to limitations of underwater acoustic communication.

A. Design Constraints

In underwater cellular network design, a design constraint refers to some limitation on the conditions under which a cellular network is developed, or on the requirements of the network. The available bandwidth for an acoustic network typically is not more than 15 KHz [9]. This bandwidth must be shared among all users. In this section, the design of a cellular network begins with selection of the frequency reuse pattern and the cell radius. The total bandwidth B is divided among N adjacent cells, which forms a cluster. The clusters are then replicated over an arbitrarily large area. In doing so, it is required that the co-channel signal-to-interference ratio be greater than some minimum, and that the bandwidth per user be $W \geq W_0$.

B. Underwater Acoustic Transmission

The ocean is a dynamic and complex environment. Water movement is never-ceasing and conditions are always changing with the time of day and weather. It is generally very difficult to

predict. Acoustic signals travelling through it are distorted by a variety a factors. The major contributors are absorption, refraction and reflection. Through these three factors, the signals picked up by receivers are duplicated forms of the original, of varying levels of strength and distorted by a certain degree of spreading or compression.

C. *Propagation Loss*

Propagation loss causes a sound wave's amplitude to gradually diminish as it travels. There are two main contributors to this loss. The first is spreading loss and the second cause of transmission loss is due to attenuation loss includes losses due to absorption, leakage out of ducts, scattering and diffraction from the actual water medium. Absorption describes those effects in the ocean in which a portion of the sound intensity is lost through convention of heat [10]. Spreading loss does not represent a loss of energy, but refers to fact that the propagation of the acoustic pulse is such that the energy is simply spread over a progressively larger surface area, thus reducing its density. Spreading loss is not frequency dependent. Underwater communications are currently characterized by low data rates and long propagation delays. The long propagation delays are a result of the speed of sound being slow, and the low data rates are primarily a result of utilizing low-frequency acoustic signals to minimize absorption, which can be very high as shown in Fig. 1. If shorter range of communication is used then higher operating frequencies can be used.

As mentioned before, an important difference between the design of underwater acoustic cellular systems and the RF terrestrial cellular systems is the fact that underwater propagation shows a frequency dependent absorption, in addition to distance-dependent path loss. Attenuation or path loss that occurs in an underwater acoustic channel over a distance r for a signal of frequency f is given by [11].

$$A(r,f) = r^{k} a(f)^{r} \tag{1}$$

Where k is the spreading factor, and a(f) is the absorption coefficient. The acoustic attenuation, expressed in dB, is given by

$$10\log A(r,f) = k.10\log r + r.10\log a(f) \tag{2}$$

The first term in the above equation indicates the spreading loss and the second term shows the absorption loss. Spreading loss consists of cylindrical spreading and spherical spreading. Fig. 2 and Fig. 3 illustrate these two types of spreading loss. Cylindrical spreading usually occurs in shallow water and spherical spreading in deep water environment. In low frequency (100-3KHz), the absorption coefficient is given by [12].

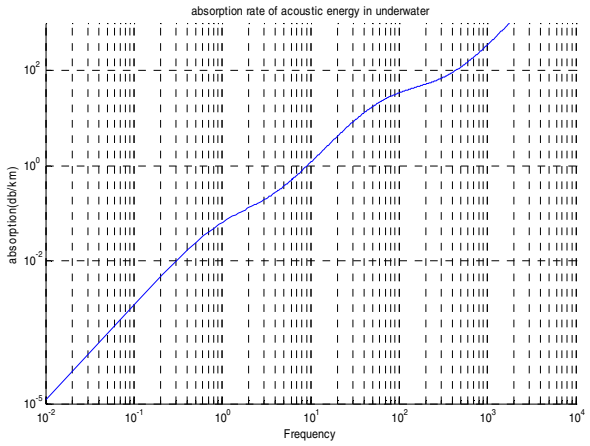

Fig.1. Absorption of underwater acoustic signal

$$10\log a(f) = 0.11\frac{f^2}{1+f^2} + 44\frac{f^2}{4100+f} + 2.75.10^{-4} f^2 + 0.003 \tag{3}$$

where the quantity 10log a(f) has unit of dB/km and f has unit of kHz. Without loss of generality, we will assume in the numerical examples a practical spreading factor k=1.5.

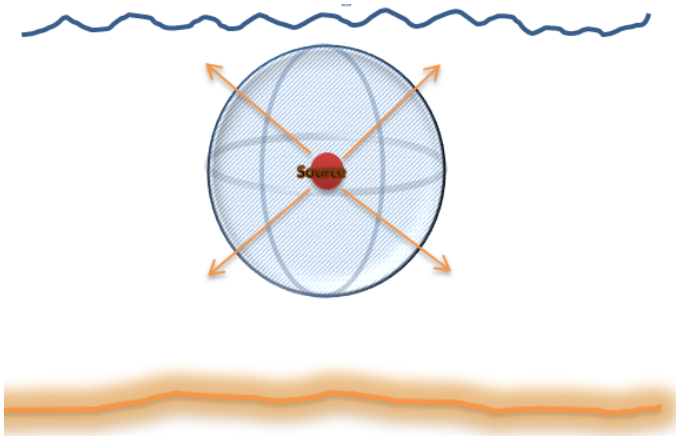

Fig. 2. Spherically spreading of sound wave

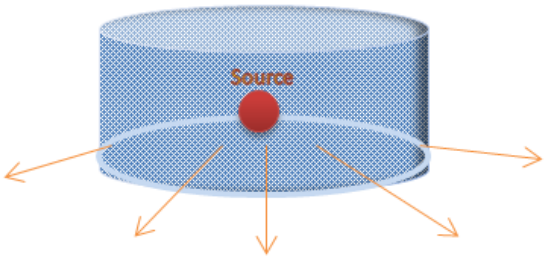

Fig. 3. Cylindrically spreading of sound wave

Using the acoustic path loss (2), the power of the signal received at a distance d from the transmitter is given by

$$P(r) = \int_{f_{min}}^{f_{min}+W} s_t A^{-1}(r,f)\,df = s_t \int_{f_{min}}^{f_{min}+W} r^{-k} a(f)^{-r}\,df \quad (4)$$

where s_t is the power spectral density of the transmitted signal which we assume to be constant and the integration is carried out over the frequency band occupied by the signal, starting at some f_{min} and extending over a bandwidth w. By substituting a(f) from (2) into (4), we have:

$$P(r) = s_t.r^{-k}\int_{f\,min}^{f\,min+W} \exp(-(0.011\frac{f^2}{1+f^2}+4.4\frac{f^2}{4100+f} +2.75.10^{-4}f^2+0.0003).r.\ln 10\,df$$
$$= s_t.r^{-k}\int_{f\,min}^{f\,min+W} \exp(-(A\frac{f^2}{1+f^2}+B\frac{f^2}{4100+f}+Cf^2+D))df$$

where the coefficients A, B, C and D are given by

$$A = 0.01\ln 10 \qquad B = 4.4r\ln 10$$
$$C = 2.75\times 10^{-5} r\ln 10 \qquad D = 3\times 10^{-4} r\ln 10$$

In order to evaluate the integrals, we make the following approximations,

$$\frac{f^2}{1+f^2}\approx 1 \quad , \quad \frac{f^2}{4100+f}\approx\frac{f^2}{4100} \quad (5)$$

Since the signal frequency in underwater acoustic communication is about several KHz, the above approximation is valid. Then P(r) can be calculated as follows

$$P(r) = s_t.r^{-k}.\int_{f_{min}}^{f_{min}+W} \exp(-(A\frac{f^2}{1+f^2}+B\frac{f^2}{4100+f} +Cf^2+D))df$$
$$\approx s_t r^{-k}.\int_{f_{min}}^{f_{min}+W} \exp(-(A+B\frac{f^2}{4100}+Cf^2+D))df$$
$$= s_t r^{-k} K.\int_{f_{min}}^{f_{min}+W} \exp(-Ef^2)df$$

where

$$E = \frac{B}{4100}+C \qquad K = \exp\left(-(A+D)\right)$$

Now by using the definition of the error function,

$$\mathrm{erf}(X) = \frac{2}{\sqrt{\pi}}\int_0^x \exp(-\lambda^2)d\lambda \quad (6)$$

we obtain

$$P(r) = s_t.r^{-k}.K.\int_{f_{min}}^{f_{min}+W}\exp(-Ef^2)df = s_t.r^{-k}.\frac{K}{\sqrt{E}}.\frac{\sqrt{\pi}}{2}\left[\mathrm{erf}(f_{min}+W)-\mathrm{erf}(f_{min})\right] \quad (7)$$

By substituting E and K into (7) and introducing the parameter γ

$$\gamma = 17.6\exp(-0.974r).r^{-(k+\frac{1}{2})} \quad (8)$$

the power of the signal received at a distance r from the transmitter is given by

$$P(r) = s_t.\gamma.\exp(-0.974r).r^{-(k+\frac{1}{2})} \quad (9)$$

Now by using (9) and the assumption that all transmitters transmit the same power spectral density s_t, we can calculate the signal to interference ratio (SIR) by the following expression

$$SIR = \frac{P(r)}{\sum_i I_i} = \frac{\int_{f_{min}}^{f_{min}+W} s_t A^{-1}(r,f)\,df}{\sum_i \int_{f_{min}}^{f_{min}+W} s_t A^{-1}(X_i,f)\,df} = \frac{s_t\gamma.\exp(-0.974r).r^{-\left(k+\frac{1}{2}\right)}}{\sum_i s_t.\gamma.\exp\left(-0.974|X_i|\right).|X_i|^{-\left(k+\frac{1}{2}\right)}}$$

where X_i is the interference user distance to the desired receiver. Therefore signal to interference ratio for underwater acoustic channel is equal to

$$SIR = \frac{\exp(-0.974r).r^{-\left(k+\frac{1}{2}\right)}}{\sum_i \exp\left(-0.974|X_i|\right).|X_i|^{-\left(k+\frac{1}{2}\right)}} \quad (10)$$

As this equation shows, under the approximations given by (5), the signal to interference ratio is independent from frequency and thus, this ratio is usable for cellules with different frequencies. In the next sections we may apply (10) to obtain underwater cellular network designing parameters.

III. CELL RADIUS AND THE REUSE NUMBER

The design of a cellular underwater network is addressed from the view point of determining the cell size and the frequency reuse pattern needed to support a desired number of

users operating over a given area within a given system bandwidth.

A. Calculation of Cell Radius

The signal bandwidth depends on the multiple-access technique used. If time-division multiple-access (TDMA) is used, it equals the bandwidth allocated to one cell, $B_0=\frac{B}{N}$ where N is the reuse number. N is given by form $N=i^2+ij+j^2$ in which i and j are integers. If frequency–division multiple-access (FDMA) is used, it equals the width of a frequency channel allocated to one of U users sharing a cell, $B_0=\frac{B}{NU}$ [13]. Let us assume (without loss of generality) TDMA is used. Assuming hexagonal cell geometry, as illustrated in Fig. 4, the SIR is dominated by the six nearest co-channel cells, and the worst SIR, which occurs at the cell edge, is given by

$$SIR \approx \frac{P(R)}{6P(D)} \tag{11}$$

where R is the cell radius and D the distance to the nearest co-channel cell. In a two-dimensional system geometry, the two distances are related by $D=QR$, where $Q=\sqrt{3N}$ and N is the reuse number [8]. By using (9), the SIR condition can be written in terms of the cell radius R and the reuse factor Q as

$$SIR \approx \frac{P(R)}{6P(D)} = \frac{\exp(-0.974R).R^{-\left(k+\frac{1}{2}\right)}}{6\exp(-0.974D).D^{-\left(k+\frac{1}{2}\right)}}$$

$$\approx \frac{1}{6}\exp(-0.974(R-D)).\left(\frac{R}{D}\right)^{-\left(K+\frac{1}{2}\right)}$$

$$\approx \frac{1}{6}\exp(-0.974R(1-Q)).Q^{\left(k+\frac{1}{2}\right)} \tag{12}$$

Fig. 5 shows the SIR as a function of cell radius for different values of the reuse number. As is seen, the SIR increases with increasing both R and N.

Since SIR has more than one minimum value, according to the signal to interference ratio which was obtained before for underwater channel, we have,

$$SIR \geq SIR_0$$

$$\Rightarrow -0.974R(1-Q) \geq \ln(6SIR_0Q^{-\left(K+\frac{1}{2}\right)})$$

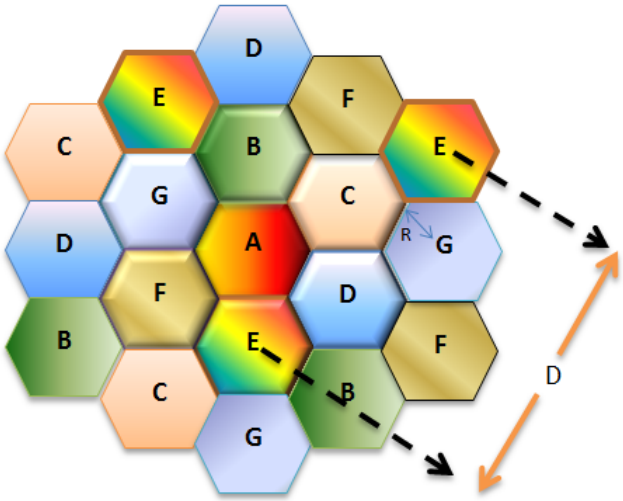

Fig. 4. Concept of cellular networks

Thus to satisfy the condition $SIR \geq SIR_0$ we should have

$$R \geq \frac{\ln(6SIR_0Q^{-\left(K+\frac{1}{2}\right)})}{-0.974R(1-Q)} = R_0(N) \tag{13}$$

In other words, in order that the SIR to be greater than the design value SIR_0, the cell radius should be greater than the minimum value of $R_0(N)$. The minimal cell radius depends on the reuse number N, and also on the required SIR and the system bandwidth.

The second system requirement is that W is greater than or equal to W_0 ($W \geq W_0$). For a given density of users ρ, the number of users per cell is $\rho\alpha R^2$, where $\alpha=\frac{3\sqrt{3}}{2}$ for the hexagonal cell geometry (α = π if the cells are modelled as circular). The bandwidth allocated to one cell is B/N, therefore, the bandwidth per user should satisfy

$$W = \frac{B/N}{\rho\alpha R^2} \geq W_0 \tag{14}$$

The above inequality shows that the cell radius should be less than some maximum value,

$$R \leq R_1(N) = \frac{1}{\sqrt{\alpha\rho}}\sqrt{\frac{B}{NW_0}} \tag{15}$$

Finally, the number of users in a cell should be greater than 1, otherwise the cellular concept is meaningless. This fact yields an additional condition

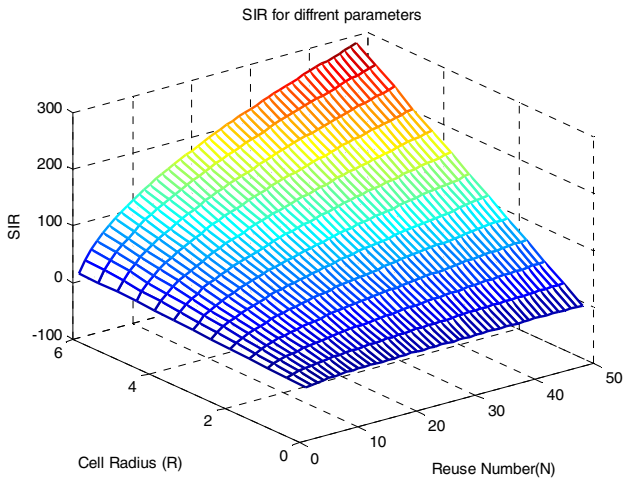

Fig. 5. Acoustic SIR for different Values of N and R

$$R \geq \frac{1}{\sqrt{\alpha\rho}} \tag{16}$$

Combining the conditions (13), (15) and (16), we find that the cell radius should satisfy

$$\overline{R}_0(N) = \max\left\{R_0(N), \frac{1}{\sqrt{\alpha\rho}}\right\} \leq R \leq R_1(N) \tag{17}$$

This expression defines the admissible region of R and N. Only those values of R and N that belong to this region constitute a valid design of underwater cellular network. Fig. 6 illustrates the admissible region for a system with ρ=1user/km^2, $B = 15\text{kHz}$, SIR_0=20dB, and W_0=0.14kHz. This region is bounded by $R_0(N)$, $R_1(N)$ and the straight line $\frac{1}{\sqrt{\alpha\rho}}$.

We observe that $R_1(N)$ decays faster than $R_0(N)$. The point at which $R_0(N)$ falls below $\frac{1}{\sqrt{\alpha\rho}}$, determines the maximal reuse number. For each admissible value of N, there is a range of cell radii that can be chosen to design the system. In practice, it is desirable to use a small value of N, because it facilitates the frequency allocation process and minimizes the loss incurred by insertion of necessary guard bands. However, we may want to choose somewhat greater than minimum to ensure a margin for the selection of the cell radius.

A slight change in the system requirement (SIR_0, W_0) may lead to a situation in which the range of solution becomes narrows, and also to situation in which there is no solution. These situations are illustrated in Fig. 7 for a system with $\rho = 0.35\text{user}/\text{km}^2$, $B = 60\text{kHz}$, $SIR_0 = 23\text{dB}$, and $W_0 = 3\text{KHz}$. Stricter performance requirements cause the admissible region becomes more narrow. Increasing SIR_0 causes R_0 to increase, and increasing W_0 causes R1 to decrease.

B. Number of Users and Bandwidth per User

Once the reuse number is fixed, the cell radius R can be chosen as any value between the minimum and the maximum. The choice depends on the system optimization criterion. A natural criterion is maximization of the number of users supported per Hz of occupied bandwidth [8].

$$C = \frac{\rho\alpha R^2}{B/N} \tag{18}$$

To maximize this quantity for a given value of N, under the constraints $SIR \geq SIR_0$ and $W \geq W_0$, the maximum value of the cell radius should be chosen, $R = R_1(N)$. With this choice we have,

$$\begin{aligned} C_{max} &= \frac{\rho\alpha R_1^2(N)}{B/N} \\ &= \frac{\rho\alpha\left(\frac{1}{\sqrt{\alpha\rho}}\sqrt{\frac{B}{NW_0}}\right)^2}{B/N} = \frac{1}{W_0} \end{aligned} \tag{19}$$

Whenever the cell radius is chosen greater than $R_0(N)$, the SIR will be greater than the design value SIR_0; when $R = R_1(N)$, the SIR will equal some $SIR_{max}(N)$. Alternatively, it may be desired that the per user bandwidth W be maximized. In that case, the smallest cell radius should be chosen, $R = \overline{R}_0(N)$. This selection results in the maximum value of W which is given by

$$\begin{aligned} W_{max}(N) &= \frac{B/N}{\rho\alpha_0\overline{R}_0^2(N)} \\ &= \frac{B/N}{\rho\alpha_0\left(\max\left\{R_0(N), \frac{1}{\sqrt{\alpha\rho}}\right\}\right)^2} \end{aligned} \tag{20}$$

Hence, depending upon the chosen value of N, the associated number of users per cell $U = \rho\alpha R^2$, depends on the cell radius. Fig. 8 illustrates the bounds on the quantity U for a system with $\rho = 0.35\text{user}/\text{km}^2$, $B = 60\text{kHz}$, SIR_0=20dB, and $W_0 = 900\text{Hz}$

IV. CAPACITY ANALYSIS

The fact that the range of admissible network topologies is determined by the desired user density (among other parameters) gives rise to the question of user capacity.

Acoustic communication channel capacity determines the maximum data rate that can be supported (theoretically) by an

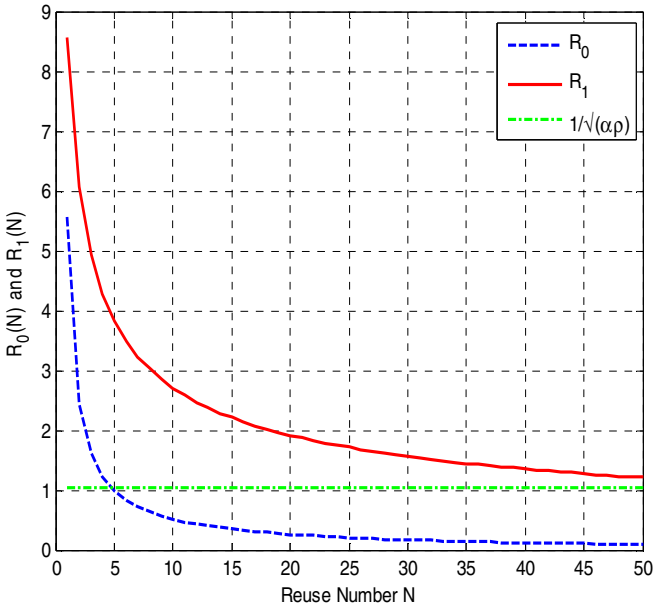

Fig. 6. Region of acceptable values (R,N)

acoustic channel for a given source power and source/receiver configuration. We define the capacity of an underwater acoustic cellular network as the maximal user density that can be supported within a given bandwidth. To assess the user capacity, we turn to the design condition (17). This condition implies that in order for a valid design to exist, the following inequality must hold

$$\bar{R}_0(N) \le R_1(N) \tag{21}$$

Substituting for $\bar{R}_0(N)$ and $R_1(N)$ this condition can be expressed in terms of the user density and the system bandwidth. In this manner, we observe that for any given, there are two possibilities: (a) $R_0(N) \le R_1(N)$ or (b) $\frac{1}{\sqrt{\alpha\rho}} \le R_1(N)$. If (a) is true, then in order for a solution to exist, condition (18) implies that the user density has to be $\rho \le (B/W_0)/\alpha N R_0^2(N)$. If (b) is true, then in order for a solution to exist, the bandwidth should be $B \ge NW_0$. Combining the two cases (a) and (b), we obtain the maximal user density that can be supported for a given N,

$$\rho_{\max}(N) = \begin{cases} (B/W_0)/\alpha N R_0^2(N) & B/W_0 \ge N \\ 0 & B/W_0 < N \end{cases} \tag{22}$$

We now define the system capacity as the maximum of conditional capacities $\rho_{\max}(N)$ taken over the reuse number N

$$\rho_{\max}(N) = \rho_{\max_N}(N) \tag{23}$$

Therefore the maximal user density depends explicitly on the bandwidth of the system and it also depends on the system requirements (SIR_0, W_0). Fig. 9 illustrates the maximum value of bandwidth per user.

V. Conclusion

Since the available bandwidth in underwater is severely limited, frequency reuse and cellular networks concepts are very important. Simple rules of cellular radio system design do not apply. The acoustic path loss depends both on the transmission distance and the signal frequency and thus it imposes a bound on the range of admissible cell radius and frequency reuse numbers N that can be used to meet the system requirements specified by the co-channel SIR and per-user bandwidth (SIR_0, W_0). Reuse number N and cell radius R must satisfy a set of constraints in order to constitute an admissible solution for a cellular network topology. The range of solutions depends on performance requirements and system parameters ρ and B. Relationships between various system parameters are complicate, but design rules are (relatively) simple. This constraint in turn implies a limitation on the overall user capacity, which is defined as the maximal density of users that can be supported within a given bandwidth B. Capacity increases as the operational bandwidth moves toward higher frequencies. We showed that there exists a a set of constraints that the cell radius and the reuse pattern R and N must satisfy in order to constitute an admissible solution for the cellular system topology. The constraints that acoustic propagation imposes on the system design, and consequently on its capacity, serve as a motivation for further research into the spatial reuse methods that will enable effective interference mitigation while remaining efficient in terms of both bandwidth and power usage [14].

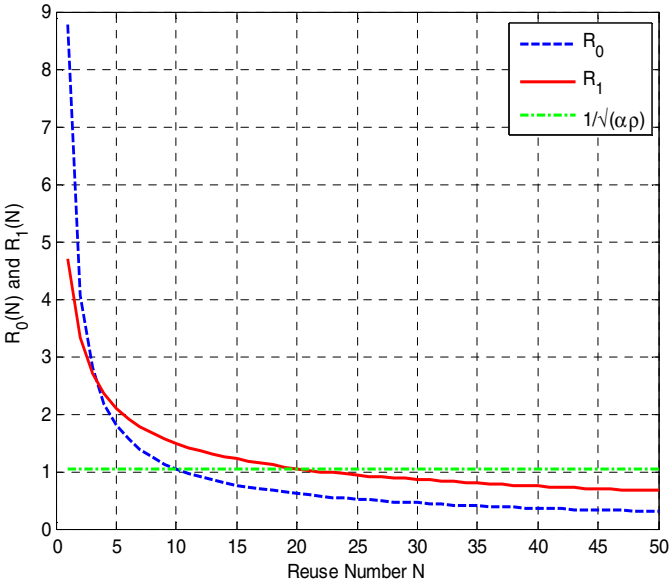

Fig. 7. Region of acceptable values (R, N) by changing the design parameters (SIR_0, W_0)

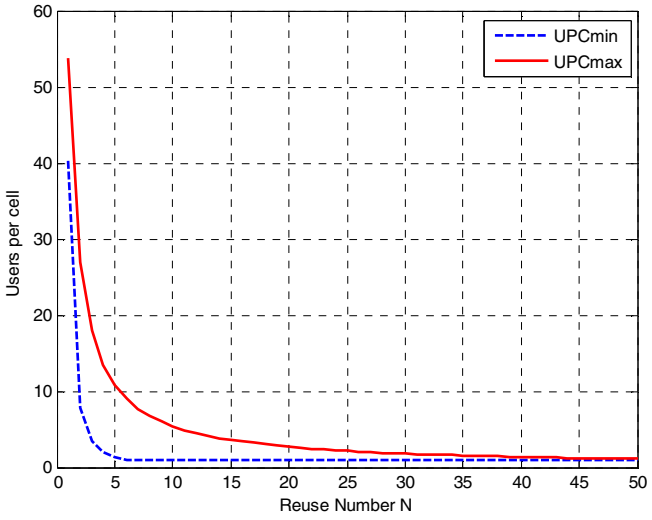

Fig. 8. Bounds on the number of users per cell U as a function of the reuse number N

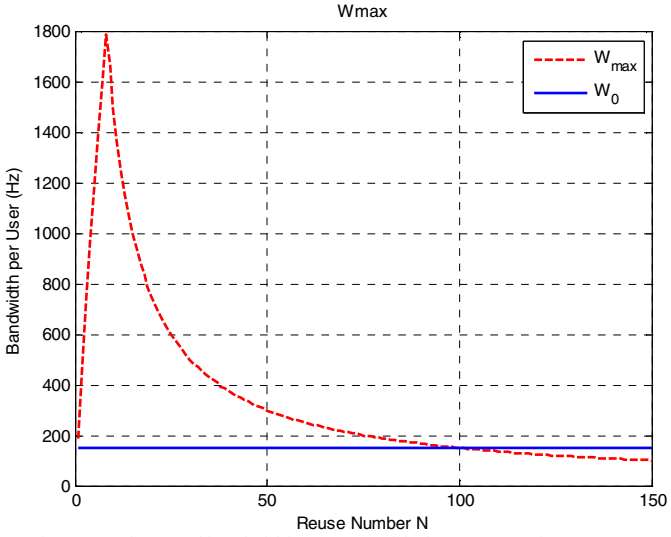

Fig. 9. Maximum of bandwidth per user with the reuse number

REFERENCES

[1] J. Preisig, "Acoustic propagation considerations for underwater acoustic communications network development," *ACM SIGMOBILE Mobile Computing and Communications Review*, vol. 11, no. 4, pp. 2-10, Oct. 2007.

[2] Z. Jiang, "Underwater Acoustic Networks – Issues and Solutions," in *Proc. IEEE Int. Conf. on Systems, Man and Cybernetics*, 2003.

[3] J. H. Cui, J. Kong, M. Gerla, and S. Zhou, "Challenges: Building scalable mobile underwater wireless sensor networks for aquatic applications," *IEEE Network, Special Issue on Wireless Sensor Networking*, vol. 20, no. 3, pp. 12-18, May/Jun. 2006.

[4] D. Pompili, T. Melodia, I.F. Akyildiz, "routing algorithm for delay-insensitive and delay-sensitive application in underwater sensor networks," *in Proc. of ACM Conference on Mobile Computing and Networking (MobiCom)*, Los Angeles, CA, September 2006.

[5] M. C. Domingo, R. Prior, "Energy Analysis of Routing Protocol For Underwater Wireless Sensor Networks," *Computer Communications*, vol. 31, no. 6, pp. 1227-1238, Apr. 2007.

[6] I. F. Akyildiz, D. Pompili, and T. Melodia, "Challenges for Efficient Communication in Underwater Acoustic Sensor Networks." *ACM Sigbed Review*, vol. 1, no. 2, Jul. 2004.

[7] D. pompili, T. Melodia, and l. F, Akyildiz, " Deployment Analysis In Underwater Acoustic Wireless Sensor Network," in *Proc. of ACM International Workshop on Underwater Networks*, Los Angeles, CA, USA, Sept. 2006 .

[8] M. Stojanovic, "On the Design of Underwater Acoustic Cellular Systems," in *Proc. of IEEE oceans 2007-Europe,* pp. 1-6, Jun. 2007.

[9] M. Cardei, "Energy-efficient scheduling and hybrid communication architecture for underwater littoral surveillance," *Computer communication*, vol. 29, no. 17, pp. 3354-3365, Jan. 2006.

[10] Paul C.Etter, Underwater Acoustic Modeling Principle, Techniques And Applicat ions. Elsevier Science Publishers, 1991.

[11] M. Stojanovic, "On the relationship between capacity and distance in an underwater acoustic channel," in *Proc. first ACM international workshop on Underwater Networks*, 2007.

[12] M. C. Domingo, R. Prior, "Energy analysis of routing protocol for underwater wireless sensor networks," *Computer communication*, vol. 31, no. 6, pp. 1227-1238, Apr. 2008

[13] T. S. Rappaport, *Wireless communications principles an practice*, Englewood Cliffs, NJ: Prentice-Hall, 1996.

[14] B. Sirnivasan, V. Rodoplu, "Capacity of Underwater Acoustic OFDM cellular Networks," in *proc. of IEEE oceans*, pp. 1-10, 2010.

Amirmansour Nabavinejad (S'12) was born in Isfahan, Iran, in 1978. He received B.S. and M.S. degrees in electrical engineering from Islamic Azad University of Iran, in 2003 and 2006, respectively. Currently he is a lecturer at Mohajer Technical University of Isfahan and Sepahan Institute of Higher Education, Isfahan, Iran. His research interests are in Digital Communications, Signal Processing Applications, Information Theory, Coding, Underwater Data Transmission, Acoustic Channel Modeling, Acoustic Imaging and Cellular Networks.

Samar Shahabi Ghahfarokhi was born in Isfahan, Iran, in 1984. She received the B.S. degree in electrical engineering (Electronics) from Yazd University, Yazd, Iran, in 2007. Currently, she is working toward the M.S. degree in the Faculty of Electrical Engineering and Information Technology, Ilmenau University of Technology, Ilmenau, Germany. Her research interests include Telecommunication Systems, Information Theory, Data Communication Networks, Cellular Networks, Digital Signal Processing, and Digital Image Processing.

Research on the Scheme and Performance of Linear SA in CDMA Application

Jijiang Chen[1], Jing Zhou[2], Jianfeng Lu[3]

1.Nanjing University of Posts and Telecommunications, Nanjing P.R. China
2.PAP Division of XX city, Nanjing P.R. China
3.The XX Regiment of The Air Force, Nanjing P.R. China
chenjijiang060703@126.com, angelazj928@vip.qq.com, air_jerry@yahoo.cn

***Abstract*—Firstly, this paper researches on the scheme of amplitude weighting(AW) for smart antenna(SA) beam-forming in linear array. With the proposed mathematical model in this paper, QPSK base-band AW is an effective method for linear SA to realize multi-user and multi-direction transmission, by which the perfect directional beam-forming can be realized with low complexity and low cost. Secondly, this paper analyses the performance of linear SA with 6 array elements(AEs) in different application scenarios. Compared with carrier phase-shifting, the implementation scheme of beam-forming by AW has the feature of easy to implement and high reliability, so that the popularization and application of SA is possible.**

Keyword-smart antenna (SA); beam-forming; amplitude weighting (AW); QPSK;6 array elements(AEs)

I. INTRODUCTION

Recently, smart antenna(SA) application in CDMA mobile communication system is a very important research direction as well as the basis of future multiple-input multiple-output(MIMO) system. Consequently, the application research of SA has great practical value. SA, based on the phase-controlled antenna array(PCA) technique, is an effective method to increase the frequency and power efficiencies for mobile communication systems. With the directional beam-forming of SA, we can realize the instant tracking and orientation for mobile terminals in a cellular mobile communication system. In CDMA mobile communications system, generally, due to the complexity of realization, SA is mainly employed in base station transceiver. To perform the perfect directional beam-forming, the direction of arrival (DOA) of mobile station (MS) signal should be acquired firstly from uplink, and then with this DOA the directional beam-forming of downlink is possible.

The effect of space division multi access (SDMA) formed by SA directional receiving and transmission is expected to be utilized to separate multi access interference (MAI) and multi path interference (MPI) in CDMA system, which can improve system spectrum utilization greatly and increase the number of users in a given channel bandwidth or CDMA code-channel. The effect of SA SDMA is originated from the directional reception and transmission principle of phase controlled array antenna. If directional reception and transmission is to be realized in base station (BS), DOA of MS must be known.

Reference [1] states that it could realize downlink beam-forming in base-band after the direction of arrival (DOA) estimation in the uplink, but it has not given the implementation scheme of beam-forming with QPSK base-band signal. Reference [2] presents the block diagram of downlink beam-forming, which is base-band weighting and can form k-beam. Pointing out in [3, 4, 5, 6], the directional transmission of SA can be achieved with the method of beam-forming by base-band weighting, but the specific implementation principle and implementation method has not been shown. Many authoritative monographs [7, 8, 9, 10] on SA only give the principle of PCA, i.e. the basic method of directional transmission by carrier phase-shifting weighting. Literatures [11, 12, 13, 14] on downlink beam-forming only give the interrelated matrix solutions of downlink beam-forming, and have not given the relation among the interrelated matrix solutions, DOA and the direction vector of SA or the related processing. Many patents [15, 16, 17, 18] related to TD-SCDMA system also remain at the level of matrix solutions. One chief engineer of ZTE R&D center has said in [19] "In addition, comparing to extensive research of uplink adaptive beam-forming technique, the downlink performance has become the 'bottle-neck' for the systems performance, so that there is an urgent need for the method of effective downlink adaptive beam-forming." The top authority [20] of TD technique said "The current application of SA technique is an initial state of multi-antenna technique. In the future it will become more powerful multi-antenna technique, which would have the functions of beam-forming, space-time multiplexing (i.e. MIMO) and SDMA." Therefore, it has been shown in those patents and articles that the research on SA in CDMA basically remains at the stage of theoretical research by mathematics, which sharply does not match the conclusion that SA has been widely used in mobile communication system for TD-SCDMA.

Owing to the difficulty in realizing the accurate phase-shifting in the radio frequency and the large output of side

lobe and insertion loss introduced by radio frequency power amplifier, people think that beam-forming by base-band weighting is an effective method for SA to realize directional transmission, while the relevant literature about the principle or method of beam-forming by base-band weighting have not been found.

Firstly, this paper gives the direction vector of SA and its principle of downlink beam-forming, and then derives an equivalent expression of beam-forming by amplitude weighting (AW) based on that by phase-shifting weighting (PW) in line array. According to the expression, we can derive the schematic diagram, which uses the QPSK signal by AW to achieve the beam-forming for SA in line array. The correctness of scheme will be proved by the simulation results. It also shows some simulation performance of 6-AE in line array in the CDMA application. Compared with carrier phase-shifting, the implementation scheme of beam-forming by AW has the feature of easy to implement and high reliability, so that the popularization and application of SA is possible.

II. DIRECTION VECTOR OF SA AND ITS PRINCIPLE OF DOWNLINK BEAM-FORMING

Structure of even line array is illustrated in Figure 1. Assuming that the angle between the normal plane and the receiving signal is φ, then the delay of the receiving signals between the neighboring two AEs is $d\sin\varphi$, correspondingly, the phase between them is $\frac{2\pi}{\lambda}d\sin\varphi$. Making the phases of receiving signals by each AE respectively $[\varphi_1,\varphi_2\cdots\varphi_N]$, we can draw the schematic diagram of carrier phase-shifting weighting for beam-forming, shown in Figure 2, where

$$\varphi_n=\frac{2\pi}{\lambda}(n-1)d\sin\varphi\ ,\ n=1,2,\cdots N \tag{1}$$

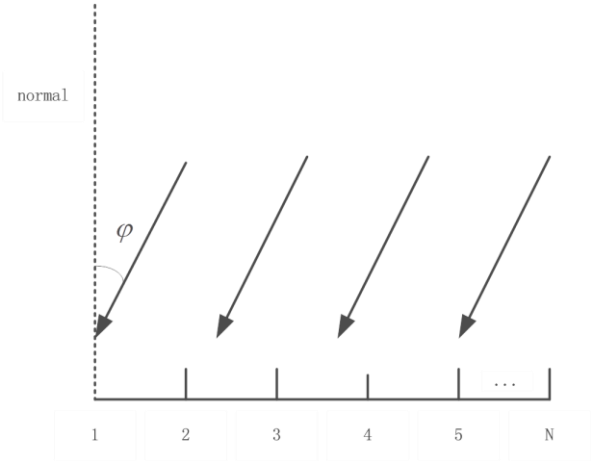

Fig.1. Diagram of even linear array

φ_n is regarded as the intrinsic phase of the nth AE, which is related to the array position and the DOA of signal, i.e. φ. The values of phase-shifter inserted are respectively $[-\varphi_1,-\varphi_2\cdots-\varphi_N]$, used to offset the impact of the intrinsic phase, shown in Figure 2. Assuming that the receiving signal of the first AE is $S(t)=\cos wt$, and then the formula of the phase-shifting weighting signal is as follows:

$$\begin{aligned}S_r(t)&=\cos(wt+\varphi_1-\varphi_1)+\cos(wt+\varphi_2-\varphi_2)+\cdots+\cos(wt+\varphi_N-\varphi_N)\\&=N\cos wt\end{aligned} \tag{2}$$

If the impact of noise is not considered temporarily, the gain of beam-forming for SA, i.e. $G_{SA}=20\lg N(dB)$ can be obtained. Because φ_n is related to the DOA, when the value of the phase-shifter is determined, G_{SA} is related to the number of code channel, thus, forming the function of directional receiving, which is regarded as the diversity reception of array antenna.

The schematic diagram in Figure 2 can also be used to understand the principle of beam-forming for transmitting. Assuming that the transmitting carriers are the same frequency and the phase-shifters are not introduced, the transmitting carrier exist the phase difference. Otherwise, there is no phase difference and can realize the diversity transmitting.

Customarily, the intrinsic phase parameters of SA above can be expressed by the complex formula, that

$$\phi=[1,e^{-j\frac{2\pi}{\lambda}d\sin\varphi},\cdots,e^{-j\frac{2\pi}{\lambda}(N-1)d\sin\varphi}] \tag{3}$$

Frequently, the parameters above are called the direction vector of SA, which are necessary and sufficient parameters for SA. Making the weighting parameter of the receiving signal is

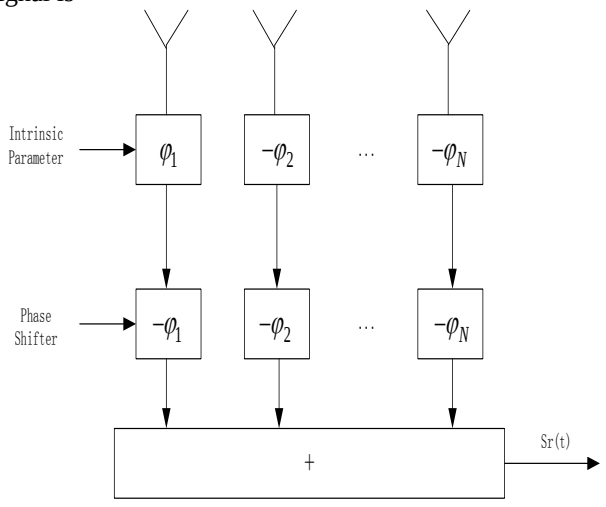

Fig.2. Schematic diagram of carrier phase-shifting weighting for beam-forming

$$w=[1,e^{j\frac{2\pi}{\lambda}d\sin\varphi},\cdots,e^{j\frac{2\pi}{\lambda}(N-1)d\sin\varphi}] \tag{4}$$

Thus,

$$Sr(t) = \sum w_n S(t) e^{-j\varphi_n} = NS(t) \quad (5)$$

Consider that the high angle θ has an impact on DOA in Figure 3, where θ is an intersection angle of DOA and array plane. And then the delay of the receiving signals between the neighboring two AEs is $d \sin\varphi \sin\theta$, correspondingly, the phase between them is $\frac{2\pi}{\lambda} d \sin\varphi \sin\theta$. The direction vector of SA is as follows:

$$\phi = [1, e^{-j\frac{2\pi}{\lambda} d \sin\varphi \sin\theta}, \cdots, e^{-j\frac{2\pi}{\lambda}(N-1) d \sin\varphi \sin\theta}] \quad (6)$$

For convenience, the impact of high angle θ is not considered.

The schematic diagram of beam-forming for multiple-direction in downlink is shown in Figure 4. In the condition of directional transmission in downlink, it needs to detect the user's DOA and then make sure the direction vector of SA., which is the sufficient parameter to realize the directional transmission.

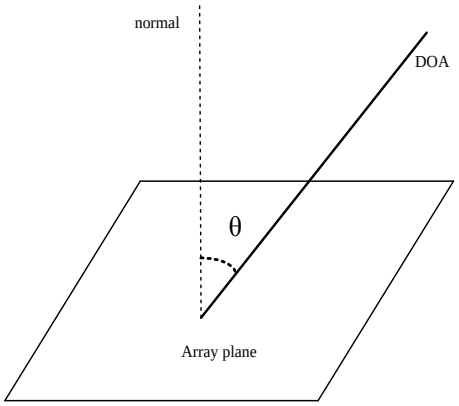

Fig.3. High angle's impact on DOA

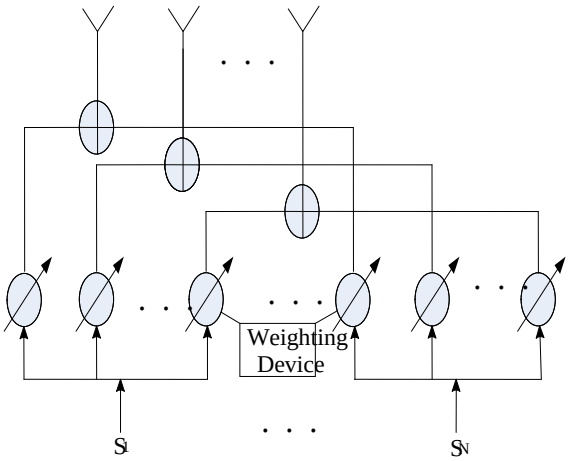

Fig.4. Schematic diagram of beam-forming for multiple-direction in downlink

In the condition of multi-user and multi-direction transmission, the PCA gives the basic principle of beam-forming, i.e., feeding a different phase current into each AE by inserting a phase-shifter in each AE circuit system, so that the radio waves given by each AE are able to realize superposition in phase, and then form the synchronism diversity transmitting gain of some specific direction.

III. THE IMPLEMENTATION SCHEME OF BEAM-FORMING BY AMPLITUDE WEIGHTING

The two carrier signals for orthogonal modulation in QPSK modulation can be shown as following:

$$\sin(wt - \theta) \text{ , } \cos(wt - \theta) \quad (7)$$

Their corresponding complex formulas can be written as:

$$\mathrm{Re}[e^{jwt} e^{-j\theta}] \text{ , } \mathrm{Im}[e^{jwt} e^{-j\theta}] \quad (8)$$

According to the above complex formulas of orthogonal carrier, the following formulas are derived

$$\begin{aligned} \cos(wt - \theta) &= \mathrm{Re}[e^{jwt} - e^{-j\theta}] \\ &= \mathrm{Re}[e^{-j\theta}] \cos wt - \mathrm{Im}[e^{-j\theta}] \sin wt \end{aligned} \quad (9)$$

$$\begin{aligned} \sin(\omega t - \theta) &= \mathrm{Im}[e^{j\omega t} e^{-j\theta}] \\ &= \mathrm{Im}[e^{-j\theta}] \cos \omega t + \mathrm{Re}[e^{-j\theta}] \sin \omega t \end{aligned} \quad (10)$$

According to the expressions above, the circuit diagram of directional transmission for SA realized by AW can be derived.

Circuit structure unit of a modulator is illustrated in Figure 5. The upper part in figure 5 is for the realization given by $\cos(wt - \theta_{mn})$, which realizes the I-phase space-frequency modulation and results in the I-phase carrier phase-shift with θ_{mn}. Where θ_{mn} is the carrier phase-shift of the mth subscriber signal in the nth AE. $I_m(t)$ is the input data of I-phase path in downlink QPSK modulator, which is the chip information stream of the input data spread and scrambled. The real part and image part of weighted coefficient w_{mn} generated by the generation circuit are

$$\mathrm{Re}(w_{mn}) = \mathrm{Re}[e^{-j\theta_{mn}}] \quad (11)$$

$$\mathrm{Im}(w_{mn}) = \mathrm{Im}[e^{-j\theta_{mn}}] \quad (12)$$

Thus,

$$\mathrm{Re}[w_{mn}] = \cos[-\pi(n-1)\sin\varphi_m] \quad (13)$$

$$\mathrm{Im}[w_{mn}] = \sin[-\pi(n-1)\sin\varphi_m] \quad (14)$$

φ_m is the DOA of the mth user.

IV. IMPLEMENTATION SCHEME OF BEAM-FORMING BY AMPLITUDE WEIGHTING IN MULTI-DIRECTION

In the third section, we obtain the circuit unit of QPSK modulator based on the fundamental of baseband beam-forming. It can be seen that the modulation process of each path signal I-phase or Q-phase includes two independent processes: space-domain modulation and frequency-domain modulation. In this section, we discuss the beam-forming method of multiple subscriber directions based on the modulator circuit unit proposed. The simplified model of QPSK modulator is given. From Figure 5, in the modulator scheme, space domain modulation signal (11) and (12) of each user is different with the result of different DOA for different subscriber m. But two orthogonal signals $\cos(wt)$ and $-\sin(wt)$ are same not only for the signals of I-phase path and Q-phase path but also for each subscriber. Thus, a simplified circuit structure is obtained as shown in Figure 6. In the simplified circuit structure, adders M_{n1} and M_{n2} contain all space domain modulators needed by each user, while multipliers M_{n3} and M_{n4} only contain two frequency modulators respectively as shown in Figure 5.

For the mth user data in Figure 6, I_{Im} and $I_{Q\mathrm{m}}$ denote the input signal of I-phase path; Q_{Im} and $Q_{Q\mathrm{m}}$ denote the input signal of Q- phase path. With the simplified circuit shown in Figure 4.Base-band beam-forming circuit needed with N transmission directions can be drawn,shown in Figure7.

The circuit block of baseband QPSK modulation beam-forming of N subscribers is given in Figure 7.

The generation process of N baseband modulation signals is similar with Figure 5.

V. THE SIMULATION RESULTS

There are different scenarios in which a signal with one or multi code channel transmits to the same direction, or multi code channels transmits to different direction, the effect of beam-forming from QPSK modulation data of every code channel will be considered in these scenarios. We have found that the polarity of QPSK modulation data in multi-channel parallel transmission will have great impact on the beam diagram of SA directional transmission.

Based on the above modulation beam-forming scheme, some simulation results are presented in this section, with simulation software matlab 7.0. Assuming that SA is a N=6 element line array with the AE space of $\lambda/2$.

Beam pattern for a code channel is shown in Figure 8. Figure 8 (a) and Figure 8 (b) respectively give the beam pattern of QPSK modulator for I and Q paths with the same data values in the direction of 90° and 30° ,where data of I path denotes the data stream $\mathrm{I}_m(t)$ after series parallel transformation, as well as that of the Q path. Because the carriers of I and Q are orthogonal, the values of data I and Q have no impact on beam diagram formed by SA. By figure 8 for the directional beam of single code channel in single direction by using 6-AE in line array, better performance could be achieved by tracking the mobile station. RAKE receiver is unneeded for that situation.

Beam pattern for two code channels and two directions is shown in Figure 9. The direction of beam slightly offsets in the direction of 30° in Figure 9 (a), when the data of 2-user fed to I path and Q path is same. It is also shown that amplitudes of two directions have a slight increase, which may be caused by introducing adjacent beam interference. While the data is opposite, the amplitudes of beam have a big drop, shown in Figure 9 (b), whose impact waiting for further study.

Beam pattern for two code channels is shown in Figure 10, which is in the direction of $60^{\circ}$and 45°. Because of less phase difference between them, the two beams can be superimposed as one. When the data of 2-user is opposite, the amplitude of beam changes slightly.

Beam pattern is given in Figure11 (a),in the direction of 30°、60°、90°、120°、150° ,where the transmitting data of each code channel is"1".If the transmitting data of $I_1 = Q_1 = -1$ is "-1" and the other is "1", the beam pattern is given in Figure 11 (b).

The simulation results above are satisfied with the requirement of infinite reflector, and also it requires that there is no beam existing in the opposite direction. However, it is difficult to satisfy the above condition in practical application.

The simulation results in the case of no-reflector are shown in Figure 13 (a), Figure 13 (b), Figure 14 (a)and Figure 14 (b) .

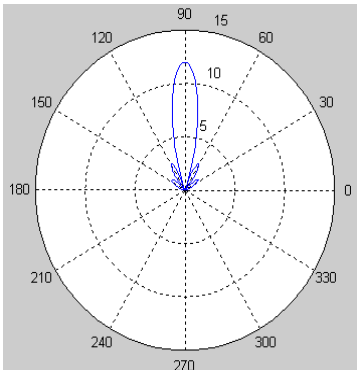

Fig. 8 (a) Direction of 90°

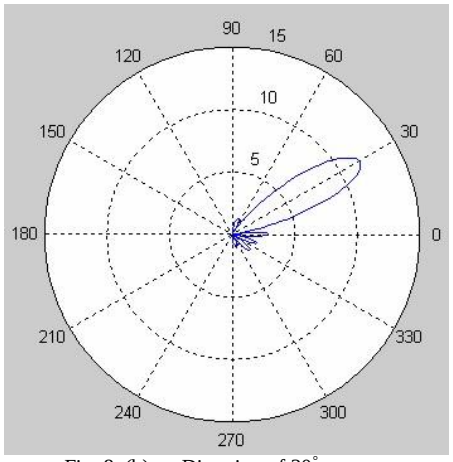

Fig. 8 (b) Direction of 30°

Fig.8. Beam pattern of single-user and single-direction.

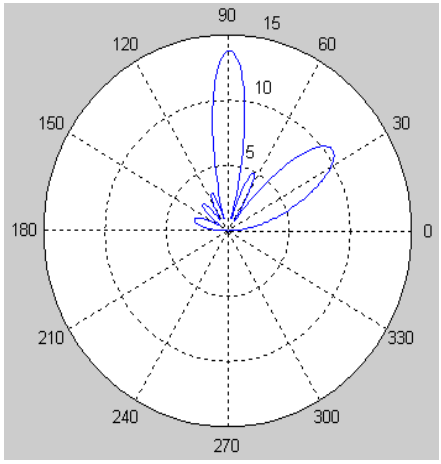

Fig. 9 (a) $I_1 = I_2 = 1\ Q_1 = Q_2 = 1$

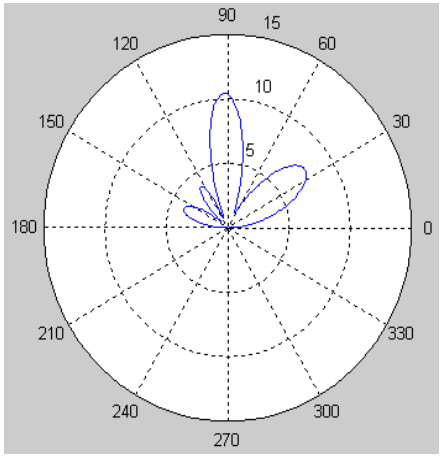

Fig. 9 (b) $I_1 = -I_2 = 1\ Q_1 = -Q_2 = 1$

Fig.9. Beam pattern of two-user and two-direction

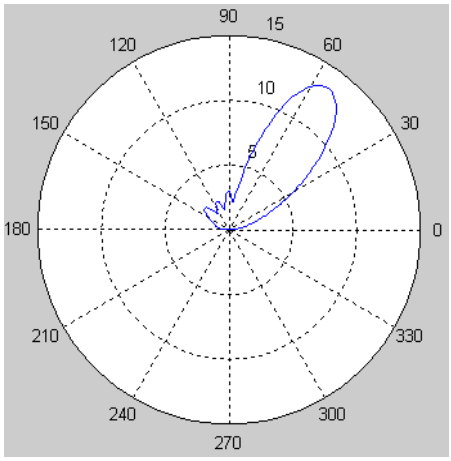

$I_1 = I_2 = 1\ Q_1 = Q_2 = 1$

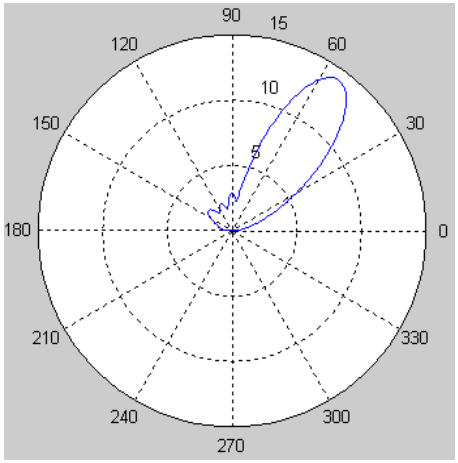

$I_1 = -I_2 = 1\ Q_1 = -Q_2 = 1$

Fig.10. 2-user and direction differs 15°

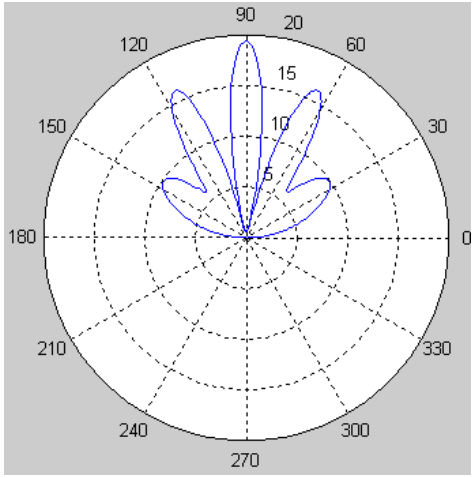

Fig. 11 (a) All transmission data "1"

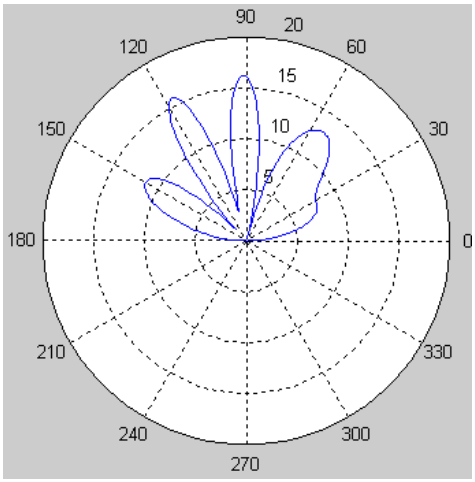

Fig. 11 (b) I_1= Q_1=-1, the other data "1"

Fig.11. Result of 5-direction

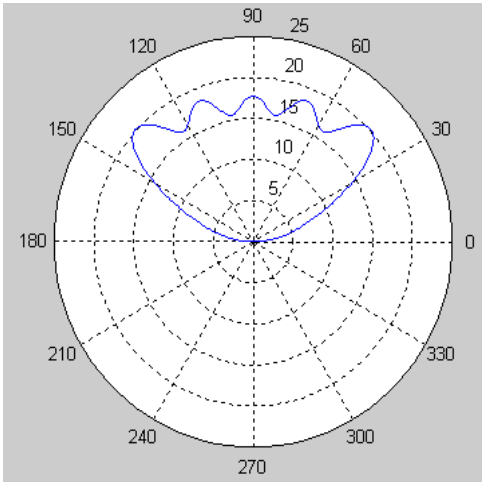

Fig.12. Result of 9-direction

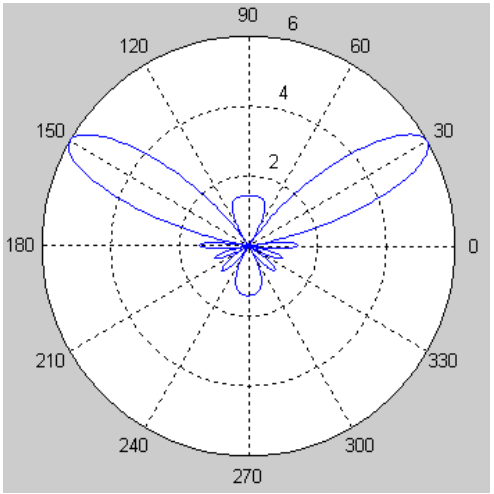

Fig. 13 (a) Direction of 30°

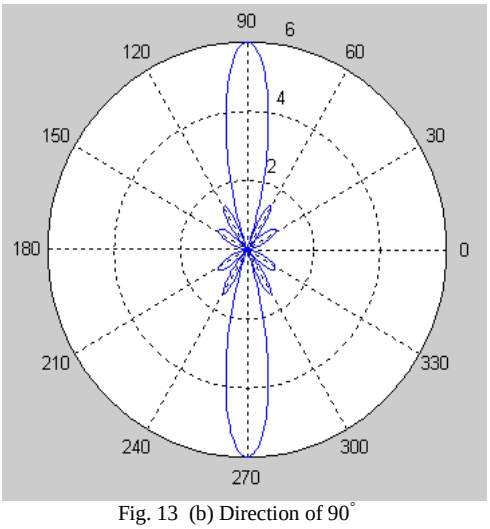

Fig. 13 (b) Direction of 90°

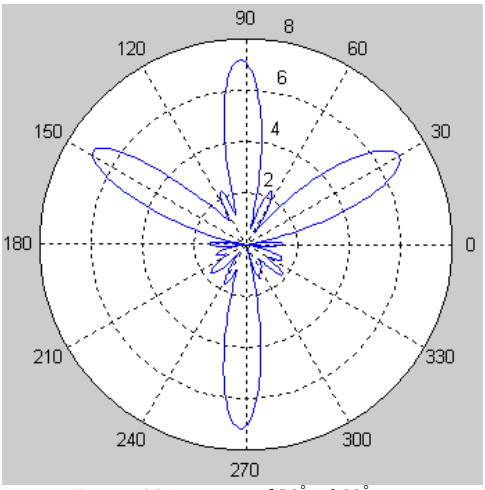

Fig. 14 (a) Direction of 30° and 90°
$I_1 = I_2 = 1 Q_1 = Q_2 = 1$

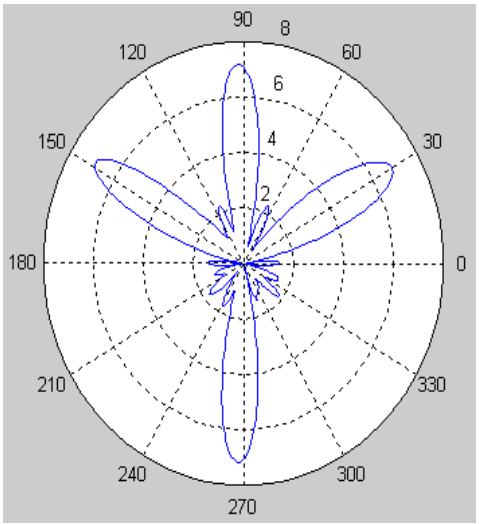

Fig. 14 (b) Direction of 30° and 90°
$I_1 = I_2 = 1 Q_1 = Q_2 = -1$

VI. CONCLUSIONS

This paper has studied the scheme and performance of linear SA with 6-AE in different application scenario in detail. With a reflector and in the situation of single direction and signal code channel, there is no MAI and MPI in the system , so the RAKE receiver is not needed.When the number of directions and code channels increases,the scheme still has a good performance.Considering that the moderate direction is the necessary condition for CDMA system maintaining stable working, it is founded that the stability of SA CDMA system is not well in the condition of transmitting to multi-direction when the direction is very near. With no-reflector,there is always another beam in the opposite. In a word,compared with carrier phase-shifting, the implementation scheme of beam-forming by AW is easy to ensure stable system performance when linear SA with 6-AE is introduced to TDD-CDMA system.

REFERENCES

[1] *Zhongxing Telecommunication Equipment Co., Ltd, Principle and realization of ireless System for TD-SCDMA , Posts & Telecom Press, 2007.12*

[2] *Liang Ma, Smart Antenna for Wireless Communications IS-95 and Third Generation CDMA Applications [M], China Machine Press, 2002.8*

[3] *Ayman F.Naguib and Aroryaswami Paulraj, Capacit Improvement with Base-Station Antenna Arrays in Celluar CDMA[J]. IEEE Trans. on Vehicular techn, 2000,43(3):691-698.*

[4] *Ayman F.Naguib, Aroryaswami Paulraj and Thomas Kailath, Performance of CDMA Cellular Networks with Base-Station Antenna Arrays: the Downlink [J]. IEEE 1994*

[5] *Hsueh-Jyh Li and Ta-yung Liu, Comparison of Beamforming Techniques for W-CDMA Communication Systems [J]. IEEE Trans.on Vehicular techn, vol.52. NO.4.July 2003*

[6] *Klaus Ingemann Pedersen, Preben Elgaard Mogensen and Juan Ramiro-Moreno,Application and Performance of Downlink Beam-forming Techniques in UMTS [J].IEEE Communications Magazine. October 2003*

[7] *Nanjing Institute of Electronic technology, Phase-Controlled Array Antenna handbook [M], Electronic Industry Press, 2008.1*

[8] *Ming Liu, Chaowei Yuan, the Technology and Application of Smart Antenna [M], China Machine Press, 2007.1*

[9] *Wei Yang, Junshi Chen, Array Antennas Technology in Mobile Communication [M], Tsinghua University Press, Beijing Jiaotong University Press, 2005.10*

[10] *Ahmed El Zooghby, Smart Antenna Engineering [M], 2005 ARTECH HOUSE,INC., Norwood*

[11] *Josef Johannes Blanz, Apostolos Papathanassion, "Smart Antennas for Combined DOA and Joint Channel Estimation in Time-Slotted CDMA Mobile Radio Systems with Joint Detection," IEEE transactions on vehicular technology, Vol.49, No.2, 2000*

[12] *Shaoli Kang, Shihe Li ,Algorithm of Downlink Beam-Forming Based on Uplink Parameter in TD-SCDMA System [J], Journal of China Institute of Communications, 2002, 23(8): 67-71.*

[13] *Qunying Wu, Shihe Li, Downlink Beam-forming in TD-SCDMA System for Time delay spread and angle spread channels[J], Signal Processing, 2002,18 (5): 427-430..*

[14] *Seungwon Choi, Donghee Shim, A Novel Adaptive Beam-forming Algorithm for a Smart Antenna System in a CDMA Mobile Communication Environment [J]. IEEE Trans. on Vehicular techn,Vol.49.NO.5, September 2000, PP:1793-1806*

[15] *Datang Mobile Communication Equipment Co., Ltd, the Method of Beam-forming for SA and Base-band Signal Processor, China Patent No. 200710098415.7*

[16] *Zhongxing Telecommunication Equipment Co., Ltd, one Generating Method of Sending Weight on Multi-user Beam-Forming, China Patent No. 200810145717.X*

[17] *Dingqiao Telecommunication Technology Co., Ltd (HuaWei), one Method of Downlink Beam-forming in TDD System, China Patent No.200710119516.8*

[18] *Putian Information technology Research institute, one Method of Beam-forming Combining Space with Time , China Patent No.200510059383.0*

[19] *Yanwen Wang, Current Research and Development of Beam-forming for SA, Zhongxing Telecommunication Technology, 2003.6*

[20] *Developing Smart Antenna Technology of TD-SCDMA with Strong Determination—An Interview to Shihe Li-the Father of TD-SCDMA Standard,Telecommunication Technology, 2008.3,pp.11-12, www.ttm.com.cn*

AUTHOR'S PICTURE & BIOGRAPHY

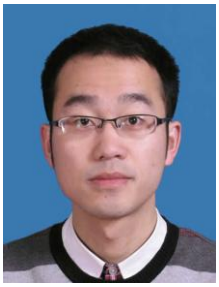

Jijiang Chen, male, from Shaoxing, Zhejiang, is graduated from College of Telecommunications and Information Engineering, NJUPT in 2010, and currently pursuing the master degree at NJUPT.Research areas are the mobile Internet, Mobile communications and wireless technology.
Email:chenjijiang060703@126.com

Jing Zhou, female, from Nanjing, Jiangsu, is graduated from College of Telecommunications and Information Engineering, NJUPT in 2010, and currently working in the PAP Division of XX city.
Email:angelazj928@vip.qq.com

Jianfeng Lu, male, from Suzhou, Jiangsu, is graduated from Harbin Flight Academy, and currently working in the XX *Regiment of The Air Force.*
Email:air_jerry@yahoo.cn

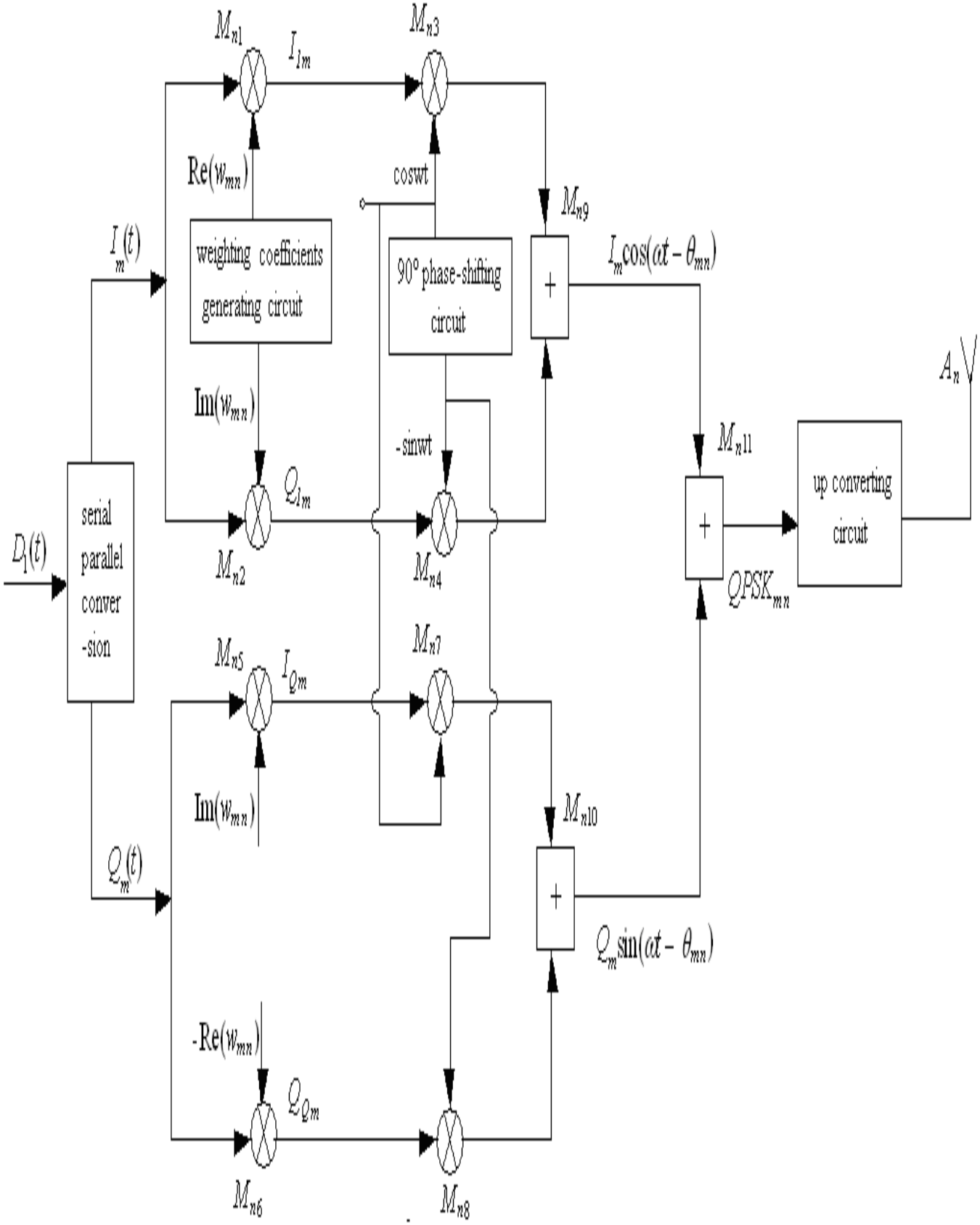

Fig5. Beam-forming modulator circuit unit

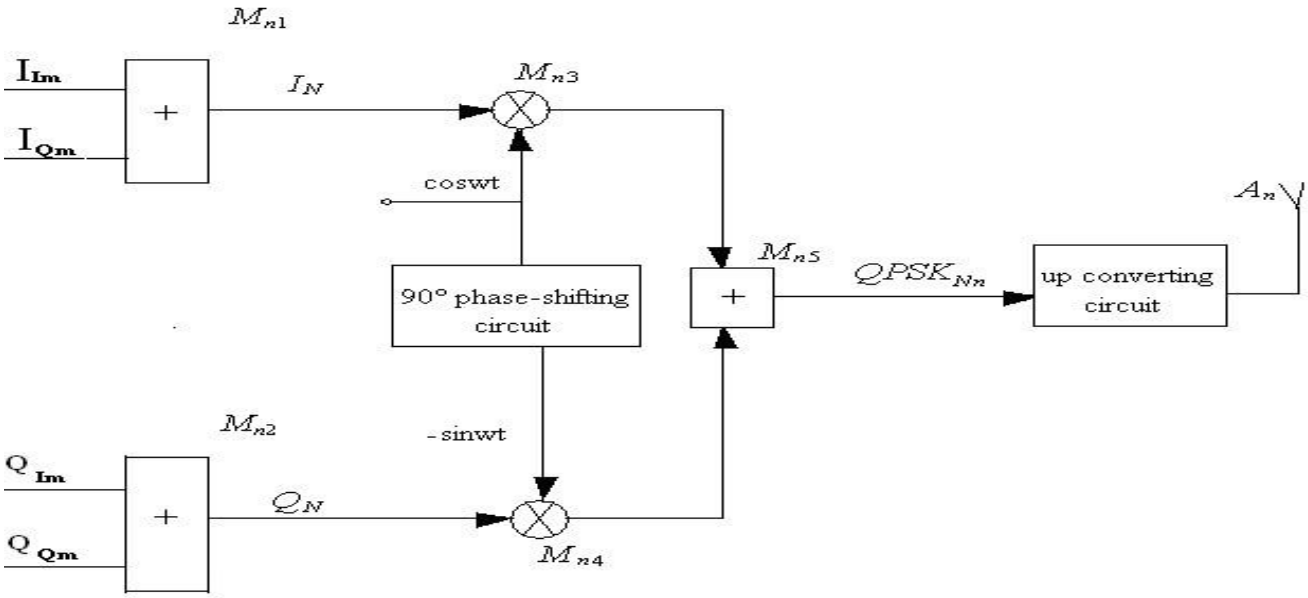

Fig.6. Simplified form of the QPSK modulation

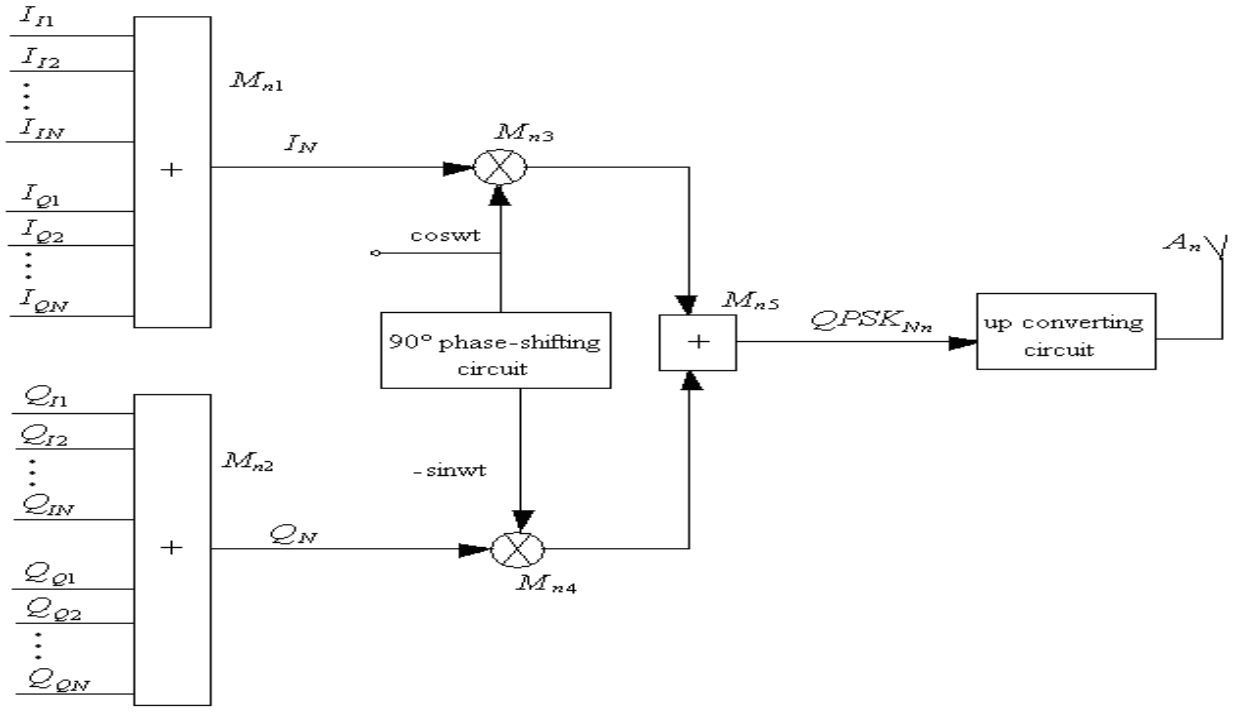

Fig.7. N-direction modulation beam-forming

Point-to-Multipoint and Multipoint-to-Multipoint Services on PBB-TE System

Wonkyoung Lee*, Chang-Ho Choi*, Sun-Me Kim*

*Optical Internet Research Department, Electronics and Telecommunications Research Institute, 161 Gajeong-dong, Yuseong-gu, Daejeon, 305-350, Korea

wklee@etri.re.kr, chhchoi@etri.re.kr, kimsunme@etri.re.kr

***Abstract*— We have implemented point-to-multipoint (PtMP) and multipoint-to-multipoint (MPtMP) services on a packet transport system (PTS) based on PBB-TE. The point-to-multipoint (PtMP) connection in the PBB-TE system has been realized by grouping point-to-point (PtP) packet transport layer (PTL) trunks and mapping a BSI onto the PtP PTL trunks using a multicast backbone destination address. For providing different capabilities for service selection and priority selection, the PTS offers customers three basic types of the port-based, C-tagged, and S-tagged service interfaces defined by the IEEE 802.1ah. To offer customers different capabilities of the layer 3 applications and services, moreover, an IP-flow service interface have been added. In order to evaluate traffic performance for PtMP services in the PTS, the PtMP throughputs for the link capacity of 1 Gbps at the four service interfaces were measured in the leaves of the ingress edge node, the transit node, and the egress edge node. The throughputs were about 96% because the B-MAC overhead of 22 bytes occupies 4 % of the 512-byte packet.**

***Keyword*— Point-to-multipoint, multipoint-to-multipoint, packet transport system, PBB-TE, MAC-in-MAC encapsulation, service interface**

I. INTRODUCTION

THE network has been evolved into simpler and more efficient structure since demands for bandwidth in today's network have been increased rapidly. In this situation, SDH/SONET platforms are being replaced by packet transport platforms as in reference [1]. The packet transport technology such as Provider Backbone Bridge – Traffic Engineering (PBB-TE) and MPLS Transport Profile (MPLS-TP) is getting the spotlight as a key point of the next generation network. Provider backbone bridge – traffic engineering (PBB-TE) defined by IEEE 802.1Qay [2] is representative carrier Ethernet transport technology that extends well-known and widely distributed Ethernet services to core of the public network while maintaining simplicity, flexibility, and cost effectiveness of the Ethernet service [3]. The PBB-TE adds transport hierarchy of MAC-in-MAC encapsulation to Ethernet frames and provides traffic engineering for connection-oriented paths and protection switching within 50 ms.

In the next generation network, the PBB-TE technology should provide multicast video streaming services and support traffic engineering for end-to-end label switched paths. There have been no proper solutions to multicast services on packet transport platforms based on PBB-TE so far [4] since the PBB-TE technology does not allow MAC learning, spanning tree protocol, and broadcast of unknown frame for providing deterministic, protected, and connection-oriented trunks and services. Moreover, it has not been easy to classify layer 3 applications and services due to layer 3 service transparency of the carrier Ethernet transport. In this study, we propose a solution to multicast services and IP flow awareness that have been weak points of PBB-TE technology. We have implemented a packet transport system (PTS) based on the PBB-TE. The PTS provides multicast services of PtMP and MPtMP and IP flow awareness. In order to evaluate the performance of the PtMP services on the PTS, we have measured traffic throughputs for the link capacity of 1 Gbps at port-based, C-tagged, S-tagged, and IP-flow service interfaces.

Manuscript received October 10, 2012. This work was supported by MKE. under Development of Packet-Optic Integrated Network Transport Technology 2008-S-009-02.

The authors are with Optical Internet Research Department, Electronics and Telecommunications Research Institute, 161 Gajeong-dong, Yuseong-gu, Daejeon, 305-350, Korea. (phone: +82-42-860-6519; fax: +82-42-860-1495; e-mail: wklee@ etri.re.kr).

II. PACKET TRANSPORT SYSTEM BASED ON PBB-TE

As shown in Fig. 1, a PBB-TE network comprises a set of backbone edge bridges (BEBs) and backbone core bridges (BCBs) that are connected by Ethernet tunnels referred as Ethernet switched paths (ESPs) [2]. Backbone edge bridges are responsible for adding transport hierarchy to customer frames in ingress edge nodes and restoring customer frames by removing the transport hierarchy in egress edge nodes. Backbone core bridges in transit nodes are responsible for swapping transport label or backbone VLAN identifier (B-VID). Each ESP as a connection-oriented path is identified by the triplet of a backbone source address (B-SA), a backbone destination

address (B-DA), and a B-VID. The ESP is also called a packet transport layer (PTL) trunk. The PTL trunk is provided by an external management system.

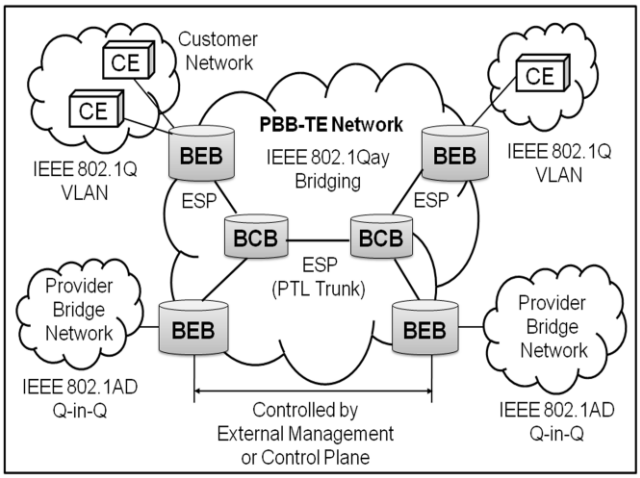

Fig. 1. The PBB-TE network

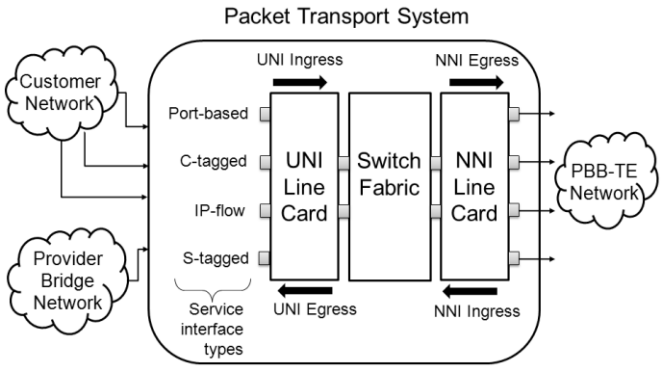

Fig. 2. The structure of the packet transport system based on PBB-TE

Figure 2 is the structure of the packet transport system based on the PBB-TE that has been implemented. The PTS consists of user network interface (UNI) line cards, network to network interface (NNI) line cards, and a switch fabric that connects between the UNI line cards and the NNI line cards. The PTS has three types of customer service interfaces called the Port-based, C-tagged, and S-tagged, which offers customers one or more types of service interfaces, each providing different capabilities for service selection, priority selection, and service access protection. To offer customers different capabilities of the layer 3 applications and services, moreover, we have added a type called the IP-flow as the customer service interface. The port-based service interfaces that attach to VLAN-unaware bridges (802.1D Bridges), routers or end-stations, classify a backbone service instance (BSI) by just an input port. The C-tagged service interfaces that attach to C-VLAN bridges (802.1Q Bridges), classify a BSI by an input port and a C-VLAN identifier. The S-tagged service interfaces that attach to a provider bridged network, map a service instance identified by an S-VLAN identifier to a backbone service instance identified by a backbone service instance identifier (I-SID). IP-flow service interfaces subdivide layer 2 flows using 5-tuple information of layer 3 such as a destination IP address, a source IP address, a destination port, a source port, and a protocol. If a port of the UNI line card receives a customer frame, a backbone service instance is allocated to the customer frame and then a PTL trunk composed of a B-DA, a B-SA, and a B-VID is created in the NNI line card. The B-SA and the B-DA are MAC addresses assigned to NNI line cards.

III. IMPLEMENTATION OF BIDIRECTIONAL POINT-TO-MULTIPOINT SERVICES

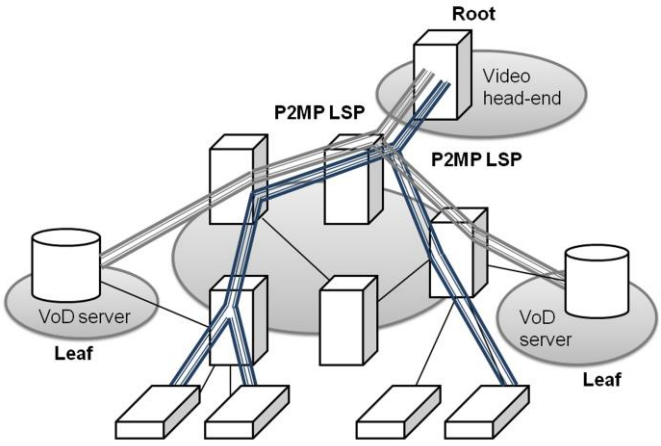

Fig. 3. A point-to-multipoint service

Figure 3 shows a point-to-multipoint (PtMP) service that is the virtual Ethernet communication between one root that distributes multicast video stream and multiple leaves that receive multicast video stream simultaneously. In the PtMP communication, the B-DA conveyed in the backbone service instance tag (I-TAG) is a multicast backbone MAC address and the B-SA is a unicast backbone MAC address as shown in Figure 4(a). In the NNI egress and the transit egress, the MAC-in-MAC frames of IEEE 802.1ah are replicated as many as the number of output port configured by the corresponding multicast MAC address and transmitted to the output ports as shown in Figure 4(b). The PtMP communication in the backward direction is transmission from single leaf to one root. Packet forwarding in the backward direction is the same with that of the point-to-point connection. The PTL trunks that built up PtMP connection are traffic engineered ESPs.

Figure 5 shows the proposed method for the PtMP service in the PTS system based on the PBB-TE. A backbone service instance is allocated to a customer frame by the backbone service lookup table in the UNI LC according customer service interfaces. PtP PTL trunks connected with each leaf node are created in the NNI LC. A multicast B-DA (MB-DA) maps the backbone service instance (BSI) with PtP PTL trunks. In the switch fabric (SW), the MAC-in-MAC frames are copied as many as the number of output slots. In the NNI LC, the MAC-in-MAC frames are replicated as many as the number of output ports in a slot. By grouping PtP PTL trunks and mapping a BSI onto the PtP PTL trunks using a multicast B-DA (MB-DA), PtMP connection in the PBB-TE system could be realized.

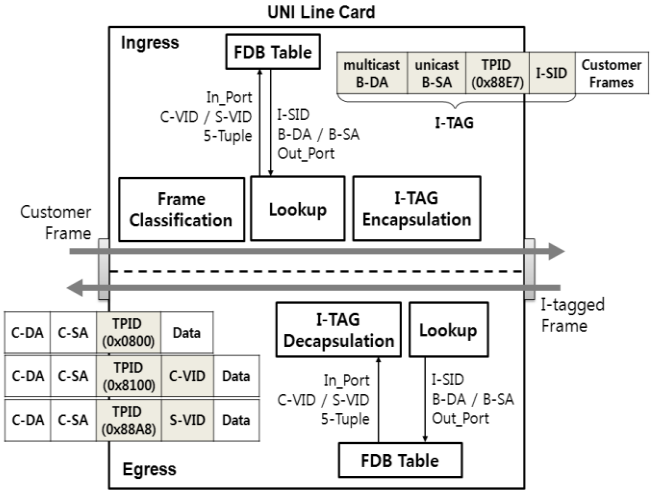

(a)

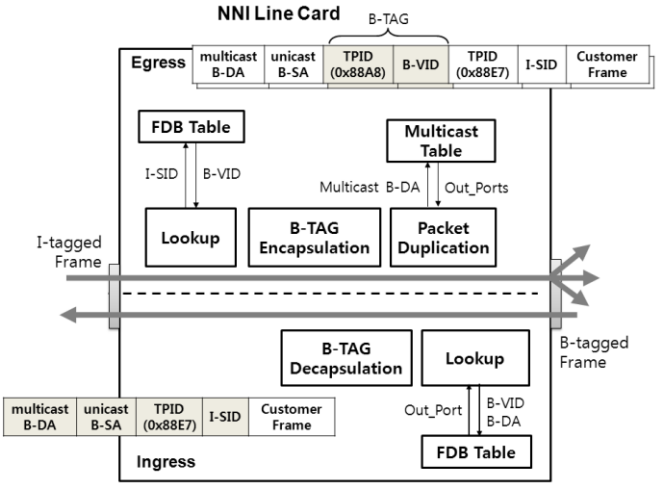

(b)

Fig. 4. The PtMP operation in (a) the UNI linecard and (b) the NNI linecard

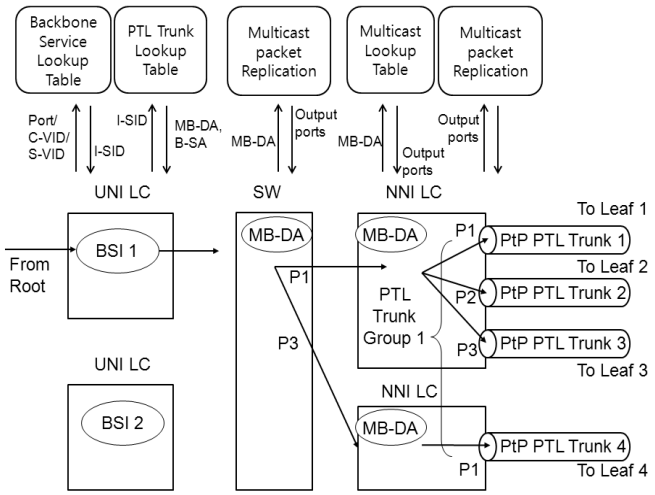

Fig. 5. The proposed method for the PtMP service in the PTS system

IV. IMPLEMENTATION OF BIDIRECTIONAL MULTIPOINT-TO-MULTIPOINT SERVICE

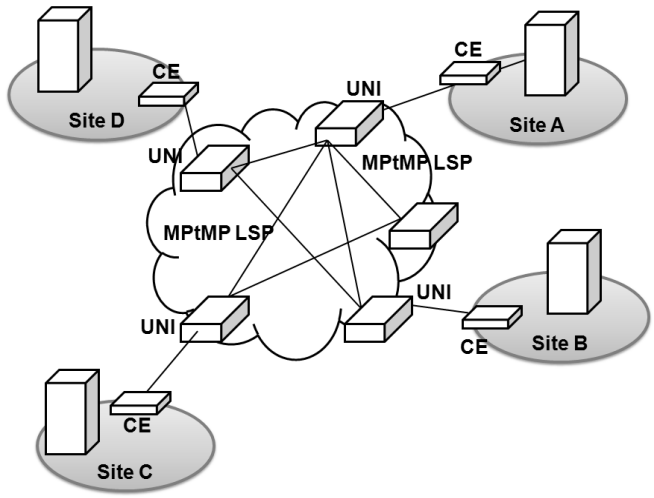

Fig. 6. A multipoint-to-multipoint service

As shown in Figure 6, Multipoint-to-multipoint (MPtMP) services provide multipoint-to-multipoint virtual Ethernet connection between two or more UNIs. More UNIs can be added to the same virtual Ethernet connection. The MPtMP configuration creates a wide area network (WAN) for customers with connectivity between every network site without restoration. The difference between MPtMP and PtMP is that the MPtMP has root endpoints only, which implies there is no communication restriction between endpoints, on the other hand, PtMP has both root and leaf endpoints, which implies there is a need to enforce communication restriction between leaf endpoints.

The MPtMP solution based on the PBB-TE technology has implemented differently from that of the PBB technology. The PBB-based MPtMP solution have used MAC learning and spanning tree protocol used in the conventional bridge, however, MPtMP solution based on the PBB-TE have realized by the combination of point-to-point paths provisioned.

To describe the MPtMP solution based on the PBB-TE, Figure 7(a) and Figure 7(b) show the MPtMP operation such as the copy and flooding of flooding packets and C-SA learning. The learned Result Lookup block of the Figure 7(a) looks the C-DA up in the C-SA learning table and checks whether the C-DA of a customer frame has been learned or not. If the C-DA is not learned, the customer frame is encapsulated with a multicast B-DA for flooding process. If the C-DA is learned, the customer frame is encapsulated with a unicast B-DA. The C-SA MAC learning, which is the learning process for C-SAs, B-DAs, B-SAs, and input ports of remote sites, has been added in the UNI egress. If the B-DA is a multicast MAC address, the flooding of packets into the PtP PTL trunks takes place in the NNI egress. If the B-DA is a unicast MAC address, the PtP transmission into a specific PtP PTL trunk takes place.

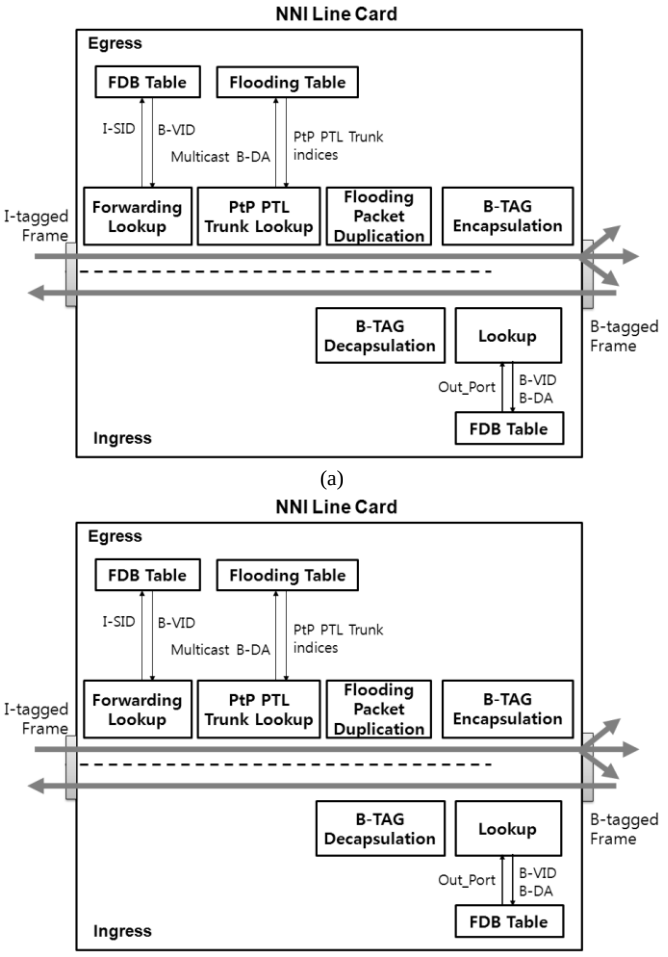

Fig. 7. The MPtMP operation such as copy and flooding of packet and C-SA learnig in (a) the UNI linecard and (b) the NNI linecard

V. EXPERIMENTS AND RESULTS

Figure 8(a) and Figure 8(b) show examples of bidirectional point-to-multipoint services using the packet transport systems. In the Figure 8(a), packets are replicates and multicasted in the ingress edge node. In the Figure 8(b), packets are replicated and multicasted in the transit node. Figure 9 describes the test configuration for the bidirectional PtMP service considering both Figure 8(a) and Figure 8(b). Packets transmitted from the traffic generator were inputted into the P11 port of the PTS 1. And then, packets were duplicated in the NNI LC of the PTS 1 and transmitted to the P12 and P13 ports simultaneously. Packets transmitted from the P12 port of the PTS 1 were inputted into the P21 port of the PTS 2 and were duplicated as many as output ports configured by the multicast B-DA of 01:00:5E:5E:00:02 in the transit LC of the PTS 2 and were output to the P22 and P23 ports simultaneously. Packets transmitted from the P22 port of the PTS 2 were inputted into the P31 port of the PTS 3, and then, packets in which B-DA, B-SA, and B-VID were removed, transmitted to the P32 port of the PTS 3.

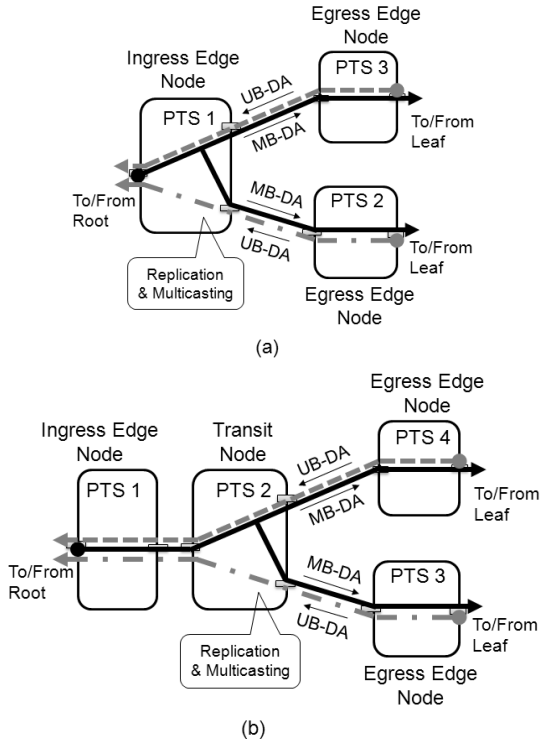

Fig. 8. Examples of bidirectional point-to-multipoint services using the packet transport systems

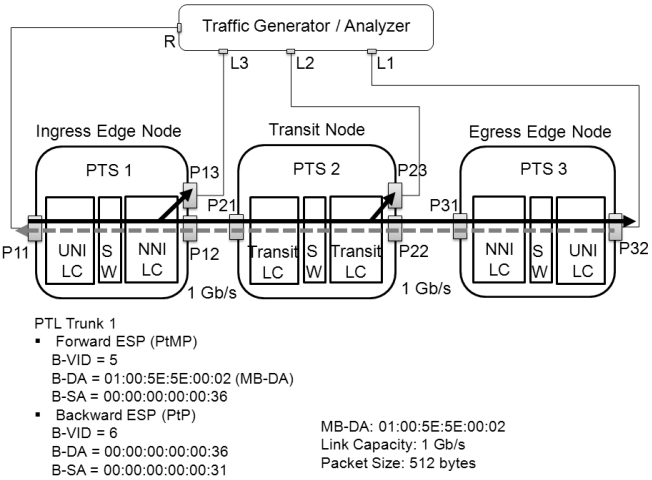

Fig. 9. Test configuration of the bidirectional PtMP service

Customer packets at the rate of about 960 Mbps except inter-packet gap and preamble were transmitted from the R port of the traffic generator to the P11 port of the PTS 1 with the four service interfaces. The customer packets were untagged frames, C-tagged frames with the C-VID of 0x64, and S-tagged frames with the S-VID of 0xC8 according to the service interface types of port-based, C-tagged, IP-flow, and S-tagged. Packets were received simultaneously at the L3, L2, and L1 ports of the traffic analyzer connected with the P13 port of the PTS 1, the P23 port of the PTS 2, and the P32 port of the PTS 3.

Figure 10 described the frames captured at the L3, L2, and L1 ports. The frames output from the P13 and the P23 ports were MAC-in-MAC frames encapsulated with backbone VLAN tags (B-TAGs), on the other hand, the frames transmitted from P32 port of the PTS 3 were the customer frames that B-TAG was

removed in the egress edge node. When the L3 port of the traffic generator sent customer frames corresponding with various service interfaces, the only R port of the traffic analyzer received the customer frames.

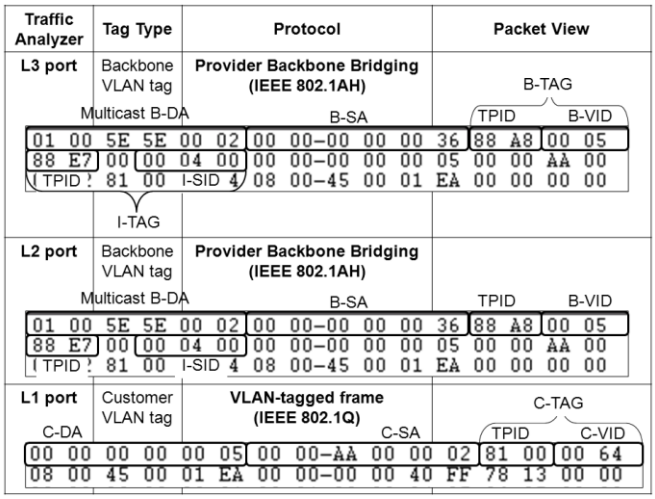

Fig. 10. Frames received in the three leaves

In order to evaluate traffic performance for PtMP services in the PTS, we have measured PtMP throughputs at output ports of the ingress edge node, the transit node, and the egress edge node. Each input traffic rate for port-based, C-VLAN tagged, S-VLAN tagged, and IP flow service interfaces was 1 Gbps including IPG and preamble. To exclude impacts of policing and shaping, policing and shaping set to be off. Table 1 shows experimental results of throughputs for the bidirectional PtMP service. Throughputs for 512-byte packet and physical link capacity of 1 Gbps were measured 100 % at the two ports of the ingress edge node and the transit node. In the egress edge node, however, 4 % of the traffic dropped. It attributed that the B-MAC overhead of 22 bytes occupies 4 % of the 512-byte pa

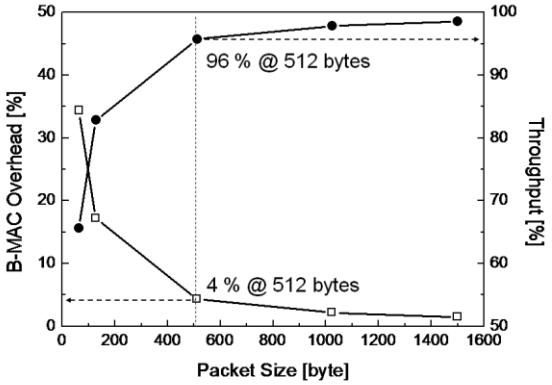

Fig. 11. Impact of B-MAC overhead on the traffic throughput according to packet sizes

Figure 11 explains the impact of the B-MAC overhead that occupying the packet on the traffic throughput according to packet sizes. The larger the packet size is, the smaller the percentage of the B-MAC overhead is, and then, the fewer packets drops. In bidirectional PtMP connection, we have measured the throughput of 96 % for the leaf without MAC-in-MAC encapsulation and the throughputs of 100 % for the two leaves with MAC-in-MAC encapsulation at four service interfaces.

VI. Conclusion

The PBB-TE technology is the carrier Ethernet transport technology that provides connection-oriented Ethernet, end-to-end QoS, and robust OAM. However there have been no proper solutions for multicast services in the PBB-TE technology since the PBB-TE technology does not allow MAC learning, spanning tree protocol, and broadcast of unknown frame for providing deterministic, protected, and connection-oriented trunks and services. Moreover, it has not been easy to classify layer 3 applications and services due to layer 3 service transparency of the carrier Ethernet transport. We have implemented the packet transport system based on PBB-TE, which provides the multicast services and the IP flow awareness. The PBB-based MPtMP solution have used MAC learning and spanning tree protocol used in the conventional bridge, however, MPtMP solution based on the PBB-TE have realized by the combination of point-to-point paths provisioned. Traffic throughputs for the packet of 512 bytes and the link capacity of 1 Gbps have been measured at port-based, C-tagged, S-tagged, and IP-flow service interfaces. The throughputs of leaves with MAC-in-MAC encapsulation (IEEE 802.1ah) were measured 100 %. After removing the MAC-in-MAC encapsulation in the egress edge node, 4 % of the traffic dropped. It attributed that the B-MAC overhead of 22 bytes occupies 4 % of the 512-byte packet. The larger the packet size was, the smaller the percentage of the B-MAC overhead was. Therefore the larger the packet size is, the impact of the B-MAC overhead of the PBB-TE technology on the traffic throughput will be reduced. This study supplements solutions for multicast and L3 level services of the PBB-TE technology, therefore the packet transport system based on PBB-TE could support broadband services such as IPTV or multicast video streaming.

Acknowledgment

This project is processed by MKE. [2008-S-009-02, Development of Packet-Optic Integrated Network Transport Technology]

References

[1] B. Pratt, "Multi-Layer Switching in Packet Optical Transport System," *OFC/NFOEC 2008*, pp. 1-6, 2008.
[2] Virtual Bridged Local Area Networks – Amendment: Provider Backbone Bridge Traffic Engineering, *IEEE Std. P802.1Qay*, 2008.
[3] K. Fouli and M. Maier, "The Road to Carrier-Grade Ethernet," *IEEE Communications Magazine*, 2009.
[4] Claus G. Gruber and Achim Autenrieth, "Carrier Ethernet Transport in Metro and Core Networks," *13th International Telecommunications Network Strategy and Planning Symposium*, 2008.
[5] Wonkyoung Lee, and et al., "Implementation of hierarchical QoS mechanism on PBB-TE system," *9th COIN*, 2010.
[6] J. Heinanen and R. Guerin, "RFC 2698 – A Two Rate Three Color Marker," *IETF Std. RFC 2698*, 1999.
[7] B. Braden, and et al., "RFC 2309 – Recommendations on Queue Management and Congestion Avoidance in the Internet," *IETF Std. RFC 2309*, 1998.

Wonkyoung Lee received the B.S. degree from the Department of Electronic Engineering, Pusan National University, Pusan, Korea in 1999 and the M.S. degree from the Department of Information and Communication Engineering, Gwangju Institute of Science and Technology, Kwangju, Korea in 2001. From 2001 to present, she is with the Optical Internet Research Department, Electronics and Telecommunications Research Institute, Daejeon, Korea. Her research interests include packet optical transport network and network management.

Chang-Ho Choi received his B.S. degree in Mining and Minerals Engineering from Chonbuk National University, Jeonju, Rep. of Korea, in 1998 and M.S. degree in Information and Communication Engineering from Chonbuk National University, Jeonju, Rep. of Korea, in 2000. He is currently working towards his PhD degree at the Chungnam National University, Deajeon, Rep. of Korea. Since 2002, he joined ETRI, Rep of Korea, his work has been focused on Ethernet and packet transport network technology research. His current interests are packet-optical transport systems and protection switching in packet transport network.

Sun-Me Kim received the B.S. degree in Computer Science from Chungnam National University, Daejeon and the M.S. degree in Computer Science from Pohang University of Science and Technology, Pohang, Korea, in 1991 and 1993, respectively. Since 1993, she has been with Electronics and Telecommunication Research Institute (ETRI), Daejeon, Korea, where she is currently a Principal Researcher. Her interested research topics are packet-circuit-optical converged switching system, multi-layer transport network control and management in packet-optical converged network and IDC network control.

Volume 1 Issue 3, Nov 2012, ISSN: 2288-0003

ICACT-TACT JOURNAL

Global IT Research Institute

1713 Obelisk, 216 Seohyunno, Bundang-gu, Sungnam Kyunggi-do, Republic of Korea 463-824

Business Licence Number : 220-82-07506, Contact: secretariat@icact.org Tel: +82-70-4146-4991